INVESTIGATING THE ROLE OF MAPK SIGNALING DYNAMICS AND CHEMOTROPIC REGULATION IN YEAST

by
Patrick Conlon

A dissertation submitted to Johns Hopkins University in conformity with the requirements for the degree of Doctor of Philosophy

Baltimore, Maryland
March 2015

Abstract

All eukaryotes possess MAPK pathways which allow cells to respond to diverse environmental stimuli, including stress, mitogenic, and developmental cues. Deviation from strict MAPK signaling regulation has been associated with the development of many human diseases, including cancer and neurodegenerative diseases. To better understand how cells utilize these pathways to make decisions on their fate, researchers often gain valuable insight from studying related pathways in simpler eukaryotic models, such as yeast, due to their genomes being smaller, better defined, and easier to perturb. In this dissertation, we employ new tools to study MAPK signaling dynamics and chemotropic regulation during the pheromone response in *Saccharomyces cerevisiae.* In the first aim, we examine the role of membrane binding by the MAPK scaffold protein, Ste5, in mediating the chemotropic behavior of cells exposed to gradients of pheromone. Our findings indicate that modulation of scaffold binding to the membrane does not alter directional sensing, but rather sets a chemotropic sensitivity range by modulating the dose response of downstream pathway activity. In the second aim, we explore how the spatial and temporal patterns of Fus3/Kss1 activity contribute to developmental outcomes in cells, including the decision to bud, mate, and undergo polarized morphogenesis in the presence of pheromone. We first apply the Erk Kinase Activity Reporter (EKAR) to specifically report Fus3 and Kss1 activity in live yeast cells. Using this reporter, we are able to elucidate important features of MAPK activity dynamics and cell-to-cell variability. Specifically, we find activity kinetics to exhibit strong cell-cycle dependence and that intracellular activity gradients develop over time as projections grow. In the third aim, we systematically examine mating at the genome-level with the goal of identifying new or previously unidentified mediators of chemotropism in yeast. First, we devised and executed an imaging-based genome-wide screen of mating efficiency and identified groups of mutants exhibiting mating defects. We then explored the nature of the defect in two groups of protein trafficking mutants: the ESCRT

proteins and a membrane-localized component of the exocyst complex, Sec3. Our results indicate previously unidentified roles for these proteins in supporting optimal mating pathway activation and chemotropic behavior.

Thesis committee: Drs. Andre Levchenko (advisor), Jin Zhang, and Jef Boeke

Preface

There are a number of people I would like to recognize who made completion of this thesis possible. First, I would like to thank my advisor, Andre Levchenko, for creating a work environment that allowed me to become an independent scientist and providing the resources to pursue new ideas. I would also like to thank the members of my committee, Jef Boeke, Jin Zhang, and Andre Levchenko, for their critical feedback in many areas of this work. Their comments and suggestions were very helpful and much of the work presented in this thesis reflects their influence.

I would also like to thank Rita Gelin-Licht and all the members of our lab; Peter Pryciak, Jeremy Thorner, Andreas Doncic, Robert Piper, Nicholas Davis, and Maya Schuldiner for valuable discussions in the early stages of this work; Pamela Meluh, Anna Sliva, Katrina Caravelli, Sondra Bahr, and Derek Prosser for providing plasmids and other experimental resources; Michael Erickstad and Alex Groisman for assistance and discussions with microfluidic device design; and Silvia Gabriela Chuartzman and Pnina Weisman for technical guidance in the high-throughput screening work.

Lastly, I wish to thank my family and friends for their unwavering support, especially Katie Coppola. None of this would have been possible without their support.

Table of Contents

List of Tables

List of Figures

I. Introduction

Signaling through the mating MAPK pathway

Pheromone-induced signaling activities

A fundamental characteristic of living cells is the ability to sense and respond appropriately to changes in their environment. To mount these specific responses, cells often enlist the help of kinase cascades consisting of the mitogen-activated protein kinases (MAPK) module. Depending on the external signal present, the temporal and spatial properties of MAPK regulation may prompt cells to proliferate, differentiate, or adapt to different stresses. All eukaryotes contain MAPK signaling networks, and many of the signaling components found in mammalian systems have similar counterparts in the budding yeast, *Saccharomyces cerevisiae* (Figure 1.1). As a unicellular model, the mating response in yeast is a slow and carefully orchestrated cell-state transition that requires diverse processes to be regulated by the mating MAPK, Fus3. To prepare for fusion with a mating partner, yeast cells must arrest their cell-cycles in G1 phase, polarize their cell growth, re-organize their membranes, and upregulate many genes that are important for maintaining these processes[1–3] (Figure 1.2).

Haploid yeast cells exist as two mating types, MATa cells and MATα cells, which differ in the type of pheromone peptide they secrete and pheromone receptor they express. The mating response is initiated in haploid yeast cells when G protein-coupled receptors bind to pheromones that the opposite mating partner secretes. Ligand-bound Ste2 receptor (for MATa cells) activates a heterotrimeric G protein, causing GTP-to-GDP exchange on the Gα subunit (Gpa1) and subsequent conformational changes that unmask the Gβγ (Ste4-Ste18) heterodimer[4]. Once free, Gβγ establishes multiple key binding interactions that are required for proper signal transmission. It recruits the Far1-Cdc24 complex, thereby activating Cdc42[5]. It also recruits Ste20, which in turn is activated by Cdc42[6–8]. The third major effector recruited by Gβγ is Ste5[9,10], a scaffold protein for the three MAPK subunits: Ste11, Ste7, and Fus3[11–13]. By virtue of being tethered to

Ste5 at the plasma membrane, Ste11 is activated by Ste20[14], thus triggering the MAPK cascade. Serving an integral role for early and long-term pathway modulation[15–18], Ste5's membrane recruitment is also a target of inhibition by G1 cyclins, allowing cells that have surpassed the Start checkpoint in G1 to complete their mitotic cycle before mating[19]. The primary goal of activating the MAPK cascade is to generate dually phosphorylated Fus3, which plays many roles in downstream mating processes. Kss1, the MAPK responsible for invasive growth and a homologue of Fus3, is also phosphorylated upon pheromone stimulation, but this activation is more transient[20] and mating functions largely overlap with Fus3[21–24]. Phosphorylation of Dig1, Dig2, and Ste12 to induce transcription of mating genes is required for mating and a central role of MAPK function[25–28]. However, for mating to be optimal, additional targets are activated to drive processes as diverse as cell-cycle arrest and morphogenesis. Known Fus3 substrates include the cell-cycle-arrest and polarized-growth mediator, Far1, and many proteins important for signaling through the MAPK pathway, including, Ste5, Ste11, Ste7, Sst2, and Msg5, among others[22,24,29,30]. While many of these substrates have been established, there are likely many more that have yet to come to light, as phosphoproteomics data would indicate[31,32].

The localization of Fus3 also appears to be important for the mating response. In vegetatively growing cells, Fus3 is found in both the cytoplasm and nucleus, but is enriched in the nucleus upon pheromone exposure[33–35]. Kss1 is predominantly in the nucleus and its localization does not change after pheromone exposure[23]. Interestingly, while both MAPKs are enriched in the nucleus and perform their most important functions there, levels of phosphorylated Fus3 appear strikingly low compared to regions outside the nucleus, although the dynamics of this localization have not been established[36,37]. This would be consistent with Fus3's rapid exchange at both the shmoo-tip and nucleus during pheromone stimulation[34], and a potentially different susceptibility to phosphatases in these regions[35–37]. Dynamic patterns of Fus3 phosphorylation may also be important in the development of projection formation when cells are exposed to high doses of pheromone[38]. These combined observations support the notion that phosphorylated Fus3 needs to

be highly mobile, so that when substrates become present, Fus3 will be able to activate them wherever they are located.

Ste5 scaffold protein dynamics

Ste5 is a key regulatory component in the pheromone response, playing roles to both localize and activate the mating specific MAPK, Fus3. Similar to Fus3, Ste5 is localized in both the cytoplasm and nucleus of vegetatively growing cells. Upon pheromone exposure and subsequent dissocation of Gβ, Ste5 is rapidly recruited to the plasma membrane (PM) and is observed to be uniformly distributed around the perimeter of the cell. After a period of several minutes, localization of the scaffold at the membrane is gradually lost, but then begins to re-appear again as projection formation ensues. In addition to binding Gβ through its RING-H2 domain[10,39], stable tethering to the PM is also mediated by binding to membrane phospholipids and phosphoinositides through an N-terminal amphipathic helix (PM motif) and an internal pleckstrin-homology (PH) domain, respectively[15,16]. All three of these interaction motifs are distinct and required for full retention of membrane binding and activation of pheromone signaling[16]. Long-term and stable localization of Ste5 at the PM also depends on its movement along actin cables assembled by Cdc42 and the formin Bni1 working at the projection growth site. Oligomerization of Ste5 proteins may also be important for its localization and activity at the PM[11,39], but the arrangement and functional purpose of these self-associated states are not clear. Interactions with additional proteins at the PM, such as the scaffold protein Bem1 (which binds the Cdc42 GEF – Cdc24), may also influence Ste5's membrane localization.

Another important property of Ste5, is its ability to exclusively bind and activate Fus3, and not Kss1[40,41]. Activation of Fus3 ensures phosphorylation of substrates that are involved in mating cell differentiation and not filamentous growth. Ste5 has also been shown to be important in both signal amplification and attenuation mechanisms. Interestingly, it has been reported that competition of Ste5 phosphorylation by Fus3 and dephosphorylation by Ptc1 contributes to a

switch-like morphological response[42], whereas membrane localization of Ste5 promotes a graded transcriptional response of mating genes[43]. Early in the response, Ste5's recruitment to the PM seems to be negatively regulated by Fus3 activity leading to its slow disappearance from the membrane[18,44]. Later in the response, Ste5's localization to the membrane appears more stable than Fus3, as indicated by FRAP studies[34]. Cortical abundance of Ste5 at the PM was also shown to be dependent on MAPK cascade activity[45]. These results support a potential role for Ste5 to downregulate the pheromone signal early in the response, but to sustain the pheromone signal later in the response, once the cell has fully committed itself to mating.

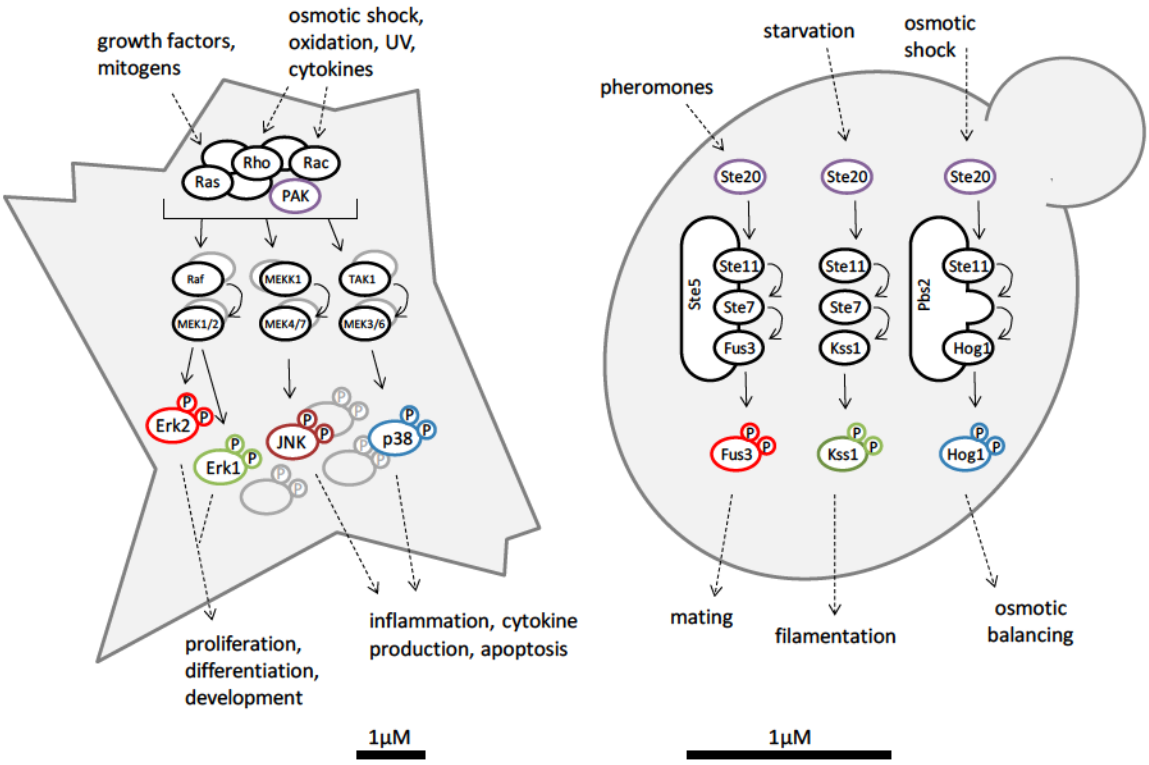

Figure 1.1. Comparison of MAPK pathways in mammalian and yeast cells. Input signals and output responses of conserved MAPK pathways are indicated for each system. Colors are the same for homologous kinases.

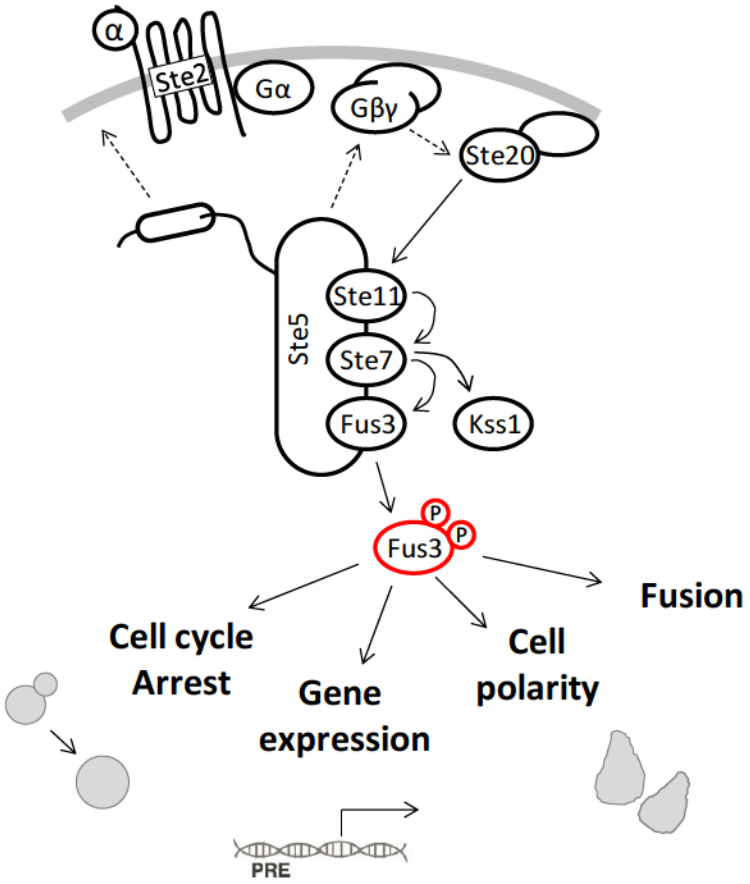

Figure 1.2. Schematic diagram of the mating MAPK pathway in yeast. Phosphorylated Fus3 is highlighted in red and downstream mating responses are indicated.

Mechanisms of pheromone gradient sensing

In order to attain diploid cell status, haploid yeast cells have an innate ability to seek out and fuse with mating partner cells, even when they are not immediately adjacent to each other. To reach the cell fusion stage with a mating partner, yeast cells are able to polarize their cell growth in the direction of the ambient pheromone gradient source. This process is referred to as chemotropism, or growth in the direction of a chemical gradient. Remarkably, yeast cells are able to distinguish pheromone gradients as shallow as 1% across their cell width and can polarize their cell growth to reach lengths several times longer than their original size. Chemotropism in response to pheromone is a dynamic process and can be characterized by two important subprocesses: establishment of the growth site and maintenance of polarized growth (Figure 1.3). Understanding how the actin cytoskeleton and polarity machinery become positioned at the projection growth site has been the topic of many studies over the past couple of decades. Several important signaling components and interactions have been identified and will be summarized below. Recently, mechanisms for re-orientation, or gradient tracking in shallow gradients, have also been proposed.

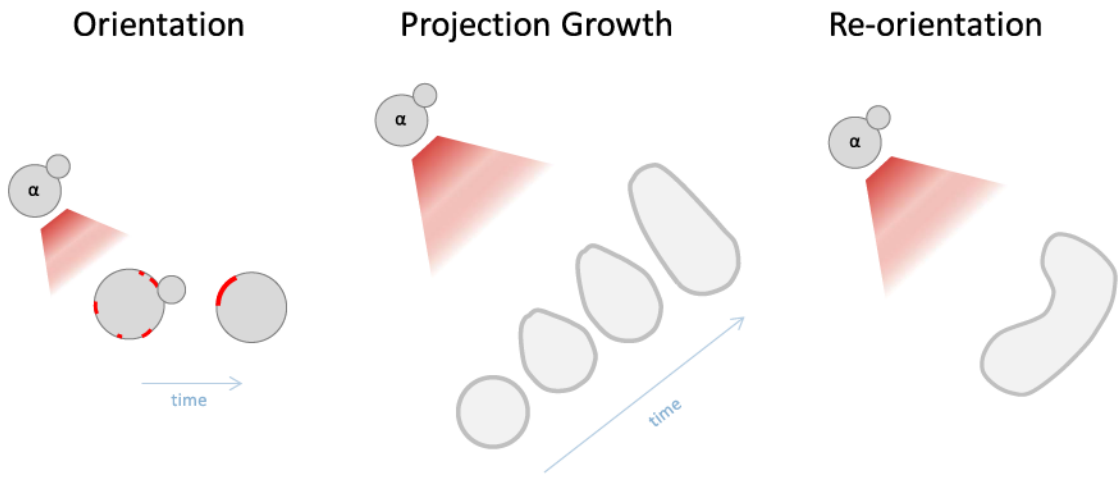

Figure 1.3. Schematic diagram depicting modes of chemotropic behavior in pheromone gradients. Orientation is characterized by wandering and establishment of the growth site. Projection growth is characterized by polarity maintenance and requires sub-maximal signaling. Re-orientation combines aspects of both orientation (polarity patch wandering) and projection growth. Arrows indicate progression over time.

Role of the Ste2 receptor

The alpha-factor receptor Ste2 is a G-protein-coupled receptor that is often studied as a model GPCR in eukaryotic systems. The receptor spans the plasma membrane seven times, contains an extracellular N-terminus, and a large 134 amino acid intracellular C-terminus that facilitates many of the interactions important for signaling. In vegetative cells, the alpha-factor receptor Ste2 is found localized uniformly around the plasma membrane, in small punctate vesicles within the cytoplasm, and in the vacuole. In response to alpha-factor, the receptor Ste2 is rapidly internalized, visibly disappearing from the plasma membrane for approximately 30 minutes after stimulation[46–49]. The rate of internalization is increased 5 to 10-fold above the basal internalization rate[50]. Rather than being recycled back to the membrane from early endosomes (as appears is the case for Ste3 in MATalpha cells), Ste2 is transported through the endocytic pathway to the vacuole where it is degraded[51]. After the initial loss of receptor sites at the membrane, receptors begin to re-accumulate at the membrane approximately 60 minutes after stimulation, which is largely due to an increased synthesis rate during pheromone treatment[47,50].

On a molecular level, the internalization of Ste2 upon pheromone treatment requires the hyperphosphorylation of its C-terminal tail[52,53] and subsequent ubiquitination of the lysine residue found in the SINNDAKSS sequence within this tail region[54]. The casein kinases Yck1 and Yck2 are required to phosphorylate the serine residues on this sequence and are required for Ste2 ubiquitination and internalization, both in basal and pheromone-induced cells[55]. Additionally, monoubiquitination, rather than polyubiquitination, seems to be particularly important as a signal for internalization and protection against proteasomal degradation[56]. In this manner, cytoplasmic, or 'signaling', portions of the receptor remain in-tact at both the plasma membrane and as the receptors become internalized on vesicles.

Interestingly, removal of residues at the C-terminus of Ste2 results in an increase in the number of receptors at the plasma membrane, an increased sensitivity to pheromone, and a defect in the recovery of cell division after pheromone treatment[51,57,58]. While a truncated ste2-T326

mutant is apparently defective in endocytosis, it may not be the endocytic defect, per say, that causes the increased sensitivity to pheromone. Specifically, another internalization-defective receptor mutant, ste2-K337R, was found to exhibit similar signaling sensitivity as an internalization-competent receptor, while only causing a defect in pheromone adaptation[58]. Removal of additional residues at the C-terminus may act to relieve repression of G protein signaling, which could be the reason for the increased pheromone sensitivity. Moreover, the ste2-T326 mutant showed a defect in mating partner selection, via the partner discrimination assay, which was suggested to be the result of the increased sensitivity to pheromone[59]. It was later determined that this receptor mutant initially orients growth in a pheromone gradient, but is not able to increase its orientation over time as is observed in wild-type cells. It was also shown that the ste2-T326 mutant and sst2Δ mutants, which are both supersensitive to pheromone, are particularly defective in orientation at higher concentrations of pheromone, indicating that proper signaling amplification and desensitization may be important for maintaining oriented growth[60–62]. In addition to the preservation of early response signaling in the endocytosis-defective receptor, overexpression of the receptor also does not appear to significantly affect signaling output of the pathway[57].

As an integral membrane protein, Ste2 is delivered to the plasma membrane through actin-dependent vesicle secretion. As the first signaling component in the mating pathway, it is reasonable to suspect that the activation and localization of Ste2 is would be important determinants in the chemotropic behavior of cells exposed to pheromone. Recently, internalization of the receptor has been found to be important for both directional sensing and shaping the polarized localization of the G-protein subunits, Gα and Gβγ[49]. Interestingly, while actin is required for the initial endocytosis of Ste2, the establishment of polarized Ste2 crescents at the plasma membrane does not require actin filaments or vesicle-mediated secretion. While the mechanism of this initial polarization is not clear, the fact that receptor polarization precedes actin-dependent cell polarization implies that early receptor polarization helps to establish the

projection growth site. It possible that the initial actin-independent polarization phase may rely on biased fusion of Ste2-containing vesicles at sites where polarity cues, such as Cdc42, are located[49]. In support of this notion, there appears to be an inherent ability of secretory vesicles to deliver proteins to the membrane in cells lacking actin cables and patches[63]. Actin-dependent recycling of endocytosed vesicles could also be a potential mechanism of membrane delivery in the absence of actin cables[64]. It has also been hypothesized that activated receptors may be protected from phosphorylation by Yck1 and Yck2. Rather than being endocytosed, this hypothesis suggests that unphosphorylated receptors and associated G proteins would accumulate on the plasma membrane over time and eventually establish the axis of polarity[49].

Role of Fus3 and G proteins

One of the important consequences of Ste2 activation is the ultimate relocalization and activation of the Rho-family GTPase Cdc42, which orients actin cables and vesicle delivery to the polarization site[65]. Cdc42 has been shown to have many direct regulators, both GEFs and GAPs, and dozens of effectors which coordinate different aspects of polarized growth. These effectors which either become activated or tethered by Cdc42 include actin, formins, PAKs, myosins, exocyst components, polarisome components, septins, vesicle targeting proteins, and other G proteins[65]. In the presence of pheromone, activation and enrichment of Cdc42 at sites of ligand-bound receptors is believed to be mediated by recruitment of the Far1-Cdc24 complex to pools of unbound Gβγ at the plasma membrane. At high concentrations of pheromone, which saturate the receptor, activation and enrichment of Cdc42 appears to occur at 'default sites' specified by the bud-site-selection protein Rsr1. This is where Cdc42 is normally activated during the cell-cycle in order to promote actin-dependent activities at sites of bud emergence. In gradients of pheromone, which do not saturate the receptor, formation of the Gβγ –Far1-Cdc24-Cdc42 chemotropic complex appears to override formation of the Bud1-Cdc24-Cdc42 budding complex, thus allowing Cdc42 to polarize toward the source of the pheromone gradient. In other words, ligand-

bound receptors can spatially bias where Cdc42 becomes activated. Highlighting the importance of the chemotropic complex, specific mutants of Far1 and Cdc24 which abrogate their interaction with each other or Gβγ, have shown to be defective in directional sensing of pheromone gradients and instead, orient their growth toward the default bud site[66,67].

In between receptor activation and the localized activation of Cdc42 at ligand-bound receptor sites, there are a number of important signaling events that both support and work in parallel with Cdc42 in mediating chemotropic growth. Dissociation of the Gα and Gβγ subunits is a primary step in polarity factor recruitment. Far1 and Cdc24, which are normally localized to the nucleus in G1 phase cells, are recruited to Gβγ by a binding interaction with Far1, thus bringing the Cdc42 GEF into close proximity with its substrate G protein at the membrane. There is additional evidence that Fus3 may either directly or indirectly support this process. Recruitment of Ste5 to Gβγ and the subsequent activation of Fus3 are critical for initiating all of the physiological mating responses, including the development of polarized growth. It has been shown that disrupting the Fus3 docking domain on Ste5 results in a defect in gradient sensing, indicating that the signaling effects and/or localization of Fus3 at the plasma membrane may be important for chemotropism[68]. Interestingly, it was also recently shown that cortical localization of Cdc24 depends on Fus3, and specifically the ability of Fus3 to down-regulate Ste5 recruitment and inhibit the Cln/Cdc28 kinase[69]. One important interaction of Fus3 is with freed Gα at the plasma membrane. Abrogating the Fus3-Gα interaction (via gpa1K21E R22E allele) diminishes the ability of cells to down-regulate cell-cycle arrest signaling and also causes a defect in chemotropism (via the partner discrimination assay)[70]. Thus localizing Fus3 to the membrane at the projection site may be important for activating proteins important for polarized cell growth and consequently, may also lead to reduced activity in the nuclear compartment where Fus3 phosphorylates Far1 and regulates gene expression to promote cell-cycle arrest. There are likely many substrates in the cytoplasm and at the plasma membrane that Fus3 may phosphorylate to support polarized cell growth. Interestingly, a nonphosphorylatable mutant of Gβ (Ste4T320A

S335A) conferred a chemotropic defect that was similar in magnitude to the defect caused by disrupting the Fus3-Gα interaction[70,71]. It was also found that phosphorylation of Gβ leads to a reduced affinity for Far1 and a concomitantly weaker interaction of the polarisome at the shmoo tip. These results imply that phosphorylation of Gβ by Fus3 destabilizes the interaction between the Gβγ dimer and Far1 enough to cause the link between activated receptors and polarity factors to be continually renewed over time. In this manner, the status of receptor activation would be continually reported to the polarity machinery[71]. In any event, it appears that Fus3's interaction with Gα and phosphorylation of Gβ are important for cells to accurately orient their growth in pheromone gradients.

In addition to G-protein regulation, Fus3 is also believed to phosphorylate and activate many other substrates that are important for polarized growth orientation and maintenance. Many of these substrates could also be effectors of Cdc42, which may possibly require both phosphorylation by Fus3 and further activation or tethering by Cdc42 to be fully functional during the pheromone response. Bni1, a formin protein, is one known substrate of Fus3 and is important for facilitating cortical actin cable assembly. Phosphoproteomics studies have also revealed a pheromone-induced increase in phosphorylation of dozens of other proteins involved in cell polarization processes, including cytoskeleton organization, vesicle transport, and cell membrane structure[31,32]. It will be interesting to see how phosphorylation state regulates their function, whether it's a means for activation, deactivation, or degradation.

Role of vesicle trafficking

In addition to the precise biochemical interactions that have been found to be important for chemotropism, it is also likely that endocytosis and exocytosis play important roles in both establishing the growth site and perpetuating the growth process. While vesicle trafficking has been rigorously studied in the context of the budding process, it is not yet clear how the delivery and internalization of vesicles contributes to signaling and polarized growth development during

the pheromone response. As discussed in the prior section, the early polarization of the receptor relies on its internalization ability[49]. It has also been proposed that differential internalization of the heterotrimeric G proteins may also be important for establishing the initial polar cap that leads to the recruitment of critical polarity factors[71]. Interestingly, the receptor and heterotrimeric G proteins tend to localize more broadly around the perimeter of the mating projection, whereas most of their downstream signaling effectors appear to be more tightly localized at the tip of the mating projection. It is not known however if the activated, or signaling-competent, forms of the receptor (phosphorylated) or heterotrimeric G proteins (dissociated or phosphorylated) have different spatial polarizations than their inactive forms. There are likely a range of spatial amplification mechanisms that operate at different phases of projection growth. The initial establishment of the growth site appears to be largely independent of actin and vesicle secretion. While the initial internalization of the receptor requires actin, polarization of both the receptor and Cdc42 have been separately shown to not require actin, as assessed from LatA treated cells[49,72]. Cdc42/Bem1 polarization even occurs in *cdc24-m1* cells, where the polarity regulators are uncoupled from the receptor. The development of a "polarity patch" consisting of Cdc42 appears to require a positive feedback loop that involves Cdc42's activator, Cdc24, being in a complex with one of Cdc42's effectors, Bem1, at the plasma membrane. Thus, by activating Cdc42, more Bem1 gets recruited, which recruits more Cdc24 and ultimately activating more Cdc42 to complete the loop[73].

In addition to the actin-independent mechanisms of projection growth site establishment, spatial amplification of polarity factors may increase over time as projections grow, and this amplification may also depend on the dose of pheromone, or the local levels of activated receptors at the membrane. For example, as Cdc42 begins to direct actin cable formation, cable-dependent vesicle transport may deliver more Cdc42 and other polarity factors to the growth site to enforce the growth trajectory for that particular projection. This has particularly been shown to be the case for polarity amplification during the budding process[74,75]. On the other hand, polarity

generation appears appears to be quite different at low doses of pheromone, compared to high doses. At low doses of pheromone, where receptors are not saturated with ligand, the growth site (or the polarity patch, as marked by a Bem1-GFP reporter) wanders around the periphery of the cell. Interestingly, this wandering appears to be caused by vesicle-mediated trafficking to the growth site, since it depended on both F-actin and Myo2. FRAP studies nonetheless showed that Cdc42 polarization was dynamically maintained in an actin-independent manner (again using LatA treatment). The mobility of the polarity patch is more constrained at higher pheromone doses, indicating that wandering requires sub-saturation and presumably a lower level of activated receptors at the membrane. It was further shown that polarity patch wandering supports the ability of a cell to reorient its mating projection and track shallow gradients of pheromone. Because secretory vesicles are not predicted to contain most polarity regulators (including Bem1, Cdc24, and other Cdc42 effectors that are not integral membrane proteins), it has been proposed that vesicle fusion perturbs the polarity patch by diluting away local polarity regulators at the plasma membrane[72]. This would allow the polarity patch to continually explore the membrane for activated receptor sites and, thus provide a mechanism for mating projections, which are initially misaligned, to improve their growth alignment over time in a pheromone gradient.

Tools for measuring chemotropic behavior

In order to assess the directional sensing, or orientation ability, of cells exposed to pheromone gradients, a variety of genetic and single-cell assays have been devised by researchers. Indirect assays, including the competition assay, the partner discrimination assay, and the confusion assay, utilize traditional genetic methods and are more amenable to higher-throughput analysis and screening. Direct assays, including zygote formation, micro-pipetting and microfluidics-based approaches, evaluate orientation ability at a single-cell level and are currently less amenable to high-throughput analysis. The details of these assays will be further discussed below.

Indirect chemotropism assays

In both the competition and partner discrimination assays, a responder cell type is mated in the presence of two mating partner cell types, which are both in greater abundance than the responder cells[46,59]. In the competition assay, the mating partner cells consist of a wild-type 'target' strain and a mutant 'competitor' strain. The relative ability of the mutant competitor cells to compete with the wild-type target cells in mating to the responder cells is assessed by measuring the mating efficiency between the target and responder cells. A good competitor cell will be competent in signaling and chemotropic behavior, but does not necessarily have to be proficient in fusion. Competitor cells that may have defects in signaling or chemotropic behavior will not compete effectively, so the mating between target and responder cells will be higher. In order to distinguish diploid formation between the target and responder cell pairs with competitor-responder cell pairs, appropriate genetic selection markers are encoded into the target and responder strains.

In the partner discrimination assay, the two mating partner cell types typically differ in their ability to secrete pheromone, but otherwise have all mating signaling components intact[59]. Instead of evaluating the competition ability of one of the mating partners, the discrimination assay evaluates how well the responder cell can choose between the two mating partner cells. Because the responder strain contains the mutation that is being evaluated, this assay typically allows a greater dynamic range to be explored since mating efficiency is being measured for a mutant, as a opposed to a wild-type strain.

The confusion assay examines the importance of the pheromone gradient during the mating process[66,76]. In wild-type cells, the addition of exogenous pheromone in the presence of mating partner cells results in a reduction in mating efficiency. This mating reduction is presumed to be caused by diminishing the ability of the wild-type cells to sense the natural pheromone gradient emitted by the mating partner cells. Thus, they become 'confused'. In mutant cells where

the gradient sensing ability is lost, however, there is no reduction in mating efficiency when exogenous pheromone is added to the mating mixture. This is because the gradient sensing ability is already lost, so abolishing the pheromone gradient will not have a further impact on mating. While several mutants with specific defects in chemotropism have been identified with the confusion assay, it may be difficult to evaluate the chemotropic defects of mutants that also exhibit severe signaling defects, since addition of exogenous pheromone may compensate for a signaling defect and improve mating. As a result, a severe signaling defect could potentially mask an orientation defect in the confusion assay.

Direct chemotropism assays

In addition to the indirect genetic-based assays described above, direct assays have also been developed to evaluate chemotropic growth at the single-cell level. The zygote formation assay involves time-lapse monitoring of the mating process in a more natural setting[71,77]. Mating partner cells are mixed on an agar surface at a relatively low density and allowed to mate. In order to assess projection orientation ability, bilateral mating crosses are typically performed, where the same mutation exists in both the MATa and MATα cell types. If a particular mutation confers a chemotropic defect, the reduction in mating will be magnified if both partner cells are defective, as opposed to just one of the partners. Once cell fusion has occurred, the orientation ability can be inferred by measuring the angle created by the two fused projections. Fusion angles will be larger for cells that exhibit poor orientation, and smaller for wild-type cells that exhibit optimal orientation. Alternatively, the angle between the projection growth site and bud scar can be measured, to assess the ability of polarity factors to undergo symmetry breaking (change from budding symmetry to pheromone-induced symmetry)[77]. In addition to orientation, projection re-orientation can also be evaluated using this assay by first stimulating the mating partner cells with pheromone in liquid culture prior to seeding them on agarose[71]. Wild-type projections can be

observed to re-orient toward their mating partners, whereas mutants defective in gradient sensing will not be able to re-orient as well.

In order to more precisely evaluate orientation and projection growth maintenance, cells can be exposed to artificial gradients either on an agar substrate or in microfluidic devices. In the first direct assay of chemotropism, a micropipette was used to generate a radial pheromone gradient around cells seeded on an agar surface[78]. Using this assay, projection orientation can be assessed by measuring the angle of the projection with respect to the gradient normal. Wild-type cells will exhibit smaller projection angles, whereas mutants defective in orientation will exhibit larger angles.

In order to increase the control and stability of the gradient, various designs of microfluidic devices have been used in assays for pheromone gradient sensing. In these devices, gradients are generated in one of two ways: either by diffusion of pheromone into chambers protected from fluid flow[68,79,80] or by diffusion of pheromone across a chamber that is experiencing fluid flow[61]. In all of these designs, the gradient extends in one direction and projection angles can be measured with respect to the gradient normal. Stability of the gradient over time is important, as cell signaling, chemotropism, and phenotypic responses are all very sensitive to pheromone concentration especially when it is in a range that largely modulates receptor saturation. Since precise signaling behaviors and developmental outcomes are often being studied, most experiments involving pheromone induction are carried out in strains with the Bar1 protease deleted. This helps to ensure the correspondence of cell response with a known level of input. In addition to measurements of growth orientation, precise measurements of projection growth rate and lineage coupling can also be obtained in microfluidic experiments. The ability to establish, sustain, and re-orient projection growth are distinct aspects of chemotropism that are best evaluated in carefully controlled environments, where pheromone gradients are either established exogenously or emanate from natural mating partners.

Tools for measuring intracellular signaling dynamics

Fluorescence-based reporters

At the core of the mating pathway is a MAPK cascade that initiates the processes important for mating. Over the years, a variety of genetic-based and single-cell assays have been developed to measure signaling at different levels of the mating pathway. Fluorescence-based reporters, including protein fusions and transcriptional reporters, have been particularly useful, since they are able to couple with single-cell microscopy and can report on both the temporal and spatial aspects of signaling dynamics. Fusing fluorescent proteins (FPs) to endogenous proteins has enabled the direct examination of protein location, translocation, expression, and degradation in live cells. These studies have also been carried out in high-throughput systematic studies using genome-wide libraries of GFP-tagged proteins[81,82]. Fusion of FPs to multiple proteins has further enabled co-localization studies and even examinations of protein-protein interactions through measurements of fluorescence-resonance energy transfer (FRET)[83]. Generally, an interaction distance of less than 10nm is necessary for FRET to occur. Other ratiometric fluorescence-based strategies have also been developed for mapping protein-protein interactions in yeast[84]. In addition to localization and protein interaction applications, fluorescent proteins can also be expressed under the control of endogenous promoters within the yeast genome, in order to report the transcriptional activity of a signaling network. For example, the promoters of highly expressed mating genes, such as Fus1, are commonly used in transcriptional fluorescence-based reporters to detect mating pathway activity[85]. Even with strong promoter activation, it takes approximately an hour to first achieve a signal from GFP expression. Because of the time required for maturation and degradation of the fluorescent protein, these reporters are considered to be 'passive' reporters and are unable to capture fast dynamics and upstream signaling events. The fusion of PEST tags, or proteasome-targeting sequences, to GFP are able to decrease its half-life to around 30 minutes[86], but this also leads to a diminished overall expression level and lower signal-to-noise ratios.

Genetically-encoded FRET biosensors

Over the past decade, there has been a rapid rise in the development of genetically-encoded FRET biosensors to visualize a diversity of intracellular signaling events, including kinase activity, GTPase activity, protein conformation changes, and small molecule/ion concentrations[83,87]. Rather than serving as passive reporters of intracellular signaling, many FRET-based biosensors are active reporters exhibiting rapid on/off switching that can more closely match the dynamics of many biological events, such as protein phosphorylation, dephosphorylation, conformational changes, and ion/metabolic fluxes. Additionally, the genetically-encoded nature of these probes, utilizing an ever-expanding catalog of fluorescent-proteins, highlights their simplicity and versatility, especially in their ability to be genetically targeted to specific subcellular compartments.

While many of these sensors have been widely utilized in mammalian systems, the development and application of FRET activity reporters in simpler eukaryotes has thus far been underappreciated. Yeast has been a model system for studying many eukaryotic signaling pathways, but its small size, fast doubling time, and non-adherent nature pose challenges for studying single-cell dynamics over extended periods of time. Only recently have microfluidic technologies enabled long-term imaging of yeast cells with user-defined control of the extracellular environment[79,88,89]. As opposed to dish or open-volume imaging platforms, microfluidic devices have the advantage of being able to keep dividing and growing yeast cells in the focal plane of the microscope, thus providing focal stability and the ability to track individual cells and cell shapes over time. This in turn enables biosensors and other fluorescence-based reporters to be monitored in single cells. Studying dynamic processes using FRET-based reporters in yeast also poses challenges relating to signal strength, photobleaching, and phototoxicity[90]. Because of their small size, concentrations of fluorescent molecules tend to be lower. Phototoxic effects, such as cell-cycle arrest or dying, can also be observed if yeast cells are

exposed to high doses of GFP-wavelength-range light. Thus, adjusting the illumination intensity and imaging frequency is especially important for time-lapse experiments involving multiple wavelengths captures, such as with FRET. To date, applications of FRET biosensors in yeast have mostly involved the detection of small molecules, including metabolites and second messengers, and ions[91–94]. Recently, a FRET biosensor was also developed to measure Cdc42 activity at the plasma membrane in vegetatively growing yeast cells[95]. As further advances in biosensor design and fluorophore development are made in mammalian systems, activity biosensors should continue to see increased utility in yeast cells, where signaling and developmental processes often occur over short and experimentally-convenient time scales.

II. Role of Ste5 membrane binding in pheromone gradient sensing

Introduction

The MAPK scaffold protein Ste5 is essential for yeast mating. Upon dissociation of the Gβγ complex, Ste5 is rapidly recruited to the plasma membrane (PM) where it serves two primary signaling functions. First, it brings the MAPKKK, Ste11, into close proximity with its upstream PAK activator, Ste20, which gets activated and localized to the plasma membrane by Cdc42. Once activated, Ste20 phosphorylates and activates Ste11 to initiate the MAPK cascade. Second, Ste5 selectively binds and activates Fus3, the mating-specific MAPK. Thus, by being recruited to the plasma membrane and binding the mating MAPK components, Ste5 is able to prevent Ste11 from signaling to MAPKs that are involved in other pathways[2].

Because of its role in activating Fus3 and initiating MAPK cascade, the regulated localization of Ste5 at the PM is important for activating the overall mating response. In addition to binding to Gβ, Ste5 also binds to the membrane through an N-terminal amphipathic helix and a PH domain, which interact with membrane phospholipids and phosphoinositides, respectively[96,16]. Membrane localization of Ste5 may also be facilitated by indirect interactions, such as with Bem1, another scaffold protein that binds Ste20, Cdc24, and Cdc42[97,98]. While Ste5's initial recruitment to the plasma membrane is rapid and uniformly distributed, polarized and sustained localization of Ste5 at the incipient projection site has been shown to require the polarized localization of PtdIns(4,5)P_2 at the membrane[99]. Projection formation and maintenance, however, may only require a small number of Ste5 proteins to be present and active at the membrane, smaller than what can be readily detected by microscopic evaluation. Additionally, it has been shown that constitutive targeting of Ste5 to the membrane (via Ste5-CTM fusion) leads to robust signaling activation[96], and even polarized cell growth in the absence of pheromone induction. These results suggest Ste5's presence at the membrane and concomitant activation of Fus3 may

also play a role in regulating the chemotropic behavior of cells. Here, we sought to examine the effects of Ste5 membrane binding more closely through assays of gene expression, localization, and pheromone gradient sensing.

Results

Localization of Ste5 and modulation of membrane binding

In order to assess the importance of the Ste5 – plasma membrane (PM) interaction on the mating response, we examined previously identified mutants of Ste5, in which the PM binding affinity was either stronger or weaker than wild-type Ste5[96]. The stronger affinity mutant, $Ste5^{T52L}$, enhances the hydrophobicity of the embedded amphipathic helix in Ste5's N-terminal PM domain, and resulted in an increased signaling response. Conversely, the weaker affinity mutant, $Ste5^{dn8E}$, adds repulsive negative charge to regions flanking this PM domain, and resulted in a decreased signaling response. These perturbations do not affect Ste5's Gβ or PIP2 binding regions, which are found at separate regions in the protein[96]. In order to more closely evaluate the localization and signaling effects of these mutants, we prepared 3xGFP-tagged chimeras of these mutants and integrated them into the genome, in place of the endogenous Ste5 gene. In basal cells, localization of Ste5-3xGFP, $Ste5^{T52L}$-3xGFP and $Ste5^{dn8E}$-3xGFP was found to be cytosolic and slightly enriched in the nucleus for each of the strains (Figure 2.1a). Low levels of $Ste5^{T52L}$-3xGFP were also detected at the plasma membrane in some cells. After 3hrs of saturating pheromone treatment, $Ste5^{T52L}$-3xGFP and $Ste5^{dn8E}$-3xGFP both showed strong localization at the projection tip, similar to wild-type Ste5.

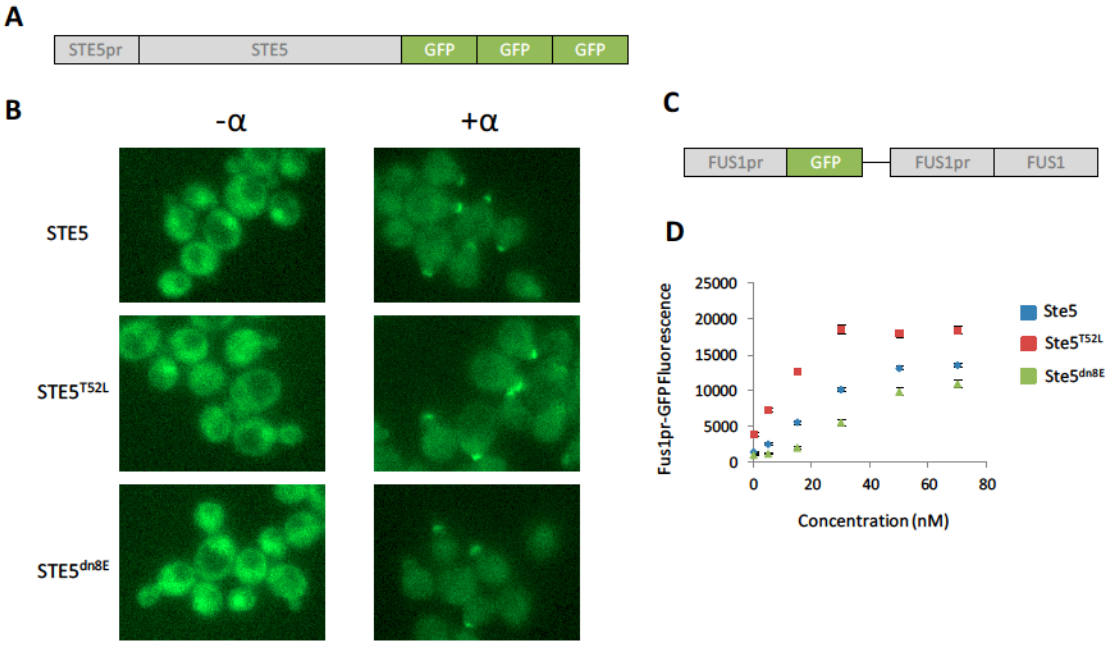

Figure 2.1. Signaling and localization of Ste5 PM binding mutants. A) Schematic of Ste5-3xGFP construction. B) GFP fluorescence images of wild-type (PC67) and mutant Ste5 strains (PC74, PC75) before and after 3 hours of 10uM alpha-factor treatment. C) Schematic of FUS1pr-GFP construction and integration. D) Dose response of mating gene expression for PC51 cells expressing an integrated Fus1pr-GFP reporter and plasmid-borne Ste5 mutants.

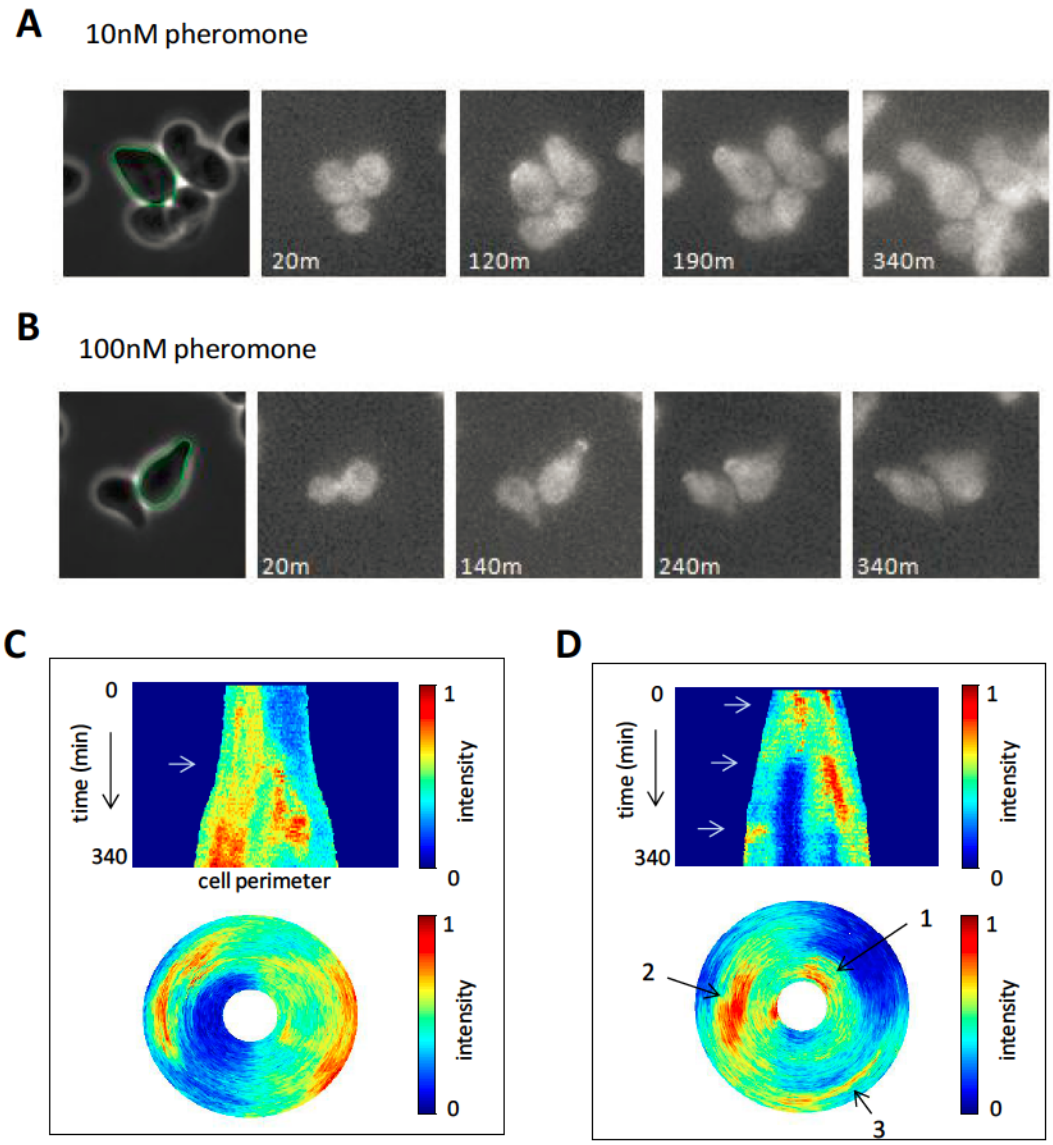

Figure 2.2. Membrane localization dynamics of Ste5 during pheromone-induced morphogenesis. Time-lapse images and kymographs depicting Ste5-3xGFP fluorescence for cells stimulated with either 10nM (A) or 100nM (B). Kymographs depict the membrane-localized GFP signal and are shown as both linear (top) and radial (bottom) plots. C) Kymograph set of membrane-localized GFP for 10nM cell in (A). D) Kymograph set of membrane-localized GFP for 100nM cell in (B).

In order to evaluate the signaling effect of the Ste5 PM-binding mutants, we used a Fus1-GFP reporter to measure mating gene expression in *bar1Δ* cells expressing wild-type or mutant Ste5. Dose responses of each strain resulted in increasing levels of Fus1-GFP as the pheromone concentration increased from 0 to 70nM (Figure 2.1b). $Ste5^{T52L}$ resulted in a higher level of gene expression at all doses, whereas $Ste5^{dn8E}$ resulted in slightly lower levels of gene expression at all doses, relative to wild-type. Interestingly, gene expression reached maximum levels at lower doses for $Ste5^{T52L}$ compared to wild-type Ste5 and $Ste5^{dn8E}$, suggesting that signaling capacity can be regulated by how strong the Ste5 – PM interaction is in the cell.

Previous studies indicate that pheromone signaling and gene expression dynamics depend on the dose of pheromone a cell is exposed to[68,38]. In particular, phosphorylation of Fus3 has been found to undergo oscillatory dynamics in cells treated with high doses of pheromone[38]. At high doses, cells form multiple mating projections over time, indicative of a 'default' mating response. To determine if these periods of high Fus3 phosphorylation (captured from immunoblot experiments) might be caused by the dynamic localization of Ste5 to sequential mating projections, we tracked Ste5-3xGFP at the membrane at different doses of pheromone (Figure 2.2). At all doses, Ste5 localization at the PM was found to precede projection growth. At lower doses of pheromone, near the receptor K_D, Ste5 was found to localize broadly around the membrane. These cells formed single projections that were sustained in time. At higher doses of pheromone, which saturated the receptor, Ste5 was found to localize to the current site of projection growth. Ste5 maintained tight localization to the projection tip while each projection grew, and then completely vacated this site and re-localized to a new projection site as growth of the subsequent projection commenced. These results suggest that dynamic localization of Ste5 to new sites of polarized cell growth may be important for regulating the signaling processes that drive pheromone-induced morphogenesis.

Design and operation of improved microfluidic gradient sensing device

In order to evaluate chemotropic behavior in controlled gradient environments, we designed and validated a microfluidic gradient sensing device that improved upon a device we previously developed[79]. One pitfall of our initial device was that gradient stability and cell seeding uniformity were difficult to control. We improved gradient stability across the cell chambers by merging the side flow channels at both the top and bottom of the flow path (Figure 2.3a,b). Mixing of the two side channels at the top of the flow path is removed by inserting a bypass channel that diverts the mixed fluid layer away from the cell chambers. Simulations with COMSOL (Burlington, MA) predicted this flow architecture to improve gradient stability when pressure imbalances occurred in the flow channels (Figure 2.3c). Addition of cell seeding inlets along the length of the side channels also improved cell seeding uniformity in the cell chambers, which is important for experiment quality.

Wild-type *bar1Δ* cells exposed to a pheromone gradient of 0-60nM developed a range of phenotypes that were noticeable after prolonged exposure (Figure 2.4a). Cells at high concentrations (above ~40nm) formed multiple mating projections and were labeled as 'default' cells. At intermediate concentrations (10-40nM) 'chemotropic' cells formed single, sustained projections that typically aligned with the pheromone gradient. At the lowest concentrations (below 10nM), cells were predominantly 'cell-cycle arrested' and 'budding' cells, based on whether they had stopped or continued to divide. The fraction of cells exhibiting each phenotype was recorded for a range of concentration bins (Figure 2.4b). We found the transitions from 'arrested' to 'chemotropic' phenotypes and 'chemotropic' to 'default' phenotypes to be mostly graded, as indicated by the appearance of multiple phenotypes at doses near these transitions.

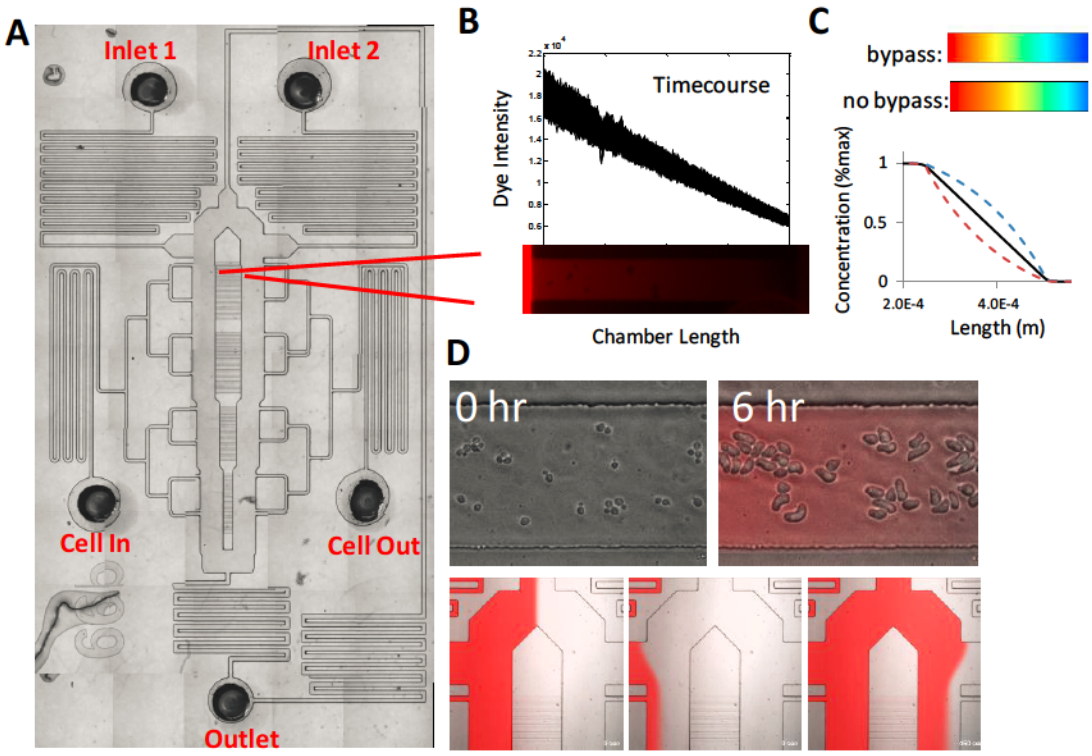

Figure 2.3. Design of microfluidic device for stable gradient generation. A) Overview of device. B) Alexa555 intensity traces of a cross chamber over a 12 hr period. C) Comsol simulation of the diffusion profile caused by a pressure difference on either side of the cell chambers with or without the bipass channel in place D) Cells sensing gradient of pheromone at 0 and 6hrs post-induction (top). Alexa555 traces for gradient, full off, and full on dose delivery modes (bottom).

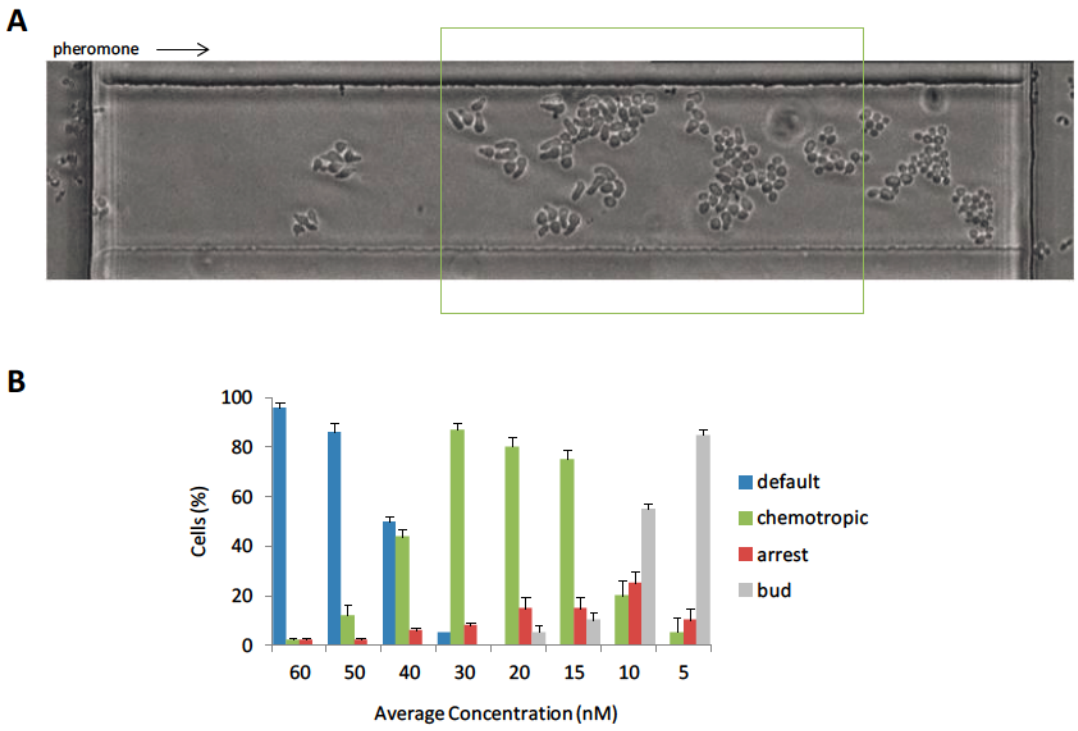

Figure 2.4. Existence of multiple mating phenotypes upon pheromone gradient exposure. A) Representative cell chamber showing cells exposed to a 0-60nM pheromone gradient after 6 hours. B) Percentage of cells exhibiting specific mating phenotypes (default, chemotropic, arrested, budding) for each of the indicated concentration bins.

Effect of modulating Ste5 membrane binding on gradient sensing

In order to assess the effect of Ste5 – PM binding on morphogenic development, we exposed the Ste5 mutants to gradients of pheromone in our microfluidic devices. Remarkably, $Ste5^{T52L}$ cells resulted in projection formation at all doses in the 0-60nM gradient (Figure 2.5). The onset of chemotropic growth and multiple-projection formation each occurred at lower doses compared to wild-type Ste5. In contrast, $Ste5^{dn8E}$ cells behaved similarly to wild-type cells, with morphological transitions occurring at slightly higher pheromone concentrations. Interestingly, the dose range at which chemotropic growth was the predominant phenotype was also the dose range at which gene expression was most highly sensitized for each of the three strains (Figure 2.6b,c). These results indicate that Ste5 PM binding may affect the ability of cells to undergo chemotropic growth by modulating downstream pathway signaling. In order to see if modulating PM binding resulted in changes in projection growth orientation, we quantified the projection angles of chemotropic cells within each concentration bin (Figure 2.6a). We did not find any significant differences in projection orientation for either of the PM binding mutants relative to wild-type cells. Morphological inspection of chemotropic mutant cells also showed similar projection sizes and re-orientation ability as wild-type cells.

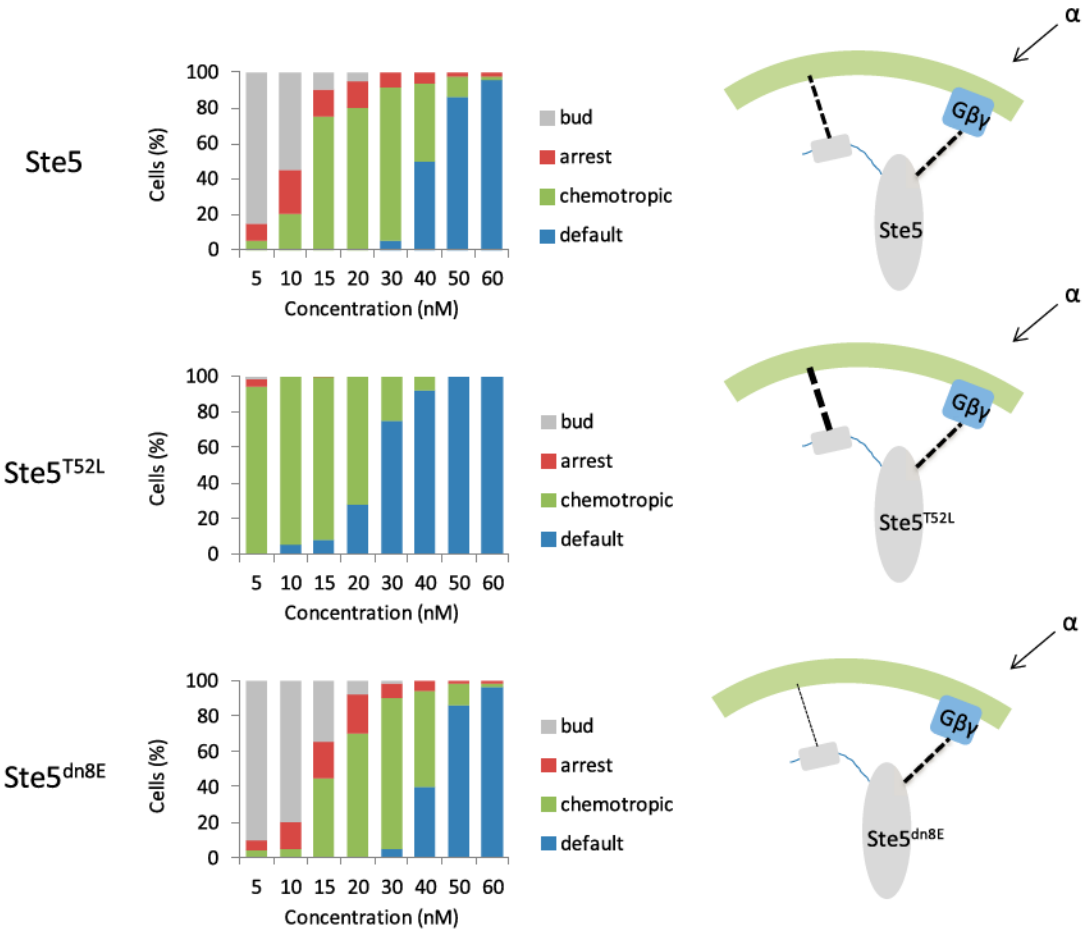

Figure 2.5. Effect of Ste5 PM binding affinity on morphogenic development. Ste5, Ste5^{T52L}, and Ste5^{dn8E} cells (PC67, PC74, and PC75 respectively) were exposed to a 0-60nM pheromone gradient and phenotypes were scored after 6 hours of stimulation. Schematic diagrams of the different scaffold – PM binding interactions are shown at the right.

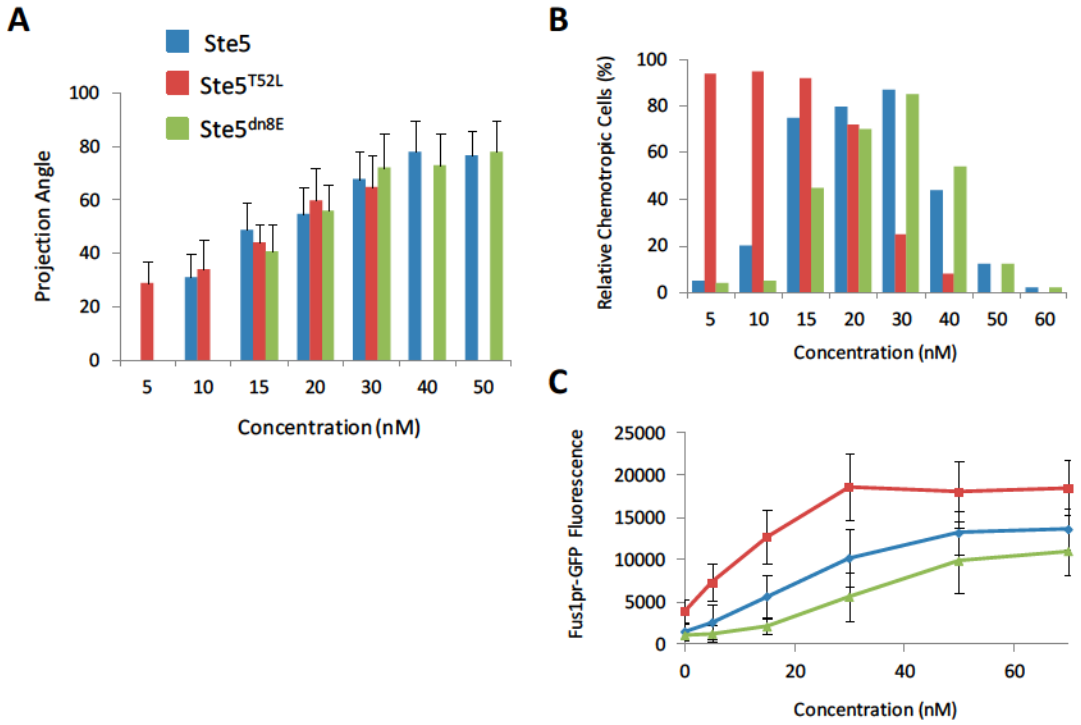

Figure 2.6. Effect of Ste5 PM binding affinity on gradient sensing and chemotropic range. A) Average projection orientations for Ste5, Ste5^{T52L}, and Ste5^{dn8E} cells exhibiting the chemotropic phenotype. B) Relative percentage of chemotropic cells at difference pheromone concentrations for each of the Ste5, Ste5^{T52L}, and Ste5^{dn8E} strains. C) Dose response of gene expression for each fo the strains. Error bars represent SD. Colors are consistent for each graph.

Conclusions

In summary, we found the binding affinity between Ste5 and the plasma membrane to be an important interaction in regulating pathway signaling and morphogenic behavior. We show localization of Ste5 to the membrane to be a highly dynamic and pheromone-dependent process. Localization to the incipient growth site precedes projection growth and is consistent with recent reports showing the requirement of early PIP_2 anisotropy in polarizing Ste5 at the projection tip[99]. Additionally, Ste5's rapid re-localization to subsequent projection tip sites supports its role in driving dynamic Fus3 activation patterns. Furthermore, we designed and utilized an improved microfluidic device to evaluate the chemotropic behavior of Ste5 mutants with altered PM binding affinities. Rather than affecting projection orientation ability, we find PM binding affinity to modulate the onset of chemotropic growth of cells exposed to pheromone gradients. With stronger membrane binding showed leftward shifted chemotropic range that correlated with the range, in which gene expression was sensitive to concentration changes. Similarly, weaker membrane binding showed a slighter rightward shift in the chemotropic phenotype and gene expression sensitivity range. Thus, in addition to the signaling modulation that is controlled by upstream receptor-ligand binding, these results support a role for Ste5's PM binding interaction in modulating pathway signaling. Ensuring an optimal level of Ste5 activity at the membrane, by controlling interaction strength, may have been evolved to maintain long-term alignment of upstream and downstream signaling processes.

Materials and Methods

Yeast strains and plasmids

All yeast strains used in this study are congenic with W303 and prepared using standard genetic and molecular biology methods. Deletion mutants were generated using *natMX4, hphMX4* and *kanMX6* selection marker fragments amplified from pAG25, pAG32[100] and pFA6a-kanMX6[101], respectively, and verified by PCR. To avoid changes in pheromone concentration, all strains were in a *bar1Δ* background and derived from PC51 (MATa *ade2 his3 leu2 trp1 ura3 can1 ste5Δ*::ADE2 *bar1Δ*::natMX4). To create integrated Ste5-3xGFP constructs, integrating plasmids were prepared containing the STE5pr-STE5-3xGFP construct in the p405 plasmid backbone. Linearization of the integrating plasmids at sites inside the Ste5 promoter and subsequent transformation into PC51 resulted in genomic integration of the Ste5-3xGFP chimeras at the endogenous Ste5 gene locus. Single-copy integrants were selected from GFP fluorescence screening of the transformed clones. For example, pPC10 was linearized with XbaI and then transformed into PC51 to make PC67. Similarly, pPC11 and pPC12 were used to make strains PC74 and PC75, respectively. In order to make pPC10 and pPC11, the STE5pr-STE5-3xGFP fragment was digested from pPP1968 and pPP2252, respectively, with SacI/PstI, then ligated into p405. To make pPC09, the 3xGFP fragment was digested from pPP1968 with SpeI/PstI, then ligated into pPP2336. pPC12 was made by cloning the SacI/PstI from pPC09 into p405.

Microfluidic device design and operation

The device was constructed from a single-layer polydimethylsiloxane (PDMS) (Sylgard 184; Dow Corning) molding made using soft lithography[102] and sealed to #1.5 cover glass. The master mold was a silicon wafer with a two-level relief corresponding to the height difference between the flow channels and the cell chambers (5 μm for the cell chambers and 100 μm for the flow chambers). The cell chamber layer was made by spin-coating a 5μm layer of SU-8 2005 photoresist (Microchem, Boston, MA) onto a 4" silicon wafer followed by UV patterning through

a mask. The flow channel layer was made by spin-coating a ~80μm layer of positive photoresist, followed by UV patterning through a second mask. The mold was then used to make a ~5mm thick PDMS cast, which was cut into individual chips. After use the PDMS chips were separated from the cover glass, washed, and recycled.

Cells were seeded into the device through the cell inlet channels that bifurcate into the side flow channel. Once in the flow channel, pressure was elevated dramatically to mobilize cells into the narrow cell chambers. A gradient of pheromone was then delivered by inlets at the top of the device. During each experiment, the gradient stability was monitored at the merge point of the two flow channels by measuring the fluorescence of a dye that is dissolved in the media containing pheromone.

Live-cell microscopy and image analysis

All strains were grown overnight in Synthetic Complete medium with 2% dextrose (SCD) or SCD^{-URA} (for episomally expressed constructs), diluted the next day, and grown to mid-log phase (OD ~ 0.8) just prior to imaging. For GFP localization studies, time-lapses were performed with cells on agarose pads. For chemotropism studies involving spatial gradients of pheromone, experiments were performed using our microfluidic gradient devices. For all experiments involving alpha-factor stimulation, media was supplemented with 20 ug/ml casein (Sigma) to prevent absorption of alpha-factor to vessel walls[18]. Imaging was performed with a Zeiss Axiovert 200M epifluorescence microscope equipped with an automated stage using either a 40x/1.3NA or 100x/1.4NA plan-apo oil immersion objective, where noted. Images were acquired with a 16-bit Cascade 512 camera. Excitation was provided by an Excite Exacte light source (Excelitas Technologies) at 25% power. GFP excitation and emission was passed through a Semrock Dual Band filter set: FF01-468/553-25 (excitor), FF01-512/630-25 (emitter), FF493/574-Di01-25x36 (dichroic). Exposure times were 100ms for the GFP channel. Images were captured using Slidebook 5.5 (Intelligent Imaging Innovations) and subsequently processed

and analyzed using Matlab. For experiments evaluating FUS1pr-GFP fluorescence, cells in each field were segmented by applying an adaptive threshold on the GFP channel image and then aligning fluorescence intensities to these masked cell regions. For Ste5 localization experiments, membrane-localized GFP intensity for individual cells was tracked in time by adapting an image processing routine[103] that segments and tracks cells using the phase-contrast channel. Cells that were out of focus or segmented incorrectly were omitted from analysis. Cell fluorescence values were background-subtracted using a region immediately adjacent to cells.

III. Single-cell dynamics and variability of MAPK activity in yeast

Summary

In response to pheromones, yeast cells activate a MAPK pathway, consisting of Fus3 and Kss1, in order to direct processes important for mating, including gene induction, cell-cycle arrest, and polarized cell growth. While transcriptional reporters and fluorescence-based assays have been able to elucidate signaling activities at multiple steps in the pathway, measurements of MAPK activity in living cells have remained elusive, and our understanding of single-cell signaling behavior is not clear. Here, we applied the mammalian Erk activity reporter, EKAR, to visualize Fus3 and Kss1 activity in live yeast cells. Upon stimulation with pheromone, EKAR-expressing cells showed a robust increase in FRET signal that was specific to both Fus3 and Kss1. We demonstrate that overall mating MAPK activity exhibits rapid reversibility, a graded dose-dependence around the K_D of the receptor, and a biphasic kinetic profile that closely resembles Fus3/Kss1 phosphorylation. Single-cell analysis revealed significant response variability, which closely depended on cell-cycle position and correlated with mating gene expression. Additionally, we find MAPK activity to be sustained at multiple locations in the cell and that spatial gradients of activity develop over time, emanating from mating projections. These findings illustrate new features of MAPK signaling dynamics in a unicellular differentiation system.

Introduction

In response to changes in their environment, cells often undergo phenotypic transitions through the action of mitogen-activated protein kinases (MAPKs). Depending on the external signal present, the temporal and spatial properties of MAPK regulation may prompt cells to proliferate, differentiate, or adapt to different stresses. As a unicellular model, the mating

response in yeast is a slow and carefully orchestrated transition that requires diverse processes to be regulated by the mating MAPK, Fus3. To prepare for fusion with a mating partner, yeast cells must arrest their cell-cycles in G1 phase, polarize their cell growth, re-organize their membranes, and upregulate many genes that are important for maintaining these processes[1–3]. The molecular interactions supporting these activities have been studied in detail, but many questions regarding the dynamics of mating differentiation remain. In particular, how phosphorylation activity manifests itself during the overall mating response will be important in furthering our understanding of MAPK signaling behavior, by effectively filling the void between upstream and downstream signaling events.

The mating response is initiated in haploid yeast cells when G protein-coupled receptors bind to pheromones that the opposite mating partner secretes. Ligand-bound Ste2 receptor (for MATa cells) activates a heterotrimeric G protein, causing GTP-to-GDP exchange on the Gα subunit (Gpa1) and subsequent conformational changes that unmask the Gβγ (Ste4-Ste18) heterodimer[4]. Once free, Gβγ establishes multiple key binding interactions that are required for proper signal transmission. It recruits the Far1-Cdc24 complex, thereby activating Cdc42[5]. It also recruits Ste20, which in turn is activated by Cdc42[6–8]. The third major effector recruited by Gβγ is Ste5[9,10], a scaffold protein for the three MAPK subunits: Ste11, Ste7, and Fus3[11–13]. By virtue of being tethered to Ste5 at the plasma membrane, Ste11 is activated by Ste20[14], thus triggering the MAPK cascade. Serving an integral role for early and long-term pathway modulation[15–18], Ste5's membrane recruitment is also a target of inhibition by G1 cyclins, allowing cells that have surpassed the Start checkpoint in G1 to complete their mitotic cycle before mating[19]. The primary goal of activating the MAPK cascade is to generate dually phosphorylated Fus3, which plays many roles in downstream mating processes. Kss1, the MAPK responsible for invasive growth and a homologue of Fus3, is also phosphorylated upon pheromone stimulation, but is more transient[20] and mating functions largely overlap with Fus3[21–24]. Phosphorylation of Dig1, Dig2, and Ste12 to induce transcription of mating genes is required for mating and a central role of

MAPK function[25–28]. However, for mating to be optimal, additional targets are activated to drive processes as diverse as cell-cycle arrest and morphogenesis. While many of these substrates are known, there are likely many more that have yet to come to light, as phosphoproteomics data would indicate[31,32]. Interestingly, while both MAPKs are enriched in the nucleus and perform their most important functions there, levels of phosphorylated Fus3 appear strikingly low compared to regions outside the nucleus, although the dynamics of this localization have not been established[36,37]. This would be consistent with Fus3's rapid exchange at both the shmoo-tip and nucleus during pheromone stimulation[34], and a potentially different susceptibility to phosphatases in these regions[35–37]. These combined observations support the notion that phosphorylated Fus3 needs to be highly mobile, so that when substrates become present, Fus3 will be able to activate them wherever they are located. Thus, regulation of diverse mating functions may be determined by the strength, location, and timing of MAPK activity in the cell.

To observe mating pathway activity in single cells, a variety of methods have been utilized, including promoter-activity reporters[104,88] and fluorescence-based techniques[37,105]. Despite their utility, direct measurements of MAPK activity have remained elusive. Here, we demonstrate the application of a mammalian Erk reporter to visualize Fus3 and Kss1 activity in live yeast cells. Using this FRET-based reporter in live-cell assays, we are able to draw new insights into MAPK signaling behavior, cell-to-cell response variability, and the spatiotemporal dynamics of substrate phosphorylation during mating morphogenesis.

Results

Reporting Fus3 and Kss1 activity using EKAR

Genetically encoded FRET reporters have emerged as useful tools for visualizing dynamic signaling processes in cells with high temporal and spatial resolution. In particular, the Erk Kinase Activity Reporter (EKAR)[106] and its newer generation versions[107–109] have demonstrated robust Erk activity reporting in a variety of mammalian cell contexts with

sensitivity to distinct physiological stimuli[110–112]. Given the close similarity of the enzyme/substrate interaction motifs between Erk1/2 and their MAPK homologs in yeast (Figure 3.1a), we reasoned that EKAR might also be capable of reporting Fus3 and Kss1 activity during the yeast pheromone response. To test this hypothesis, we expressed a version of the EKAREV construct, EKAR2.3 (referred to as EKAR herein), under control of the strong GPD promoter in yeast and measured the FRET ratio of single cells in response to alpha-factor (Figure 3.2b, c, d). On average, we found a robust increase in the FRET ratio that consisted of a rapid initial increase followed by a slower prolonged increase that reached a maximum level approximately 90 minutes after pheromone stimulation (Figure 3.2c). As controls and to further assess the cause of this ratio increase, we measured the pheromone-induced EKAR response in strains where different components of the MAPK signaling cascade were deleted (Figure 3.2e). In wt cells expressing EKAR with a T/A phosphosite mutation in the substrate domain, there was no increase in FRET ratio after pheromone induction. Similarly in ste7Δ and fus3Δkss1Δ strains expressing intact EKAR, the average FRET ratio did not increase after alpha-factor treatment and remained below pre-treatment levels for the full 3hr time course. These results indicate that both phosphorylation of the substrate domain and the presence of the mating MAPKs are required for EKAR to illicit a pheromone-induced FRET response. In a fus3Δ strain, ratio levels initially increased to a level roughly half that of the wt strain, peaking within the first 15 minutes and then showing a mostly transient response thereafter. Remarkably, the average FRET ratio of kss1Δ cells closely mimicked that of wt cells with a strong initial increase in the first 6 minutes of stimulation, followed by a slower growth phase and then slight decay after 2 hrs. The relative activity responses in the fus3Δ and kss1Δ strains are consistent with Fus3 being the primary MAPK in the mating pathway and with it's doubly phosphorylated form increasing to a greater abundance than the phosphorylated form of Kss1. Additionally, the overall biphasic activity increase reported by EKAR in the wt strain is qualitatively similar to the combined activation of Fus3 and Kss1 based on western blot detection of phosphorylated forms (Figure 3.6). It should be noted, however, that

phosphorylation of Fus3 and Kss1 alone may not fully represent their relative activity in the cell, and that signaling activity is more directly indicated by their engagement with and phosphorylation of substrates. Altogether, these results indicate that EKAR is a reliable single-cell reporter of Fus3 and Kss1 activity in cells exposed to pheromone.

To seek further improvements and insight into the probe's performance, we evaluated the effects of expression and docking domain homology on EKAR's signaling dynamic range. Expression of EKAR from multiple integrated genomic copies (2x, 3x, and 4x copies) resulted in a greater FRET ratio change than expression from a single integrated construct (Figure 3.3). Additionally, due to the fact that EKAR's substrate domain contains a DEF (FXFP) docking site from mammalian Elk1, we wondered how altering the docking site would affect EKAR's signaling properties. Surprisingly, variants of EKAR, in which the surrounding FXFP residues were mutated to match those from Dig1, showed a slight reduction in signaling dynamic range and a concomitant increase in basal FRET signal (without pheromone present) (Figure 3.4). While the precise cause is not clear, this increase in basal FRET signal could be the result of MAPK-specific, nonspecific protein, or clustering interactions that preclude the FRET probe from remaining in a true "off" state. Despite this confounding effect, an EKAR variant with the four FXFP residues changed to alanine showed significant reductions in both basal FRET signal and dynamic range, indicating the importance of the Phe and Pro residues for Fus3/Kss1 docking and probe signaling. Additionally, to assess EKAR's potential to report Hog1 (p38 homolog) activity, we stimulated EKAR expressing cells with osmotic stress conditions and found no increase in FRET ratio (Figure 3.5). These findings further support EKAR's utility as a MAPK activity reporter specific for the mating pathway.

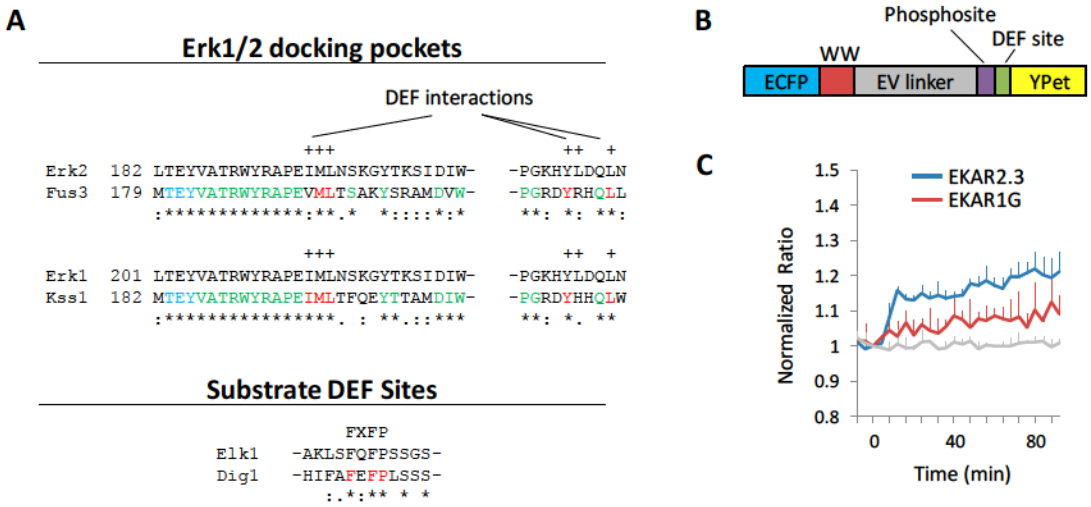

Figure 3.1. Rationalization and validation of EKAR in yeast. A) Pairwise sequence alignments of Erk2 with Fus3 and Erk1 with Kss1 showing regions that directly interact with defined MAPK substrate motifs (phosphosite and DEF motif). Both the P+1 motif and the TXY activation loop (in blue) direct proline specificity for the substrate phosphorylation site (P-X-S/T-P). Residues marked by a '+' sign form a hydrophobic pocket and have been shown to be important for binding the DEF (FXFP) motif on Elk1 (x), conferring an added mode of substrate affinity and specificity. Residues that are conserved in Fus3 and Kss1 are colored with amino acid similarity symbols below. Alignment of the DEF motifs in Elk1 and Dig1 is shown below. B) Schmatic of EKAR2.3 construct, derived from EKAREV. C) Normalized emission ratios of EKAR2.3 and EKAR1G (expressed on plasmids in PC72) after pheromone stimulation. Unstimulated EKAR2.3 construct in gray. Graph shows mean ± SD (n=4 fields of view).

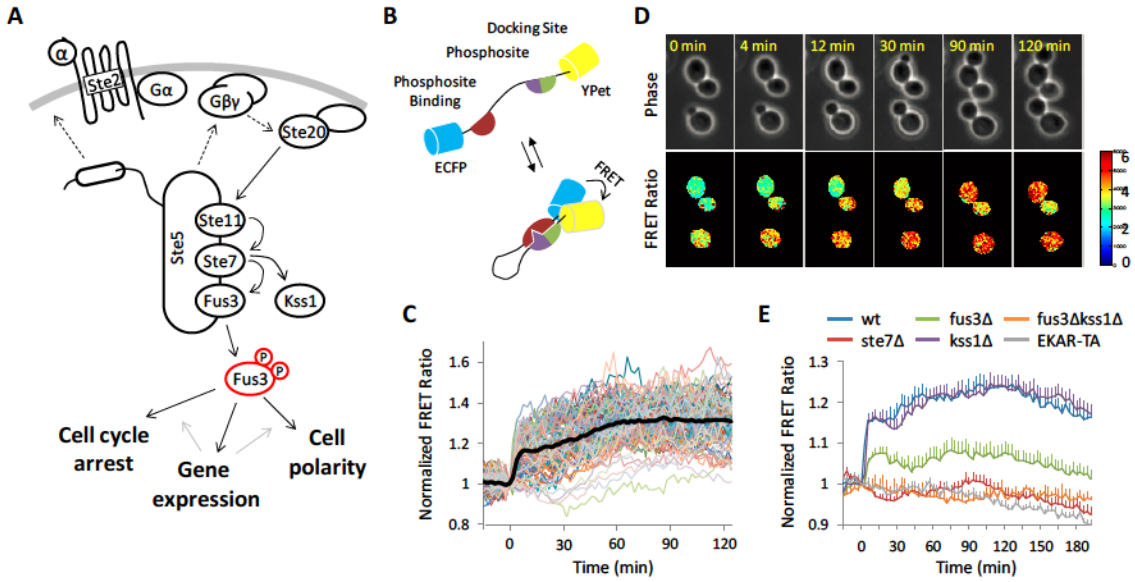

Figure 3.2. Probing Fus3 and Kss1 activity in live yeast cells using EKAR. A) Schematic diagram showing the core signaling components and physiological outputs of the yeast mating pathway. B) Schematic representation of the EKAR FRET biosensor used in this study. C) Asynchrous ells expressing integrated EKAR (PC128) were treated with 10uM alpha-factor and imaged over a 2hr period. FRET ratios of single cells are shown with average response as black line. D) Representative phase-contrast and FRET ratio images of cells from experiment shown in (C). E) Comparison of pheromone-induced responses in wildtype and mutant MAPK deletion strains expressing EKAR, and wildtype strain expressing nonphosphorylatable EKAR-TA. Means and SEMs are shown (wt (PC128): n=30 cells, ste7Δ (PC154): n=43 cells, fus3Δ (PC155): n=33 cells, kss1Δ(PC156): n=42 cells, fus3Δkss1Δ (PC196): n=32 cells, PRAP (PC162): n=40 cells).

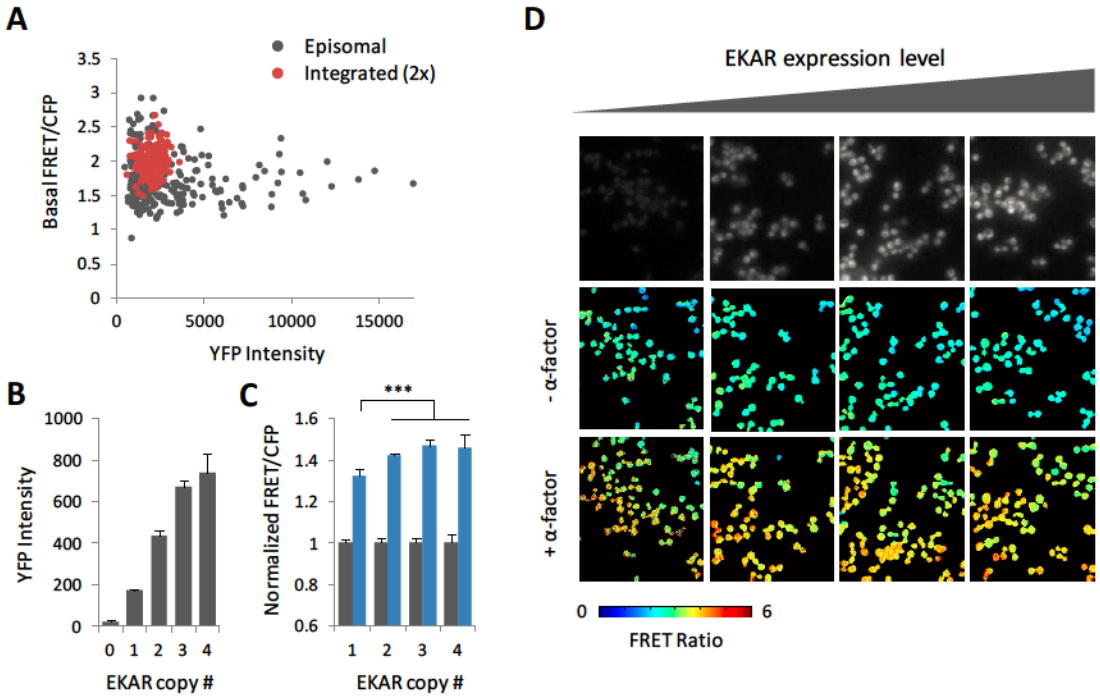

Figure 3.3. Dependence of FRET ratio on EKAR expression level. A) Single-cell FRET ratios plotted against YFP intensity for cells expressing EKAR on a high-copy episomal plasmid (gray) and cells expressing EKAR integrated into the genome. B) YFP intensities for distinct integrated clones of EKAR, and parent strain (0 copy #). Bar graph: mean ± SD (n≥3 fields of view). C) FRET ratios for integrated EKAR clones after 1 hr treatment with 10uM alpha-factor, normalized to average ratios prior to treatment. Bar graph: mean ± SD (n≥4 fields of view). ***P<0.001, one-way ANOVA. Clone 1 compared to clones 2, 3, and 4, collectively. D) Representative images for quantification shown in B and C. Top row: YFP intensity normalized to highest expressing clone. Pseudocolored FRET ratios are shown before (middle row) and after alpha-factor treatment (bottom row) for the same fields of view.

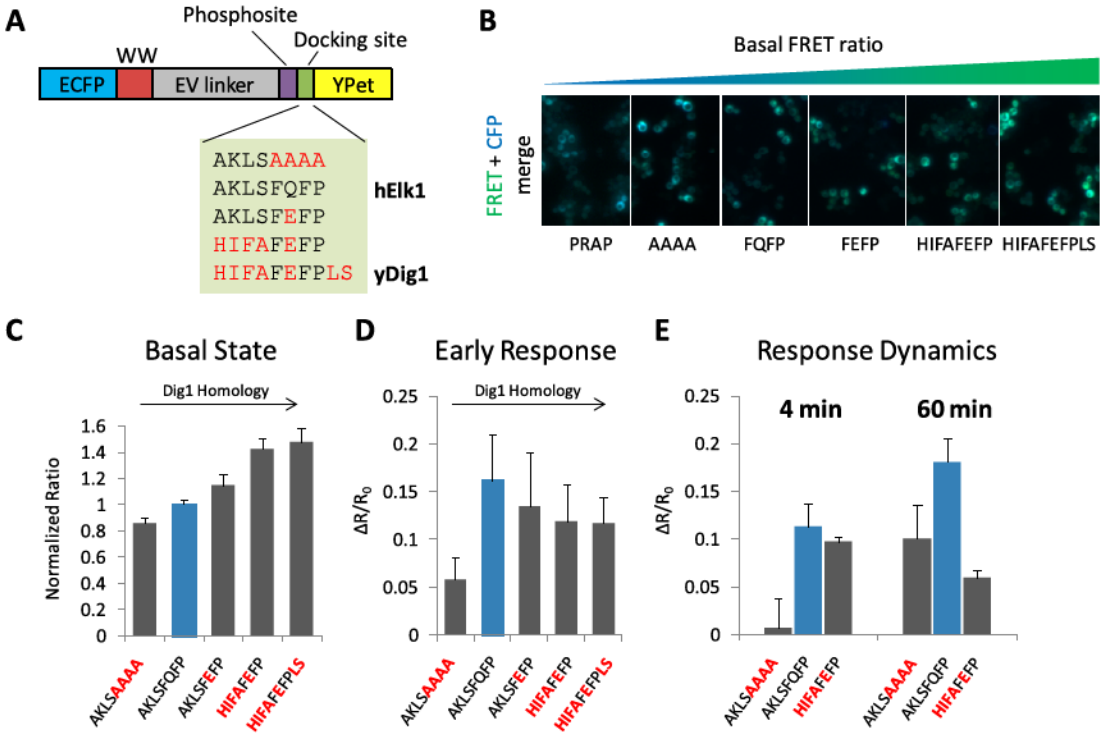

Figure 3.4. Effect of docking site homology on EKAR performance. A) Sequence variants of the DEF site showing increasing homology for the Dig1 DEF. B) Images of basal cells expressing EKAR DEF variants on episomal plasmids. Variants with increasing Dig1 homology show increasing FRET activity in the basal state (FRET channel in green, CFP channel in blue). PRAP shows the lowest FRET activity. C) Quantification of basal FRET ratio and D) ratio change after 6min of alpha-factor stimulation for same DEF variants. E) Ratio change measured at early and late time points after alpha-factor stimulation for selected DEF mutants expressed as integrated (2x) constructs.

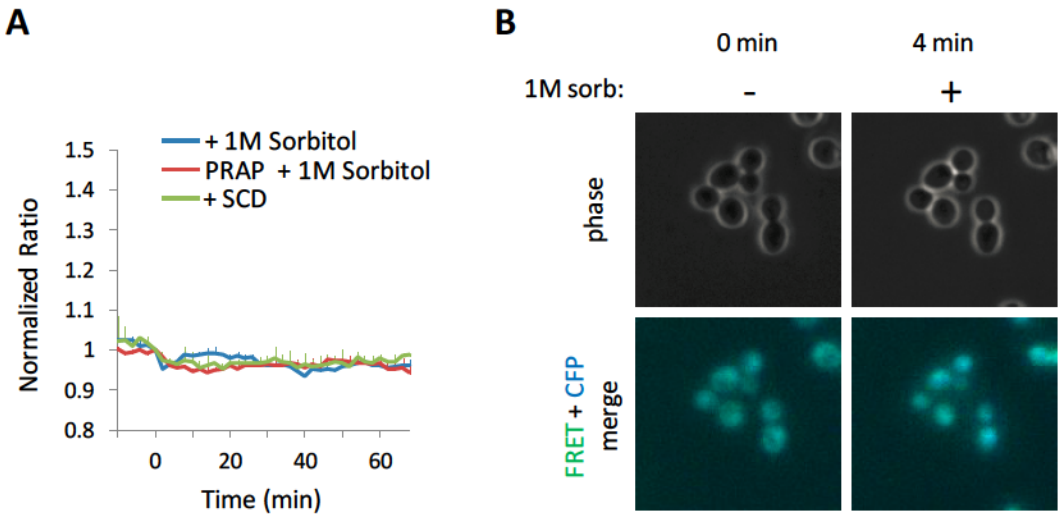

Figure 3.5. Effect of osmotic stress on EKAR response. A) Cells expressing EKAR and nonphosphorylatable EKAR (PRAP) were treated with equal volumes of 1M sorbitol or plain SCD medium. Graph shows mean ± SD (n=4 fields of view). B) Representative phase and FRET+CFP fluorescence images of cells before and after sorbitol addition. Reduction in cell volume following osmolyte challenge is observed in both channels.

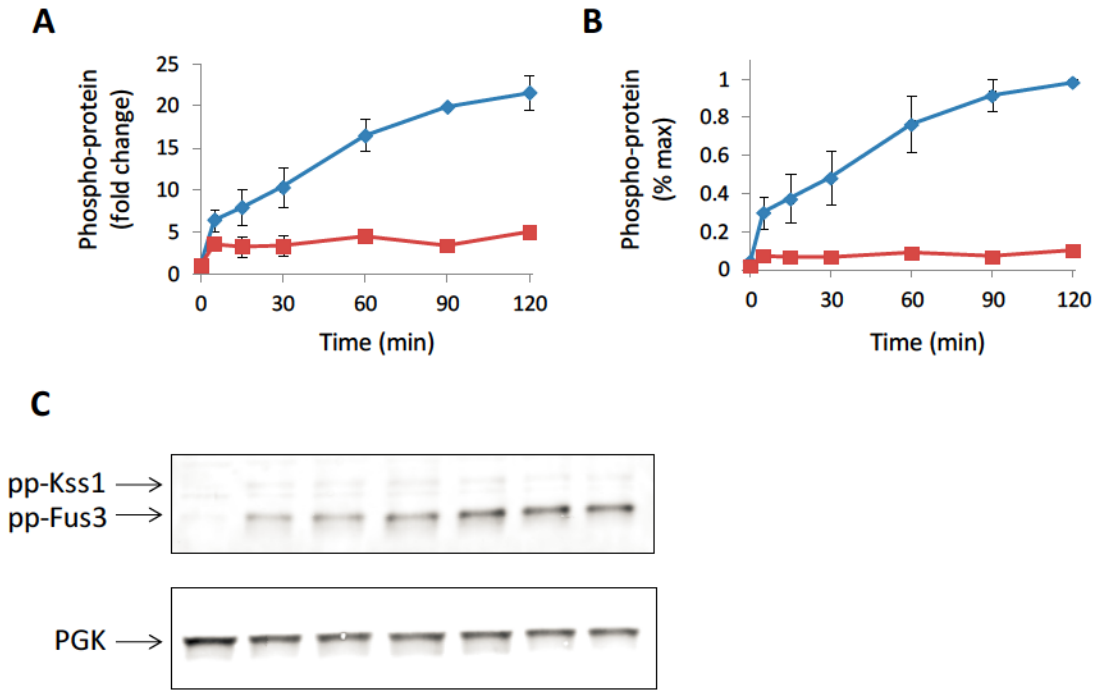

Figure 3.6. Activation of Fus3 and Kss1 in *bar1Δ* cells (PC128) upon exposure to saturating pheromone. A) Fold-change in abundance of phosphorylated Fus3 (blue) and Kss1 (red) at indicated times of pheromone treatment. B) Absolute levels of phospohrylated Fus3 and Kss1, normalized to the maximum phopho-Fus3 abundance. C) Representative blots for anti-phospho-p44/42 and anti-PGK showing respective protein bands. Error bars represent SEM (n=3).

Dose dependence of MAPK activity

The sensitivity of pathway activity to varying pheromone conditions has been widely examined[18,104,88,113,114,43]. To capture the dose dependence of Fus3/Kss1 activity using EKAR as a proxy for substrate phosphorylation, we measured the FRET response of single cells exposed to a range of pheromone concentrations. With the pheromone protease Bar1 deleted, Fus3/Kss1 activity increased incrementally from 0nM to 20nM of pheromone reaching near maximum activity levels at the 20nM dose (Figure 3.7a). During the first 90 minutes of stimulation, activity was noticeably more transient for the 4nM dose compared to the more sustained responses at 8nM and higher, indicating that MAPK activity levels are largely modulated by changes in receptor occupancy (receptor $K_D \sim 6nM$[115]). We found the dose response of MAPK activity to be mostly graded in the 30min to 2hr treatment window. This alignment of activity and upstream signal strength is consistent with previous reports of pathway sensitivity using MAPK phosphorylation and transcriptional induction[18,104,114,68]. Timelapse observation of morphological states in this pheromone range showed transitions from budding cells to enlarged, cell-cycle arrested morphologies and elongated, projection-forming cells at higher concentrations (Figure 3.7b), behavior that is consistent with previous reports[88,79,61]. To assess the effective reversibility of the pheromone-induced MAPK response, we replaced the endogenous Fus3 gene with an inhibitor-sensitive allele in an EKAR-expressing kss1Δ strain and examined the effect of direct Fus3 inhibition on its substrate phosphorylation activity (Figure 3.7c). Upon catalytic inhibition of Fus3, activity decreased precipitously (basal level reached within 15 min), indicating that substrates are dephosphorylated rapidly when Fus3 is not able to phosphorylate them. Additionally, we exposed EKAR-expressing wild-type cells to consecutive periods of pheromone, plain media, and pheromone (Figure 3.7d). Upon removal of pheromone, MAPK activity quickly decreased, returning to basal levels in 15 minutes. Restimulating the cells with an equal dose of pheromone produced a response similar to the first exposure. These results indicate that for cells to recover from cell-cycle arrest and other mating activities, both Fus3/Kss1 and their

downstream substrates are quickly dephosphorylated, thus permitting the mating pathway machinery to reset and be properly utilized in future mating attempts.

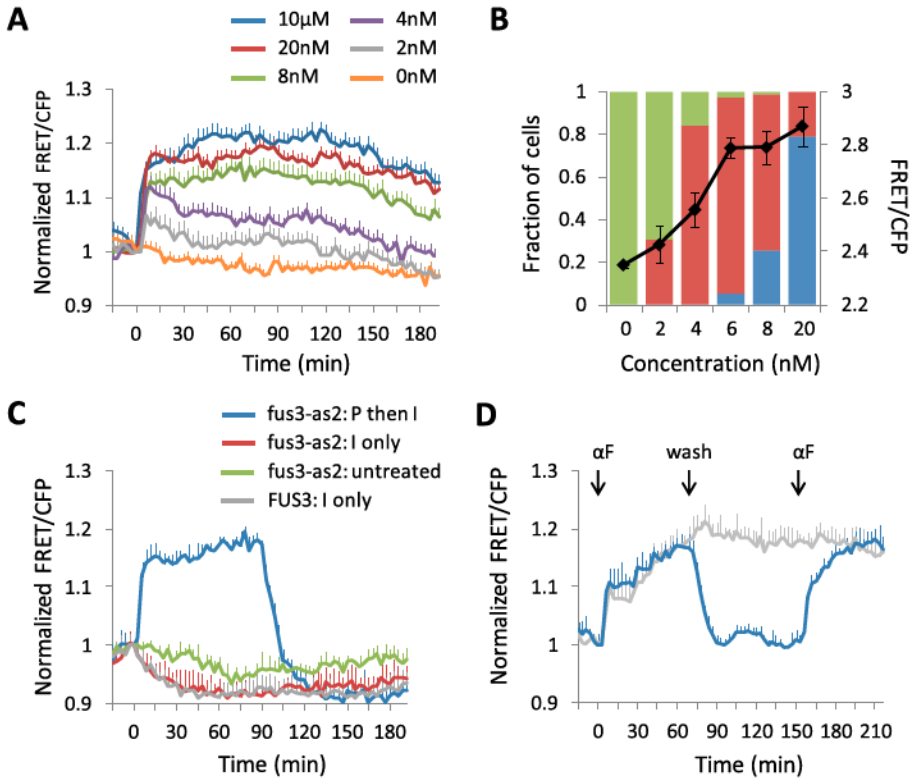

Figure 3.7. Dose sensitivity and reversibility of Fus3/Kss1 activity during pheromone response. A) Wildtype cells expressing EKAR (PC158) were stimulated with the indicated doses of alpha-factor (colored lines) and FRET/CFP levels were measured for single cells. Means and SEM are plotted (10μM: n=41, 20nM: n=40, 8nM: n=38, 4nM: n=25, 2nM: n=31, 0nM: n=35 cells). B) Fraction of wildtype cells (PC128) exhibiting specific phenotype after 3.5 hrs pheromone exposure. Colors represent cells which continued to bud (green), arrested cells which remained round (red), and cells that formed mating projections (blue). Average EKAR response measured at 2 hrs is overlayed as black line (Mean ± SD, n=4 fields of view for each condition). C) Pheromone-induced substrate phosphorylation depends on Fus3 activity. FRET responses for fus3Δkss1Δ cells expressing an inhibitor-sensitive allele of Fus3 (fus3-as2) (PC199) were monitored after treatment with 10μM alpha-factor and subsequent treatment with 10μM NM-PP1 after 87 minutes (blue line). For comparison, the same cells (red line) and kss1Δ cells expressing wildtype Fus3 (PC156, gray line) were treated with 10μM NM-PP1 alone. Green line shows cells with no treatment. Means and SD are plotted (n = 4 fields of view for each condition). D) Wildtype cells (PC128) were either treated with 200nM alpha-factor (gray line) or treated, washed 4x, and re-treated with 200nM alpha-factor (blue line) at the indicated times. Experiments were in multi-well dish format. Means and SDs are plotted (n≥4 fields of view for each experiment).

Cell-cycle dependence of MAPK activity in single cells

As in many cell differentiation systems, the timing for executing processes in response to external signals is often controlled by internal checkpoints in the cell which help to prevent signaling interferences and ensure a single, successful cell fate. In yeast, the execution of mating processes has been observed to be coordinated with cell-division status, as pheromone is only capable of arresting cells in the G1 phase of the cell cycle[104,116–119]. Cells past the Start checkpoint in G1 will complete a new cell cycle before arresting and responding to pheromone. Specifically, the inhibition of mating pathway signaling in post-Start cells has been shown to be mediated by G1 CDK targeting of the scaffold protein, Ste5, which when phosphorylated, is unable to localize to the membrane and activate the MAPK cascade[19]. Consistent with these findings, we observed a striking difference in EKAR responses among cells that promptly formed projections versus cells that budded following pheromone exposure (Figure 3.8a, b). In cells that proceeded to form projections (pre-Start cells, approximately 65% of all cells), the increase in MAPK activity was rapid and typically sustained throughout the course of mating morphogenesis (Figure 3.8c, d). In cells that proceeded to divide and bud (post-Start cells, approximately 25% of all cells), the increase in MAPK activation was significantly more delayed and often followed an initial, short-lived spike in activity. The increase in activity was found to be sustained only after bud emergence and the rate of increase was slower than for pre-Start cells. Upon closer examination of the budding stage, we also noticed the increase in MAPK activity to be less delayed in cells which had begun the budding process just prior to pheromone exposure (early-S cells). The time required to reach half maximum response ($t_{1/2}$) was 6.4 ± 4.2min, 48.7 ± 12.2min, and 34.8 ± 10min for pre-Start, post-Start, and early-S cells, respectively. Despite differences in the rates of activation, cell-cycle state did not have an effect on the eventual, steady-state activity level as cells exposed to pheromone ultimately committed to the mating phenotype. These results show that sustained MAPK activity coincides with the cell's commitment to freely undergo mating

morphogenesis and supports the upstream G1 CDK regulation of Ste5 in modulating MAPK activity.

The cell-to-cell variability of mating gene expression has been previously explored with significant sources of variability stemming from differences in both cell-cycle position and gene expression capacity[104]. Given that MAPK phosphorylation is the primary stimulus of Ste12-mediated gene induction, we were interested in exploring the correlation between MAPK activity and the downstream transcriptional response within the same cells. Cells co-expressing EKAR and P_{FUS1}-mCherry reporters were treated with pheromone and responses of each reporter were measured over time (Figure 3.9a). Because we assumed the strength of the transcriptional response should reflect aspects of both time and amplitude of the stimulus, we used the time-integrated EKAR signal as our metric. After 3.5 hrs of treatment, the final mCherry fluorescence and the integrated EKAR response were found to correlate over a range of EKAR integration times, with an optimal correlation observed from the first 70 minutes of EKAR signaling (Figure 3.9b). This time period spans the range where variation in cell-to-cell EKAR signal was maximal, in large part due to differences in cell-cycle position. Cells past Start exhibited low reporter responses, whereas both responses were higher for pre-Start cells. Despite this correspondence, there are likely separate factors influencing each of the MAPK signaling and gene expression subsystems, which are working independently of the cell-cycle.

In addition to the effect of cell-cycle on MAPK response variability, we also noticed a strong response similarity between successive generations of cells, consistent with the observed heritability of gene expression responses, which has recently been reported[120]. Responses of mother and newborn daughter cell pairs were highly symmetric when the cell-cycle phases of both cells were pre-Start at the time of pheromone treatment (Figure 3.9c). This symmetry was diminished when the cell-cycle phase of the mother had exceeded Start, due to the overall reduction in time-integrated EKAR signal for post-Start stimulated cells (Figure 3.9d, e). These results indicate that the preservation of signaling capacity across cell generations occurs at the

level of MAPK-substrate phosphorylation, which in turn may be due to the preserved stoichiometries of pathway components during cell division.

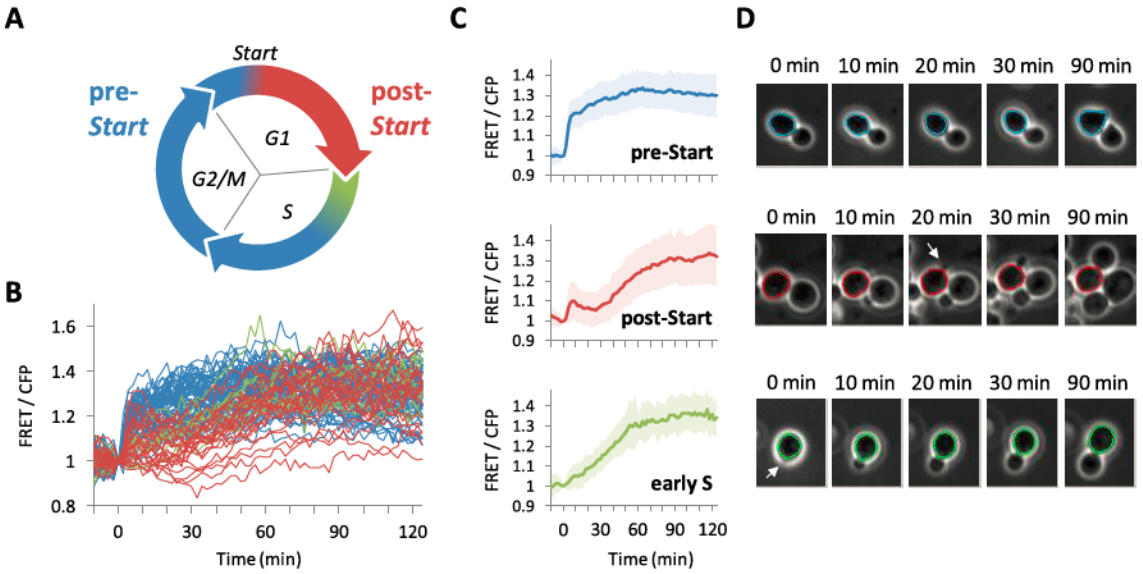

Figure 3.8. Cell-cycle dependence of Fus3/Kss1 activation in single cells. A) Diagram of cell cycle with color corresponding to cell cycle position at the time of pheromone treatment (pre-Start, post-Start, or early-S). Upon pheromone induction, pre-Start cells arrest their cell-cycle and eventually form mating projections, whereas post-Start cells undergo one more cycle of budding before arresting their cell cycle and forming a projection. Cells initiating bud emergence within a 10 minute window prior to pheromone stimulation were classified as 'early S' cells. B) Fus3/Kss1 activity in single cells. FRET ratio responses measured in pre-Start (blue), post-Start (red), and early S (green) cells after 10uM alpha-factor treatment. C) Average response for cells in each cell-cycle position group: pre-Start (top), post-Start (middle), and early-S (bottom). SD is shown as shaded region (pre-Start: n= 51, post-Start: n=25 cells, early-S: n=10 cells). D) Images of example cells in each cell-cycle group with indicated times after stimulation. Arrows indicate visualization of bud emergence (for post-Start and early-S cells). Example activity profiles for individual cells are shown in Fig S5.

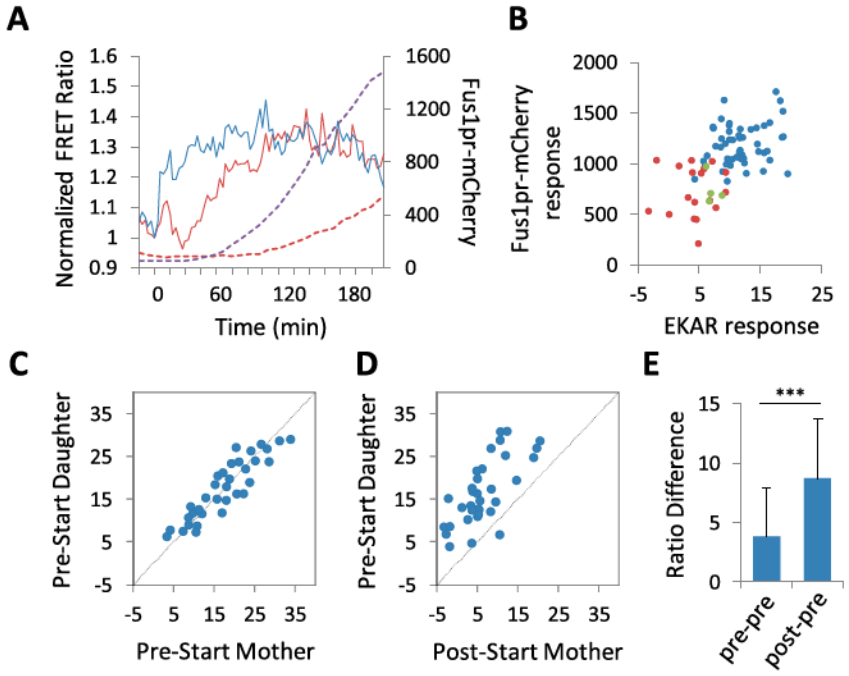

Figure 3.9. Single-cell variability of gene expression and MAPK activity reporter responses. A) and B) Correlation of transcriptional and MAPK activity responses in single cells. A) Example pre-Start (blue) and post-Start (red) cell with FRET ratio (solid line) and Fus1pr-mCherry fluorescence (dashed line) time-course after 10uM alpha-factor treatment. B) Scatter plot of Fus1pr-mCherry fluorescence at 3.5 hrs (gene expression response) and the time-integrated FRET ratio after 70 min (Fus3/Kss1 activity response) in single cells exposed to 10uM alpha-factor. Color indicates initial cell cycle phase at time of treatment (pre-Start: blue, post-Start: red, early-S: green). C), D), and E) One-hour EKAR responses measured after 10uM alpha-factor treatment in the following cell pairings: pre-start mothers and newborn pre-start daughters (C), post-start mothers and newborn pre-start daughters (D), and random pre-start cells paired together (E) (data combined from three independent experiments).

Spatiotemporal probing of mating MAPK activity

Pheromone treatment results in a rapid uptick of cellular MAPK activity that is maintained over the course of the mating response. This sustained activity implies that there is a constant need for Fus3 and Kss1 to phosphorylate substrates in their proper spatial and temporal contexts[22,68,33]. Additionally, the free mobility of Fus3 between the nucleus and plasma membrane has been shown to be important for full activation of the mating machinery[36]. Due to the importance of Fus3 and Kss1 being able to engage their substrates and regulators in multiple cellular compartments, we were interested in exploring the subcellular dynamics of MAPK activity in wild type cells exposed to pheromone. To visualize Fus3/Kss1 activity at different subcellular locations, we prepared strains with EKAR fused to targeting peptides specific for the cytosol (EKAR-cyt), nucleus (EKAR-nuc), and plasma membrane (EKAR-pm). Upon pheromone treatment, Fus3/Kss1 activity in all three compartments increased rapidly, exceeding 40% maximum activity within the first 10 minutes (Figure 3.10a). Both the cytosolic and nuclear responses were sustained and steadily increased beyond the initial spike. Interestingly, the overall nuclear response was reduced compared to the cytosolic response, even though the concentrations of both Fus3 and NLS-EKAR are higher in the nucleus. These results are consistent with the notion that phosphorylation of Fus3 in the nucleus is more transient due to a greater susceptibility to deactivating phosphatases in this compartment[36,121].

While it is known that Fus3 becomes localized and enriched at multiple cellular compartments upon pheromone exposure, it is less clear how its activity emerges and is utilized during the morphological changes that take place. To visualize the spatial patterns of Fus3/Kss1 activity, we exposed EKAR-expressing cells to gradients of pheromone in our microfluidic devices and measured cell responses over a 7-8hr period. For doses in the 5-60nM range, we found that as cells formed mating projections, gradients of Fus3/Kss1 activity emerged from the projection tips and would typically persist through most of the projection growth cycle (Figure 3.10b, c, e, f, S10). Cells exposed to 60nM doses showed higher overall activity and steeper front-

to-back (shmoo to distal end) distributions of activity compared to cells exposed to doses near the K_D of the receptor, where mating projections tracked the direction of the pheromone gradient (Figure 3.10d, Figure 3.11a). The fractional difference in activity between the front and back cell regions was approximately 2-fold higher for 60nM exposure (0.22 ± 0.12) compared to 10nM exposure (0.11 ± 0.06). Similar front-to-back activity patterns were also observed in secondary projections that formed at higher pheromone exposures. As a control, cells expressing the EKAR-TA mutant did not reveal any consistent patterns of activity (Figure 3.11a, b). Interestingly, projection-localized activity patterns were generally found to strengthen over time as mating projections grew, consistent with an increasing expression of Fus3 and the localization of its substrates/regulators to the projection tip (Figure 3.12). Back-to-front activity gradients, stemming from pockets of high activity at the distal end of the cell, were also observed, but were weaker and occurred less frequently than front-to-back gradients for both concentration ranges tested (Figure 3.11b). Altogether, these results indicate that MAPK activity is predominantly localized at the mating projection in a graded fashion and that spatial activity patterns develop over time as projection growth ensues.

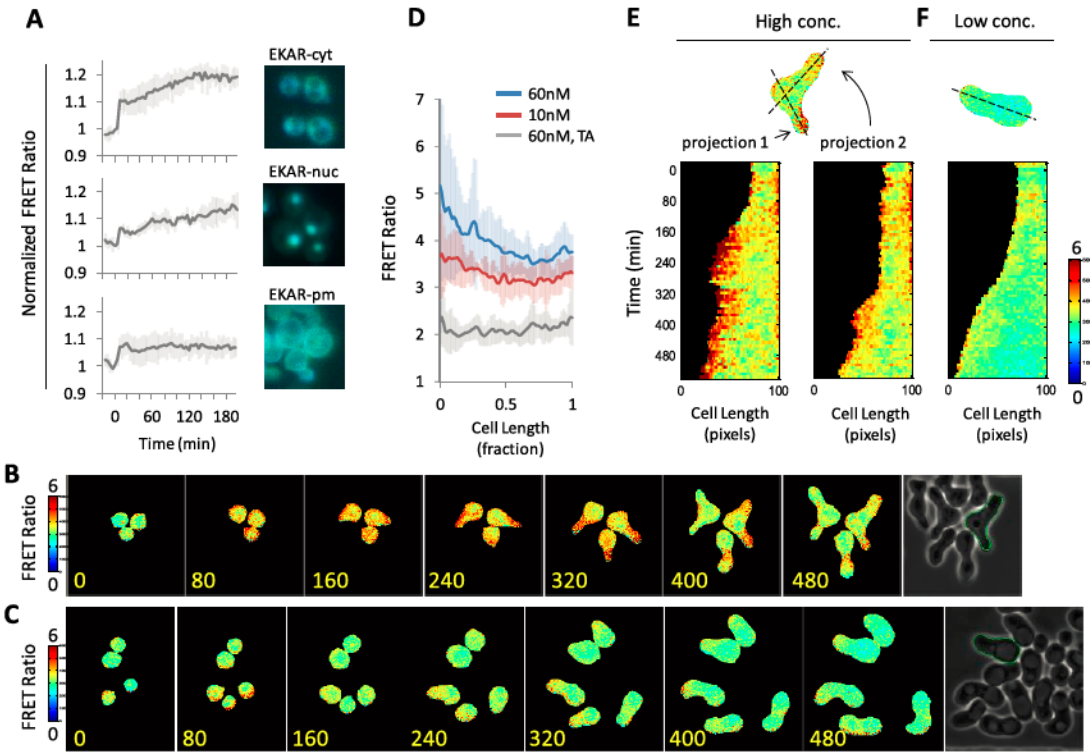

Figure 3.10. Spatiotepmoral dynamics of Fus3/Kss1 activity using EKAR. A) Probing pheromone-induced Fus3/Kss1 activity in different cellular compartments using integrated chimeras of EKAR genetically targeted to the cytoplasm (EKAR-NES), nucleus (NLS-EKAR), and the plasma-membrane (EKAR-CaaX). Left: Normalized FRET ratio time-course for each strain after 10uM alpha-factor treatment. Means and SD are shown ($n \geq 5$ fields of view for each strain). Right: Representative images of PC128, PC164, and PC152 cells showing fluorescence overlay of FRET (green) and CFP (blue) channels. B) and C) PC128 cells exposed to a 0-80nM gradient of alpha-factor in our microfluidic device. Representative FRET ratio images at 80min intervals showing cells exposed to concentrations in the 55-65nM range (B) and in the 5-15nM range (C), resulting in multiple-projection and single-projection morphologies, respectively. Pheromone is diffusing from left to right. Phase-contrast image (used for cell segmentation) of last time point is shown at right. D) Average distribution of MAPK activity in cells after development of the mating projection. The average FRET ratio measured across the length of the cell, from the projection tip to the back of the cell, for EKAR-expressing cells in the 60nM range (blue, n=24 cells), 10nM range (red, n=13 cells), and EKAR-TA-expressing cells (control) in the 60nM range (gray, n=11 cells). Distrubition was measured at 3.5 hrs for cells in the 60nM range and 4.5 hrs for cells in the 10nM range, since projection formation takes longer for these cells. Ratio data was normalized to a fractional length scale. E and F) FRET ratio kymographs for example cells outlined in the phase images in B and C, respectively. E) Ratio kymographs were generated using a line through the center of the cell along the axis of each projection (from projection tip to back of cell). F) Ratio kymograph of single-projection in a gradient-tracking cell.

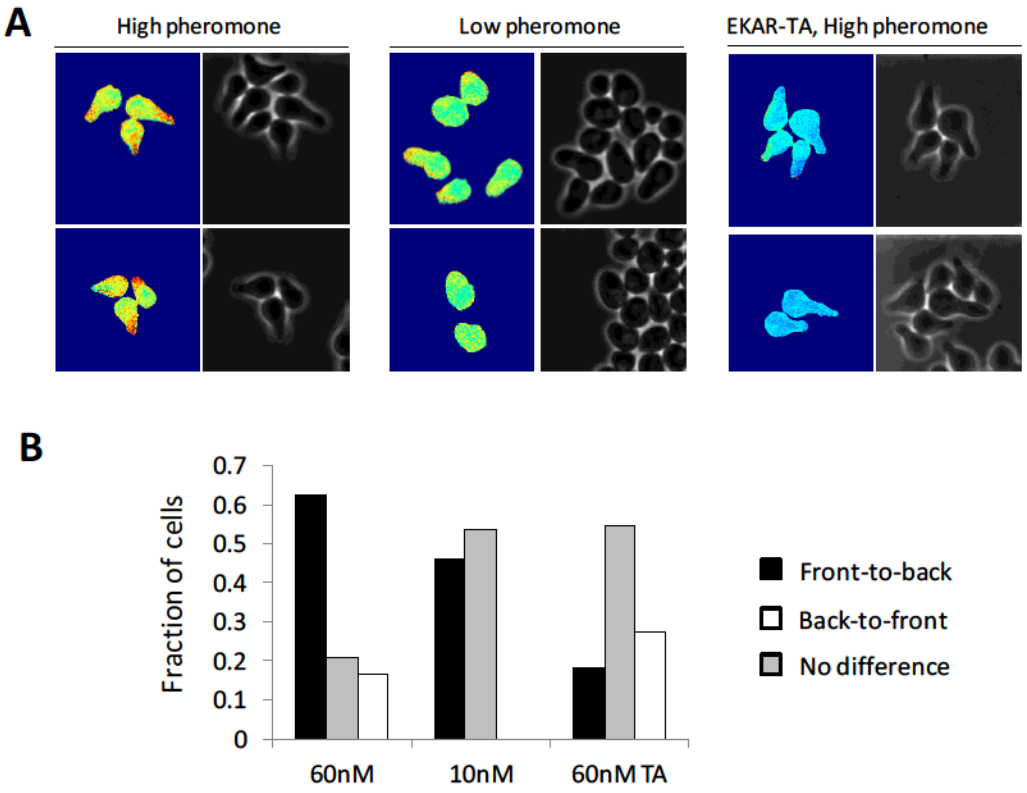

Figure 3.11. Distributions of MAPK activity gradients at high and low pheromone conditions. A) Visualization of MAPK activity during pheromone-induced morphogenesis. Representative FRET ratio and phase-contrast images shown for EKAR-expressing cells exposed to A) 60nM pheromone for 3.5 hrs and B) 10nM pheromone for 4.5 hrs, and C) EKAR-TA-expressing cells (control) exposed to 60nM pheromone for 3.5 hrs. B) Fractions of EKAR expressing cells (PC128) exhibiting distinct FRET ratio profiles after 3.5 hrs (for 60nM average) and 4.5 hrs (for 10nM average) exposure to an external pheromone gradient. As a control, the frequency of ratio profiles for EKAR-TA expressing cells (PC162) are also shown. For each cell activity profiles were measured from the average of 3 pixel-wide line distributions, measured from the projection tip to the distal end of the cell. Classification as a front-to-back (black) or back-to-front gradient (white) was by a comparison of the 20% front-most and 20% back-most pixel averages on either side of the cell, which resulted in a p-value < 0.01 (Student's T-test). Front-to-back activity differences that were not significant ($p > 0.01$) were classified as flat gradients (gray).

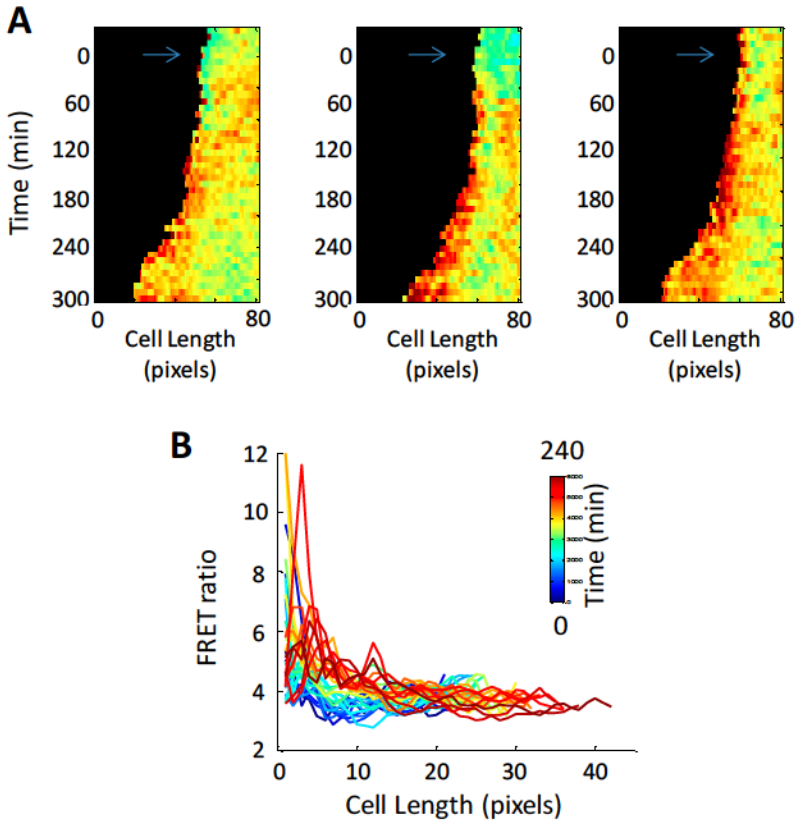

Figure 3.12. Development of intracellular Fus3/Kss1 activity gradients in single cells. A) Kymographs showing EKAR activity along the mating projection axes. Three representative cells (PC128) stimulated with a 60nM dose of pheromone are shown. Arrows indicate pheromone stimulation time. B) Distributions of EKAR activity with increasing time for an example cell stimulated with 60nM pheromone. EKAR activity is represented as the 3-pixel wide average FRET ratio along the mating projection axis from front-to-back.

Discussion

Many cell differentiation systems utilize MAP kinase signaling to help convert information in the cell's environment to actionable internal stimuli that can direct multiple processes inside the cell. In mammalian systems, distinct temporal and spatial patterns of Erk activity have proven to be important for cell-fate decisions pertaining to proliferation and differentiation in a variety of cell and stimulus-dependent contexts[111,112,122–125]. In yeast, signaling through the MAP kinases, Fus3 and Kss1, is required to initiate and perpetuate the activities important for mating. Both the timing and location of their signaling activities is thought to be important for ensuring that non-mating signaling processes are not interfered with or invoked, and that the appropriate substrates are phosphorylated when and where they need to be. Specifically, it has been suggested that the purpose of a slower rate of Fus3 phosphorylation is to keep the pathway 'on' for an extended period of time and thus prevent downstream mating responses from becoming saturated too soon[68]. It has also been observed that constitutive localization of Fus3 at either the plasma membrane or nucleus causes mating defects, further emphasizing the integral role of Fus3 at multiple locations in the cell[36]. Despite an extensive characterization of the mating pathway to date, the dynamics of MAPK activity in cells responding to pheromone have remained elusive. To capture these dynamics and address questions relating to cell-to-cell variability and spatial regulation of MAPK signaling, we applied the FRET-based mammalian Erk activity reporter, EKAR, to the live-cell imaging of yeast.

While FRET-based protein activity reporters have been instrumental in elucidating dynamic signaling behaviors in mammalian systems, their utilization in yeast and other simpler eukaryotes has been underappreciated. In this work, we leveraged the high homology of Erk1-Kss1, Erk2-Fus3, and their cognate substrate docking sites in the application of EKAR to visualize MAPK activity in live yeast cells. First, we demonstrate that EKAR can be used to detect pheromone-induced Fus3 and Kss1 activity in single cells with high specificity and signaling dynamic range. We show that overall mating MAPK activity exhibits rapid

reversibility, a graded dose-dependence around the K_D of the receptor, and a biphasic kinetic profile that closely resembles Fus3/Kss1 phosphorylation. These results support Fus3/Kss1's role as a cellular on/off stimulus for mating pathway activities that are naturally slow to develop, but may also need to be turned off quickly for cells to survive a failed mating attempt. Second, we find the dynamics of MAPK activity in single cells to be cell-cycle dependent and correlated with mating gene expression. Cells prior to Start undergo distinctly faster and more sustained early activation than cells that have already committed to or have just begun a new budding cycle. This behavior indicates that a sustained MAPK response may be counterproductive to early cell-cycle events, possibly from a combination of polarity establishment, cell-cycle arrest, and gene expression activity that may interfere with normal budding progression. This is also consistent with observations that pheromone-stimulated post-Start cells expressing a Ste5-8A allele, which is resistant to cell-cycle modulation, undergo an aberrant arrest state characterized by 2N DNA, incomplete cytokinesis, and coexpression of mating and cell-cycle gene reporters[19,126]. We further show that cell-cycle phase is important for the MAPK response symmetry observed between mother and newborn daughter cells. Finally, we explored the spatial patterns of Fus3/Kss1 activity that arise during a cell's response to pheromone. Given that phosphorylation of Fus3 and the Ste5-Fus3 interaction itself have been observed to have graded distributions at the shmoo-tip[37,105], we reasoned this could also translate into gradients of MAPK activity emanating from the mating projections. Indeed, using EKAR, we observed predominantly front-to-back gradients of Fus3/Kss1 activity in cells at both high and low pheromone doses, relative to the K_D of the receptor. Whereas overall cellular activity was high and largely nonpolarized prior to projection growth, gradients emerged just after projections became visible and strengthened over time. This indicates that continued phosphorylation activity at projection growth sites may be important for engaging morphological and cell fusion effectors, especially at later time points. Additionally, reduced levels of nuclear-localized activity, compared to the cytoplasm, may be important for

keeping the transcriptional response and pathway feedbacks in check so that the overall mating response runs optimally and is sustainable over time.

In summary, the findings presented here reveal that signaling through the mating MAPKs is highly dynamic in nature. Spatiotemporal control of MAPK activity has profound consequences in cell development, affecting both when and how different cell states emerge. Characterization of single-cell signaling dynamics through the use of substrate-based reporters will provide unique opportunities to compare and contrast signaling behaviors in complex mammalian systems with those of simpler, genetically tractable eukaryotes.

Materials and Methods

Yeast Strains and Plasmids

All yeast strains used in this study (Table S1) are congenic with W303 and prepared using standard genetic and molecular biology methods. Deletion mutants were generated using *natMX4, hphMX4* and *kanMX6* selection marker fragments amplified from pAG25, pAG32[100] and pFA6a-kanMX6[101], respectively, and verified by PCR. To avoid changes in pheromone concentration, all reporter constructs were expressed in the *bar1Δ* background and derived from PC72. To create integrated reporter constructs of EKAR, integrating plasmids were prepared containing the EKAR2.3 construct under control of the high-expression GPD promoter. EKAR2.3 (referred to as EKAR herein) is similar to EKAREV[107] except that the positions of ECFP and YPet are switched (ECFP is N-terminal and YPet is C-terminal) and a C-terminal nuclear export sequence is absent (the untargeted construct localizes to both the nucleus and cytoplasm). Linearization of the integrating plasmids at sites inside the selection marker genes and subsequent transformation into PC72 resulted in genomic integration of the P_{GPD}-EKAR constructs at the endogenous marker gene locus. The number of plasmid integrations was assessed by microscope-based fluorescence screening of transformed clones. For example, pPC48 was digested with StuI and integrated at the *ura3* locus to create PC126 and PC128 with 1 and 2 copies of P_{GPD}-EKAR

integrated, respectively. PC167, PC195, PC162, PC149, PC165, and PC152 were created in a similar fashion by StuI linearization and transformation of the plasmids pPC62, pPC63, pPC64, pPC57, pPC60, and pPC58, respectively. To evaluate the effect of higher EKAR expression levels on the performance of the reporter, PC128 was transformed with Bsu36I-linearized pPC49 to create PC158. PC158 was transformed with NheI-linearized pPC50 to create PC163. Due to an altered projection growth behavior and a noticeable degree of toxicity observed with the NLS-EKAR construct when expressed at high levels, the weaker ADH1 promoter was used for dynamics studies with this nuclear-localized reporter. The mCherry transcriptional reporter plasmid pPC61 was linearized with SwaI and integrated at the endogenous Fus1 promoter locus of PC128 to create the dual activity/transcriptional reporter strain, PC159.

All plasmids used in this study (Table S2) were constructed using standard recombinant DNA methods and propagated in *E. coli* strain DH5α. The plasmids pRS426-GPD, pRS406-GPD, pRS404-GPD, and pRS403-GPD were constructed by cloning the GPD promoter fragment from p416GPD (ATCC 87360) as a SacI-SpeI fragment into pRS426, pRS406, pRS404, and pRS403, respecitvely. pPC40 was constructed by amplifying and cloning the coding sequence of EKARcyto[106] (from the start codon to the C-terminus of mVenus) into pRS426-GPD via SpeI-XhoI (sites introduced into primers). pPC41, pPC48, pPC49, and pPC50 were constructed by cloning the coding sequence of EKAR2.3-pC (gift from Jin Zhang lab) as a BamHI-EcoRI fragment into pRS426-GPD, pRS406-GPD, pRS404-GPD, and pRS403-GPD, respectively. Reporter docking site (pPC42, pPC44, pPC45, and pPC46) and phosphosite (pPC47) variants of pPC41 were constructed using standard site-directed mutagenesis techniques (QuikChange kit, Agilent) and verified by nucleotide sequencing analysis. The BamHI-EcoRI fragments of pPC44, pPC46, and pPC47 were cloned into pRS406-GPD to make pPC62, pPC63, and pPC64, respectively. To make nuclear targeted reporters, the EKAR2.3 construct was amplified from pPC48 using a forward primer encoding nucleotides for SpeI, the NLS sequence (PKKKRKV), and a 5 a.a. linker (DDKDP) and a reverse primer encoding EcoRI. The resulting product was

cloned into pRS406-GPD and pRS406-ADH1 as a SpeI-EcoRI fragment to make pPC57 and pPC60, respectively. To make plasma membrane targeted versions of EKAR2.3, the EKAR2.3 construct was amplified from pPC48 using a forward primer encoding BamHI and a reverse primer encoding nucleotides for the 12 C-terminal residues of Ras2[36] (including the stop codon) followed by HindIII. The resulting product was cloned into pRS406-GPD as a BamHI-HindIII fragment to create pPC58. To make the cytoplasmic targeted EKAR construct, the EKAR2.3 construct was amplified from pPC48 using a forward primer encoding BamHI and a reverse primer encoding nucleotides for the nuclear export signal in *Xenopus* MAPKK[127] (LQKKLEELELDE) and the stop codon, followed by HindIII. The resulting product was cloned into pRS406-GPD as a BamHI-HindIII fragment to create pPC66. To make the P_{FUS1}-mCherry reporter plasmid, the promoter of Fus1 (500-bp region upstream of the start codon) was amplified from genomic DNA (W303 strain) and inserted into pRS403 via SacI-SpeI (sites introduced into primers). The mCherry fragment from pMS107 (gift from Maya Schuldiner lab) was cloned into the resulting plasmid via SpeI-XhoI to create pPC61.

Live-cell microscopy and image analysis

All strains were grown overnight in Synthetic Complete medium with 2% dextrose (SCD) or SCD^{-URA} (for episomally expressed constructs), diluted the next day, and grown to mid-log phase (OD ~ 0.8) just prior to imaging. For timelapses requiring less than 3 hours of imaging, experiments were performed in a multi-well dish format (8well, Thermo Nunc). Dishes were coated with 0.1 mg/ml concanavalin A (Sigma) prior to seeding cells. For timelapses longer than 3 hours or for applying spatial gradients of pheromone, experiments were performed using our microfluidic device (see Supplementary Info for description of device and operation). For experiments involving alpha-factor stimulation, all media was supplemented with 20 ug/ml casein (Sigma) to prevent absorption of alpha-factor to vessel walls[18]. Imaging was performed with a Zeiss Axiovert 200M epifluorescence microscope equipped with an automated stage using either

a 40x/1.3NA, 63x/1.4NA, or 100x/1.4NA plan-apo oil immersion objective, where noted. Images were acquired with a 16-bit Cascade 512 camera. Excitation was provided by an Excite Exacte light source (Excelitas Technologies) at 15% power for 40x and 63x magnification and 10% power for 100x magnification. Donor, FRET, acceptor, and mCherry channel images were acquired sequentially with the following excitation, dichroic mirror, and emission filters (Chroma): donor: ET430/24x, 69008bs, ET470/24m; FRET: ET430/24x, 69008bs, ET535/30m; acceptor: ET500/20x, 69008bs, ET535/30m; mCherry: . Exposure times were 60ms for the donor and FRET channels, 20ms for the acceptor channel, and 200ms for the mCherry channel. Images were captured using Slidebook 5.5 (Intelligent Imaging Innovations) and subsequently processed and analyzed using Matlab. For EKAR expressing cells, emission ratios were measured by subtracting the average background fluorescence from the emission intensities of each cell area. For experiments evaluating construct expression level, docking domain effects, and signal reversibility, the average emission ratio for cells in a field of view was calculated for each time point. Cells in each field were segmented by applying an adaptive threshold on the YFP channel image and then aligning fluorescence intensities to these masked cell regions. For all other experiments, average emission ratios and mCherry fluorescence for individual cells were tracked in time by adapting an image processing routine[103] that segments and tracks cells using the phase-contrast channel. Cells that were out of focus or segmented incorrectly were omitted from analysis. Normalized emission ratios were calculated by dividing the ratio at each time point by the emission ratio just prior to stimulation. Ratiometric images and line scans of cells were generated from emission images with background fluorescence subtracted on a per-pixel basis.

Immunoblot analysis

Cell extracts were resolved by 10% SDS-polyacrylamide gel electrophoresis and immunobloting was performed as described previously[128]. Primary antibodies used were anti-

phospho-p44/p42 MAPK (Cell Signaling, cat 4370) and anti-PGK1 (Abcam, cat 113687). Band intensity was quantified by scanning densitometry with ImageJ (National Institutes of Health).

Table 3.1. Strains used in this study.

Name	Genotype	Source
BMA64-1A	MATa ura3-1 trp1Δ leu2-3,112 his3-11,15 ade2-1 can1-100	Euroscarf
PC72	MATa ura3-1 trp1Δ leu2-3,112 his3-11,15 ade2-1 can1-100 ade2::ADE2 bar1Δ::natMX4	this study
PC126	MATa bar1Δ ura3::P_{GPD}-EKAR2.3-URA3	this study
PC128	MATa bar1Δ ura3::P_{GPD}-EKAR2.3-URA3(2x)	this study
PC158	MATa bar1Δ ura3::P_{GPD}-EKAR2.3-URA3(2x) trp1::P_{GPD}-EKAR2.3-TRP1	this study
PC163	MATa bar1Δ ura3::P_{GPD}-EKAR2.3-URA3(2x) trp1::P_{GPD}-EKAR2.3-TRP1 his3::P_{GPD}-EKAR2.3-HIS3	this study
PC167	MATa bar1Δ ura3::P_{GPD}-EKAR2.3(HIFAFEFP)-URA3(2x)	this study
PC195	MATa bar1Δ ura3::P_{GPD}-EKAR2.3(AAAA)-URA3(2x)	this study
PC162	MATa bar1Δ ura3::P_{GPD}-EKAR2.3(PRAP)-URA3(2x)	this study
PC154	MATa bar1Δ ura3::P_{GPD}-EKAR2.3-URA3(2x) ste7Δ::kanMX6	this study
PC155	MATa bar1Δ ura3::P_{GPD}-EKAR2.3-URA3(2x) fus3Δ::kanMX6	this study
PC156	MATa bar1Δ ura3::P_{GPD}-EKAR2.3-URA3(2x) kss1Δ::kanMX6	this study
PC196	MATa bar1Δ ura3::P_{GPD}-EKAR2.3-URA3(2x) fus3Δ::kanMX6 kss1Δ::hphMX4	this study
PC199	MATa bar1Δ ura3::P_{GPD}-EKAR2.3-URA3(2x) fus3Δ::kanMX6 kss1Δ::hphMX4 his3::P_{FUS3}-Fus3-as2-HIS3	this study
PC149	MATa bar1Δ ura3::P_{GPD}-NLS-EKAR2.3-URA3	this study
PC164	MATa bar1Δ ura3::P_{ADH1}-NLS-EKAR2.3-URA3	this study
PC152	MATa bar1Δ ura3::P_{GPD}-EKAR2.3-CCaaX-URA3(2x)	this study
PC202	MATa bar1Δ ura3::P_{GPD}-EKAR2.3-NES-URA3(2x)	this study
PC159	MATa bar1Δ ura3::P_{GPD}-EKAR2.3-URA3(2x) P_{FUS1}-mCherry-HIS3	this study

Table 3.2. Plasmids used in this study.

Name	Description	Source
pPC40	pRS426 P_{GPD}-EKAR	this study
pPC41	pRS426 P_{GPD}-EKAR2.3	this study
pPC42	pRS426 P_{GPD}-EKAR2.3-FEFP	this study
pPC44	pRS426 P_{GPD}-EKAR2.3-HIFAFEFP	this study
pPC45	pRS426 P_{GPD}-EKAR2.3-HIFAFEFPLS	this study
pPC46	pRS426 P_{GPD}-EKAR2.3-AAAA	this study
pPC47	pRS426 P_{GPD}-EKAR2.3-PRAP	this study
pPC48	pRS406 P_{GPD}-EKAR2.3	this study
pPC49	pRS404 P_{GPD}-EKAR2.3	this study
pPC50	pRS403 P_{GPD}-EKAR2.3	this study
pPC57	pRS406 P_{GPD}-NLS-EKAR2.3	this study
pPC58	pRS406 P_{GPD}-EKAR2.3-CCaaX	this study
pPC59	pRS406 P_{ADH1}-NLS-EKAR2.3	this study
pPC61	pRS403 P_{FUS1}-mCherry	this study
pPC62	pRS406 P_{GPD}-EKAR2.3-HIFAFEFP	this study
pPC63	pRS406 P_{GPD}-EKAR2.3-AAAA	this study
pPC64	pRS406 P_{GPD}-EKAR2.3-PRAP	this study
pES1002	pRS406 Fus3-as2	[18]
pPC65	pRS403 P_{FUS3}-Fus3-as2	this study
pPC66	pRS406 P_{GPD}-EKAR2.3-NES	this study

IV. Systematic analysis of mating and chemotropic behavior in yeast

Introduction

For mating of two haploid yeast cells to work optimally, a variety of processes are carried out within the cell. These processes include pheromone production, MAPK signaling, gene induction, cell-cycle arrest, polarity establishment, vesicle trafficking, and cell wall/membrane reorganization. While most genes play specific roles in these processes, some genes have multiple distinct functions functions. One example is Far, which serves as a cell-cycle arrest promoter and an adaptor protein that localizes Cdc42-mediated polarity at the membrane[2]. While mating requires many genes that are involved in pheromone production, MAPK signaling, and gene induction, genes involved in polarized growth and gradient sensing are also important. In the context of mating, genes supporting polarized growth processes have been characterized less rigorously than genes that support early signaling processes. The difficulty in examining the mating-specific functions of these genes is partly due to the fact that many polarity genes are also important for cell division and viability[129]. Additionally, the mating defects exhibited by polarity gene mutants may also be partial and difficult to distinguish, possibly due to some polarity genes sharing similar or overlapping functions.

Chemotropism is a unique developmental behavior that allows non-motile cells to explore their local environment. Mechanisms supporting chemotropism in yeast have implicated several upstream signaling components, including the receptor, heterotrimeric G proteins, and two immediate Gβ effectors, Far1 and Cdc24. In particular, activated receptors and heterotrimeric G proteins are thought to be early landmarks for linking polarity factors to sites of highest pheromone binding at the cell surface. Accordingly, the receptor and G proteins can be observed to polarize their localization at the plasma membrane before projection growth ensues[49]. Recently, studies have focused on how the link between Cdc42-driven polarity machinery and

activated receptors is established and utilized by cells tracking gradients of pheromone[71,72]. While mostly studied in the context of cell budding, vesicle trafficking may also play an important role in polarity establishment, maintenance, and signaling during pheromone exposure. Proteins regulating vesicle trafficking may thus help fine-tune projection growth toward mating partners, so that mating can occur optimally. In this study, we seek to systematically explore mating efficiency at the genome level with the goal of identifying new genes important for mating, and particularly chemotropic growth. In particular, we focused on specific groups of genes with endocytic and exocytic functions.

Results

Design and execution of genome-wide mating efficiency screen

In order to potentially uncover new genes important in the regulation of the mating pathway, we devised an imaging-based approach to systematically evaluate mating efficiency for individual gene mutants. The working principle of our method involves mating a mutant and wild-type yeast strain, each constitutively expressing a different fluorescent protein, similar in concept to previous assays examining yeast cell fusion[130] (Figure 4.1a). Imaging-based detection of haploids (non-mated cells) and fused zygotes (mated cells) can be used to quantify the mutant strain's overall mating efficiency. In order to apply this method in a high-throughput format, we devised an SGA-based screen of the yeast knockout and DAmP libraries that automated haploid cell mixing, mating, and imaging.

An SGA reporter library was created, based on previous methods[131132], in collaboration with the Schuldiner Lab at the Weizmann Institute, to produce a MATa mutant strains containing a cytosolic mCherry reporter. To assess mating efficiency, the MATa mCherry library strains were mixed with a wild-type GFP-expressing MATα strain on agar for 3 hrs, after which mating mixtures were collected, fixed and imaged (Figure 4.1b). After segmenting the RFP and GFP channel images, the number of mated and non-mated cells were counted, and a mating fraction

metric was used to assess the overall mating efficiency for each strain in the screen. Overall the mating efficiencies of 5,289 mutants (4,507 knockouts and 782 DAmP mutants of essential genes) were directly evaluated in the screen (out of ~5,800 total open reading frames in the yeast genome) (Figure 4.1c). An additional 669 mutants were missing from the screen, and approximately half of these were absent from our SGA mCherry library. These missing mutants included strains deleted for genes that were either vital for mating (most of the Ste genes) or vital for cell growth. The inability to mate or proliferate efficiently would have caused the strain to not pass through the stages of the SGA mCherry library creation. Thus, we concluded these genes to include those that could be highly important for mating.

Due to systematic time differences in assaying strains in 384-well format, there was some variability observed in the mean mating efficiency per plate. This variability was accounted for by normalizing all mating fractions to the average of each plate. Also, due to strain-to-strain differences in the number of cells assayed in the mating mixture, we looked to see if this affected mating efficiency. Importantly, the mating efficiency did not depend on the number of haploid cells in the mating mixture (Figure 4.1d), indicating that cells were at a density below the level which mating efficiency could be obscured by cell crowding and pheromone confusion effects.

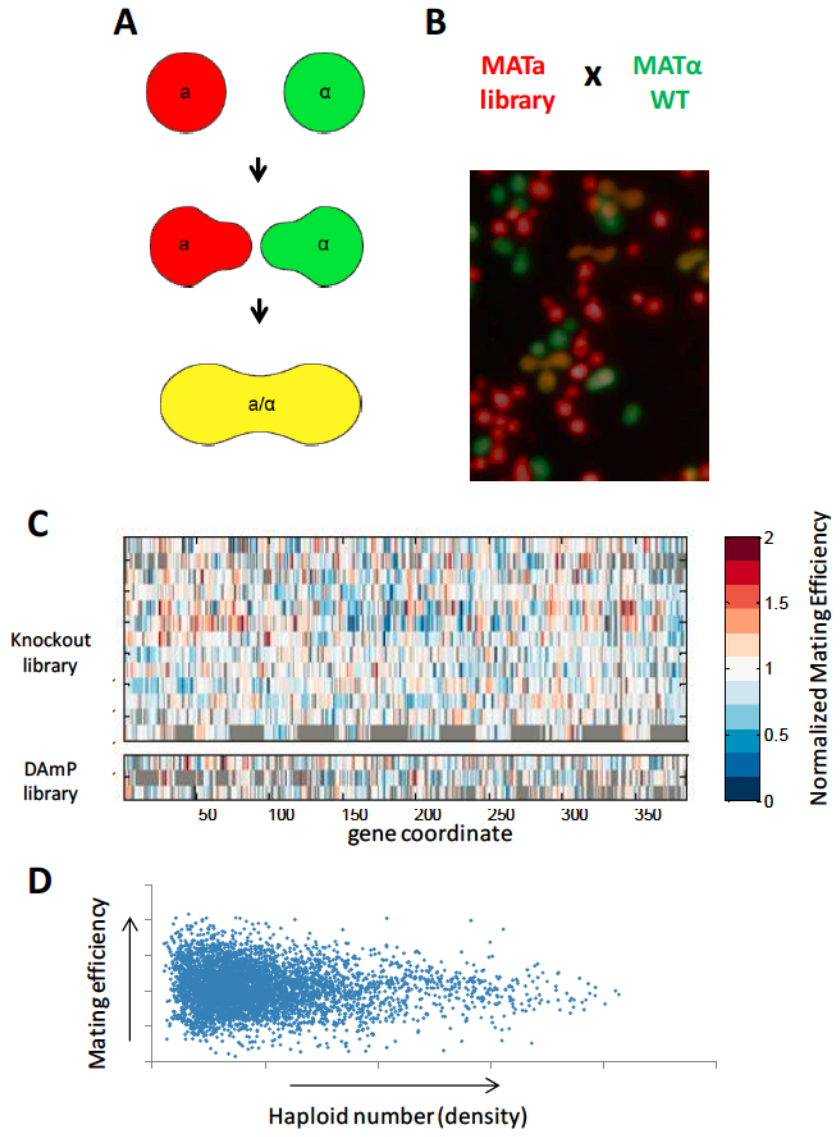

Figure 4.1. Design and execution of genome-wide mating efficiency screen. A) Schematic showing the working principle of the fluorescence-based mating screen. B) Example image of a MATa mutant, MATalpha wildtype, and MATa/alpha zygote cells in red, green, and yellow, respectively (pseudocolored). C) Heatmap of all genes in the knockout and DAmP libraries with their normalized mating efficiency indicated by color (red: high, blue: low). D) Scatter plot showing that mating efficiency is not effected by variability in the number of haploid cells in the mating mixture.

Screen validation and candidate selection

To validate the reliability of the screen, we assessed the ranks of known positive and negative mating regulator genes (Figure 4.2a). Mutants of positive regulators, or genes known to be important for mating, showed severe mating defects (predominantly in the lowest 10% of mating efficiency) and included genes such as Ste20, Ste50, Fus3, and Cdc42. Mutants of negative regulators, or genes known to be antagonistic to the mating pathway, showed highly proficient mating (predominantly in the highest 5% of mating efficiency) and included genes such as Hog1, Pbs2, and Msg5. Full lists of known regulators identified from the full screen are included in the Appendix Additionally, we manually validated groups of positive and negative regulators by performing quantitative mating assays on a panel of mutants (Figure 4.2b). We found the results of these assays to be in qualitative agreement with the screen results.

To identify potentially new genes that are important in the regulation of mating, we selected the most mating-defective and the most mating-proficient ORFs from the first screen and then conducted repeat screens with these strains, this time using a wild-type strain as a mating control. Genes in these groups with functions that were clearly not specific to mating, including mitochondrial and nonspecific transcription, translation, and metabolic genes, were omitted from further analysis. Figure 4.3 depicts genes that were found to be consistently more mating-defective than wild-type cells, organized by primary gene function. Genes were further categorized as having known involvement in mating, less defined involvement in mating, or having no characterization altogether (ie. genes without names). Notably, a large proportion of the less defined genes were found to have functions relating to cell polarity and vesicle trafficking. Genes important for chemotropism, or particularly involved in polarized cell growth and orientation ability, would likely fall into these functional categories.

As a first measure of assessing the chemotropic ability of the mating defective hits, we first performed a screen-based pheromone confusion assay. The confusion assay involves comparing the mating efficiency of MATa and MATalpha haploid cells both with and without

exogenous alpha-factor added to the mating mixture (Figure 4.2c). The mating efficiency of wild-type cells is significantly reduced when exogenous alpha-factor is present, because the MATa cells can no longer detect the pheromone gradient coming from their MATalpha partner. However, mutant MATa cells that have a defect in chemotropism will not show a reduction in mating efficiency with alpha-factor present, because these cells are already unable to orient their mating projections[67]. Thus, we used the ratio of mating efficiencies with and without pheromone to assess the chemotropic ability of the hits. When exposed to pheromone, we found a significant proportion of the mating defective hits (roughly 40 out of 150) to exhibit a mating decrease that was less severe than the wild-type decrease in mating. We identified this group as chemotropic candidates. As many of these mutants already exhibit a severe mating defect (many include genes known to be vital for mating), we found that the addition of pheromone might enhance their mating, masking separate and less pronounced chemotropic defects. Consistent with this reasoning, roughly 30% of the chemotropic candidates resulted in a higher mating efficiency with pheromone than without, indicating that these strains confer a signaling defect which can be alleviated with stronger concentrations of alpha-factor.

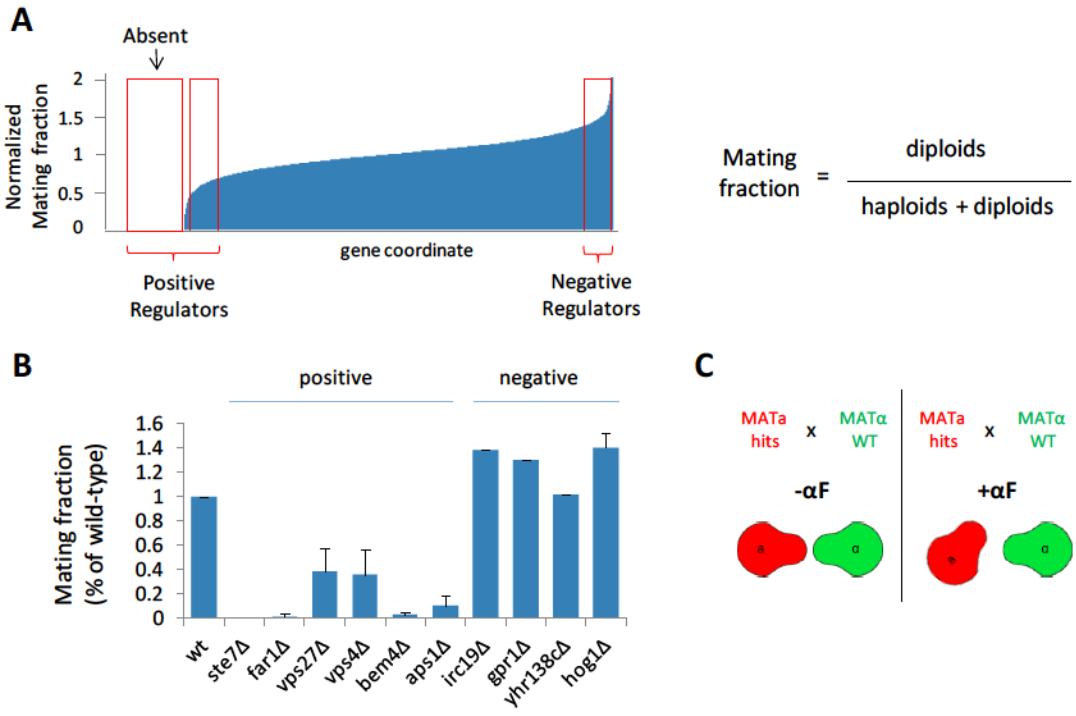

Figure 4.2. Candidate selection and validation of mutants from mating screen. A) Normalized mating fractions of mutants sorted from lowest to highest fraction. Mutants showing the most defective (lowest) and most proficient (highest) mating efficiencies were selected as genes of interest (regions highlighted in red). Mating fractions, as calculated by the equation on the right, were normalized by the average mating efficiency for each plate. B) Quantitative mating assays were performed for groups of positive and negative regulators (both known and less defined genes) to validate results of the screen. C) Schematic of high-throughput pheromone confusion screen. A wildtype cell response is depicted as showing a reduced ability to mate with its partner.

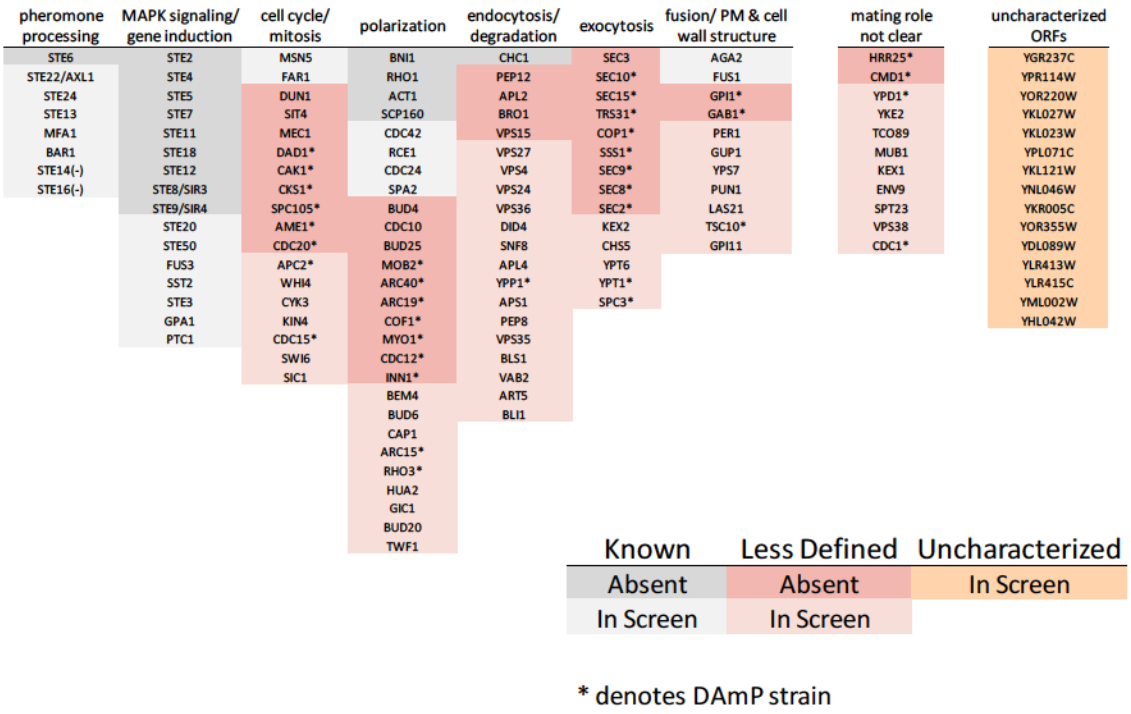

Figure 4.3. Mating-defective genes identified from screen and grouped by function. Genes are color coded based on whether they have previously known or less defined roles in mating. Genes involved in general cell transcription, translation, or metabolism processes were ommitted from the analysis.

Role of ESCRT function in pheromone signaling and chemotropism

Analysis of our mating screen results revealed a large number of genes involved in cell polarity and vesicle trafficking to be important for mating. In particular, we found several knockout mutants comprising the ESCRT (Endosomal sorting complexes required for transport) machinery to consistently rank high among our hits for mating defectiveness and confusion ratio. These genes include Vps27, Vps36, Vps24, Vps4, Did4, and Snf8, representing components of each of the ESCRT complexes (I, II, and III). ESCRT complexes have been shown to be required for the sorting of ubiquitinated receptors and biosynthetic cargoes into internal vesicles of the late endosome (also known as multivesicular bodies – MVBs)[133]. In yeast, impairment of ESCRT function has been shown to result in the accumulation of various membrane proteins at exacerbated late endosomal compartments (class E compartments), blocking their normal degradation in the vacuole[134]. It has additionally been shown that receptors, including EGFR[135] (in mammalian cells) and Ste3 pheromone receptors[48] (in MATalpha yeast cells), also accumulate at the plasma membrane, but the molecular basis for this phenotype is still being explored. Interestingly, it has been proposed that ESCRT impairment leads to enhanced recycling of receptors from early endosomes rather than a block in their initial internalization from the membrane or enhanced recycling from late endosomes[136].

In order to further dissect the cause of the mating defect we observed in the ESCRT mutants, we performed a variety of assays to characterize the signaling and morphological behavior of these cells in response to pheromone. We first created individual knockout strains of Vps27, Vps36, Vps24, and Vps4 and conducted traditional quantitative mating assays (colony-based) to confirm results from the mating screen. Figure 4.4a shows a significant reduction in mating efficiency (more than 2-fold) for each of the ESCRT mutants compared to wild-type, consistent with their positive regulator grouping in our screen. We next evaluated the pheromone-induced morphological development of the mutants in a *bar1Δ* background. Dose response experiments reveal the onset of polarized growth to be delayed in the ESCRT mutants (Figure

4.5). Relative to wild-type, *vps27Δ* and *vps4Δ* cells required higher doses of pheromone to achieve elongated and shmooing cell states. Additionally, these mutants appeared to be defective in the ability to form pointed projections as is the case when wild-type cells are exposed to saturating doses of pheromone.

To assess the gradient sensing ability ESCRT deficient cells, we co-stimulated wild-type and *vps27Δ* cells to gradients of pheromone in our microfluidic device (Figure 4.6). Interestingly, while *vps27Δ* cells were defective in forming multiple projections at high pheromone doses, single-projection cells were able to align their mating projections with similar accuracy as wild-type cells at both high and low concentration ranges (moderate increases in projection angles in Figure 4.6c were not statistically significant). Thus, ESCRT function does not appear to be specifically important for growth orientation.

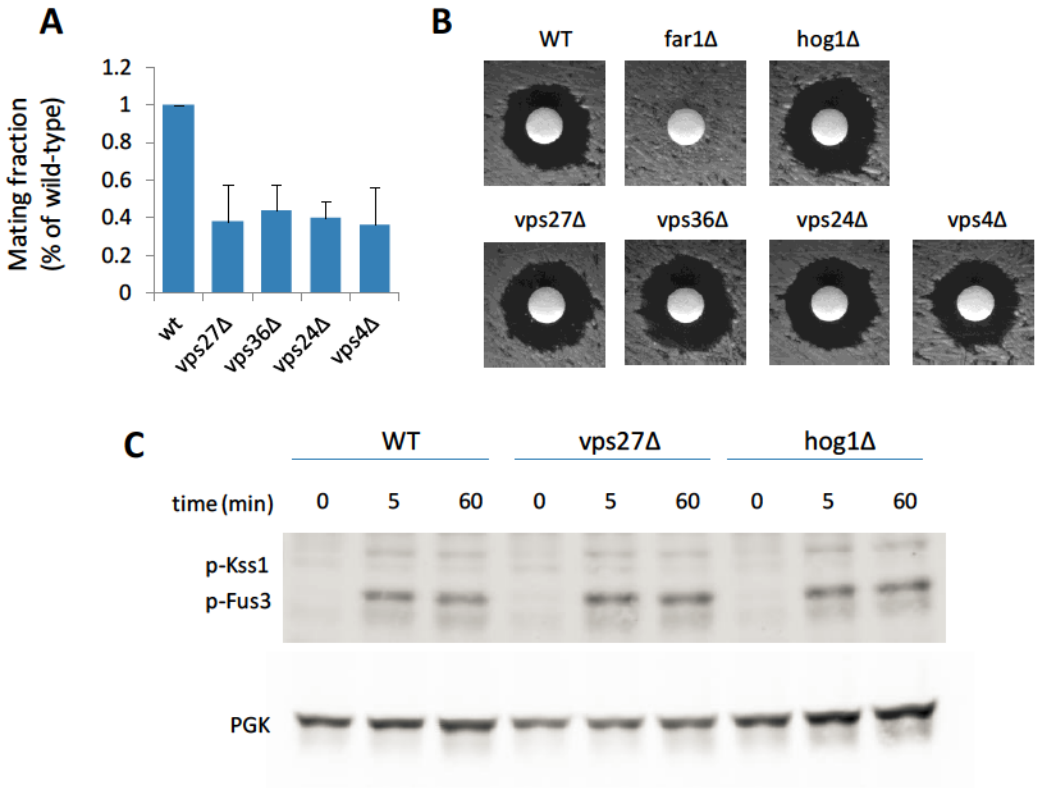

Figure 4.4. ESCRT pathway mutants are partially defective in mating but retain signaling. A) Quantitative mating assay of ESCRT mutants show mating defect relative to wild-type. B) Halo assays of ESCRT mutants with *far1Δ* and *hog1Δ* as negative and positive controls for cell-cycle arrrest, respectively. C) Pheromone-induced phosphorylation of Fus3 is retained in *vps27Δ* mutant.

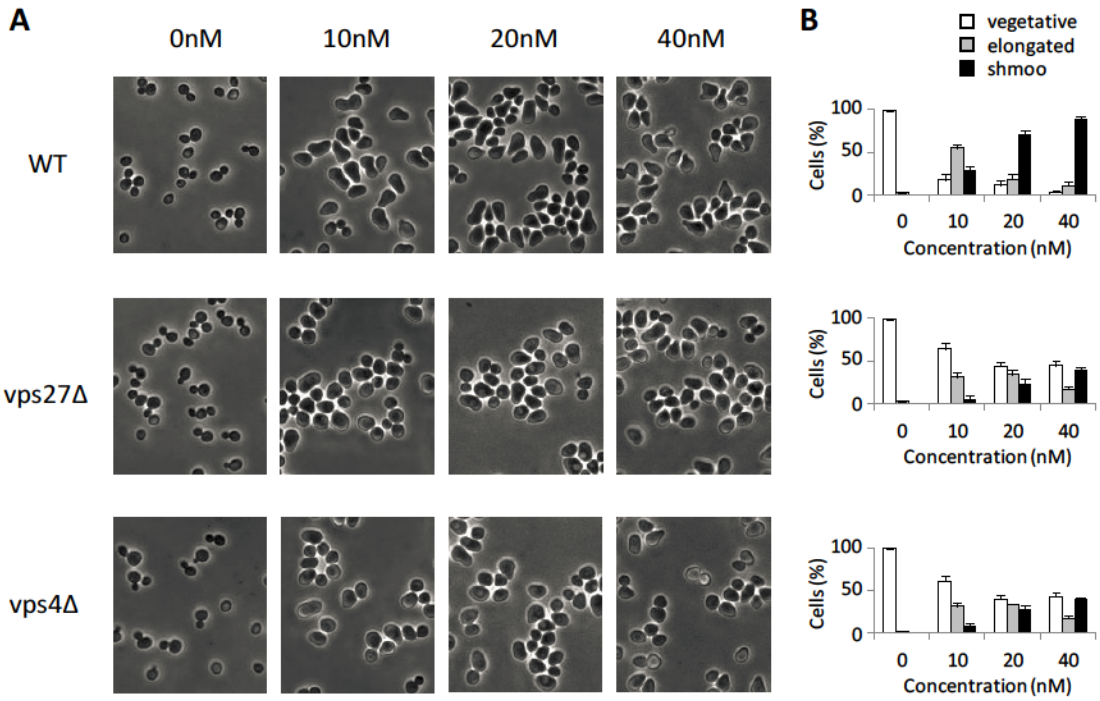

Figure 4.5. Pheromone-induced morphogenesis is altered in ESCRT-deficient mutants. Polarized growth of *vps27Δ* and *vps4Δ* mutants each show a reduced sensitivity to pheromone concentration. A) Indicated strains were treated with pheromone in liquid culture and scored as vegetative (budding), elongated (cell aspect ratio > 1.6), or shmooing (projections are pointed) after 3.5 hrs for each of the assayed concentrations. B) Percent of cells exhibiting each phenotype is shown at the right of the image sets.

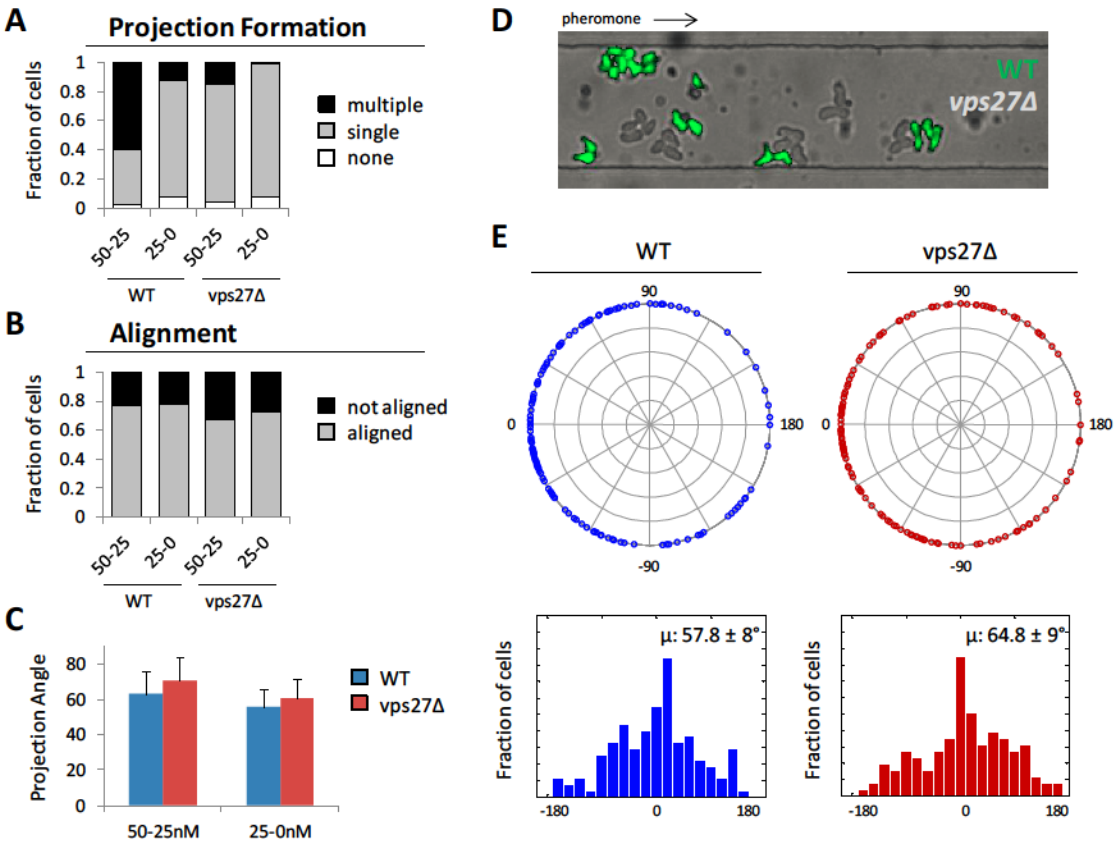

Figure 4.6. Gradient sensing is preserved in ESCRT-deficient mutants. Wild-type and *vps27Δ* cells were co-stimulated in a 0-60nM pheromone gradient and chemotropic behavior was assessed. A) Fraction of cells exhibiting multiple projection growth, single projection growth, or no projection growth (arrested or budding cells) in both the high (50-25nM) and low (0-25nM) concentration ranges of the pheromone gradient. B) Percent of single-projection cells that aligned their growth with the direction of the gradient (angles < 90deg from gradient normal). C) Average projection angles for wt and *vps27Δ* cells in the high and low concentration ranges. D) Representative image of cell chamber containing wt and *vps27Δ* cells exposed to a pheromone gradient. E) Polar plots (top) and histograms (bottom) of raw projection angles measured for both wt and *vps27Δ* cells exposed to the same pheromone gradient (n>150 cells per strain). Average angle ± 95% CI is indicated at topright of histogram.

To determine if the ESCRT deficient mating defect could be attributed to a reduction in signaling through the mating MAPK pathway, we performed separate tests for cell-cycle arrest, Fus3 phosphorylation, and pheromone-responsive promoter activity. The ability of the mutants to arrest their cell cycle and activate Fus3 was not compromised, with levels comparable to wildtype (Figure 4.4b). Additionally, pheromone-induced phosphorylation of Fus3 in a *vps27Δ* strain appeared to be comparable to Fus3 phosphorylation in wild-type cells (Figure 4.4c). However, when ESCRT mutants expressing a Fus1pr-GFP reporter were treated with pheromone for 90min, all of the mutants showed significant reductions in expression levels (between 40-60% of wt) (Figure 4.7). This seems to indicate that loss of ESCRT function leads to an overall reduction in MAPK-mediated signaling that may lead to impairment of downstream processes over time. To determine if altered receptor activity could be a cause for this defect, we assessed the membrane-localized abundance of Ste2-GFP in wild-type and vps27 cells (Figure 4.8). We found a significant increase of membrane-localized receptor in vps27 cells relative to wild-type. These results indicate that altered Ste2 trafficking and increased recycling of internalized Ste2 receptors back to the plasma membrane may disrupt normal receptor activation events.

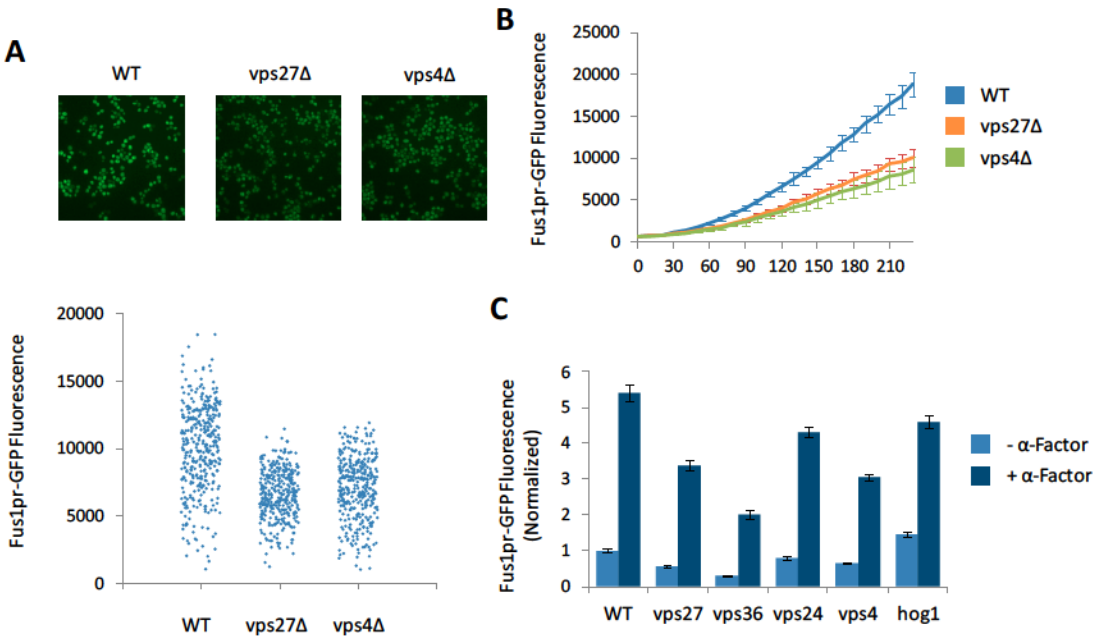

Figure 4.7. Analysis of mating gene expression in ESCRT-deficient mutants. A) Single-cell quantification of Fus1 gene expression in wt, *vps27Δ* and *vps4Δ* cells containing an integrated FUS1pr-GFP reporter. Fluorescence was quantified after 3hrs of 10uM pheromone treatment. B) FUS1pr-GFP was expressed from a low-copy plasmid in wt, *vps27Δ*, and *vps4Δ* cells. Fluorescence was measured over time after 10uM alpha-factor treatment. C) FUS1pr-GFP expressed from low-copy plasmids in ESCRT mutants. Average fluorescence was recorded before and after 3hrs of 10uM pheromone treatment.

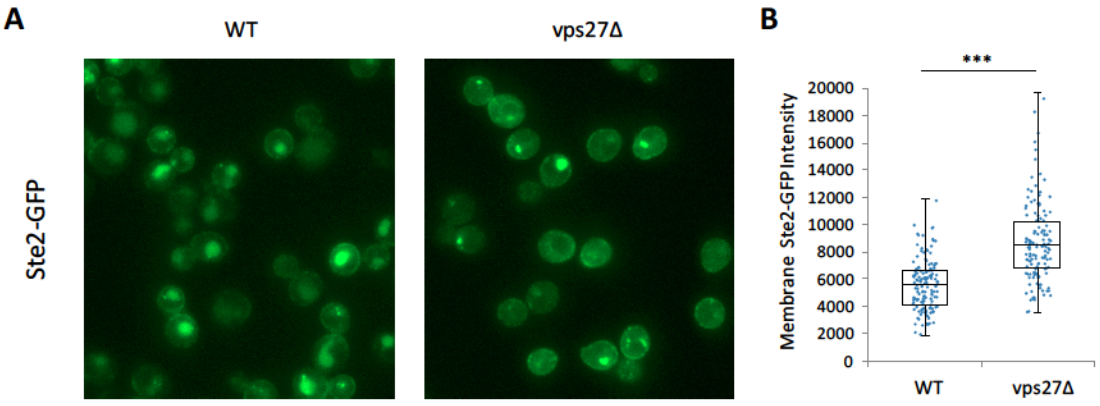

Figure 4.8. Receptor localization increased at plasma membrane in vps27 mutant. A) Fluorescence images of Ste2-GFP in wild-type and vps27 cells. B) Single-cell quantification of membrane-localized Ste2-GFP fluorescence for each strain. *** $P < 0.01$ (n>100 cells).

Evaluation of Sec3 as a chemotropic mediator

In addition to endocytosis proteins, analysis of our mating screen also identified many proteins having exocytic functions. Moreover, many of these exocytic mutants also happened to be DAmP mutants (gene is essential) and were found to have not passed the SGA mating stage, thus indicating a potentially severe mating defect. It was recently found that trafficking of polarity and mating gene mRNA to the shmoo tip, via the RNA-binding protein Scp160, is important for polarity factor protein enrichment and directional sensing of pheromone gradients[137]. These results implicate specific proteins, working in concert with vesicle trafficking machinery, to be important for chemotropic growth. The exocyst complex is an important group of proteins that coordinate the targeting and fusion of secretory vesicles to defined sites at the plasma membrane[65]. One important component of this complex, Sec3, is normally localized at the membrane and serves as a landmark protein for secretory vesicle fusion[138]. Interestingly, Sec3's polarized localization at the membrane is independent of actin-mediated transport. Additionally, Sec3 has been shown to specifically interact with Cdc42 and PIP2, which also become polarized to projection growth sites during pheromone exposure. Because of its appearance as a positive regulator in our screen, we were interested in determining if Sec3 plays a role in chemotropic growth.

In contrast to most other exocyst components, deletion of the Sec3 gene maintains cell viability, albeit a slower growth rate. Sec10 is another exocyst component, which is essential for cell viability and happens to undergo increased phosphorylation during pheromone exposure[31]. As a first assessment of morphological plasticity, we performed pheromone dose response experiments comparing the ability of *sec3Δ* and *sec10^{tet}* cells to polarize their growth, relative to wild-type (Figure 4.9). Notably, for *sec3Δ* cells we found the onset of polarized growth to require higher pheromone doses relative to wild-type cells, similar to the behavior exhibited by endocytic ESCRT mutant cells. Very few *sec10^{tet}* cells showed polarized growth behavior, even at saturating pheromone doses, indicating a much more severe defect in polarized growth ability.

To assess the gradient sensing ability the *sec3Δ* cells, we co-stimulated wild-type and *sec3Δ* cells to gradients of pheromone in our microfluidic device (Figure 4.10). Interestingly, *sec3Δ* cells were found to be defective in their ability to form multiple projections and also exhibited an impaired ability to orient their projections with the pheromone gradient. This defect was more pronounced at lower concentrations, where cells are more inclined to accurately track a gradient. The average projection angle with respect to the pheromone gradient was 64.6 ± 8° for wild-type cells and 76.9 ± 7° for *sec3Δ* cells (n>200 cells for each strain). Additionally, we found the projection growth rate of single-projection *sec3Δ* cells to be slower than single-projection wild-type cells in a pheromone gradient (Figure 4.11). These results indicate that Sec3 is important for accurate pheromone gradient sensing and may serve as a landmark for targeting vesicle traffic toward incipient projection sites.

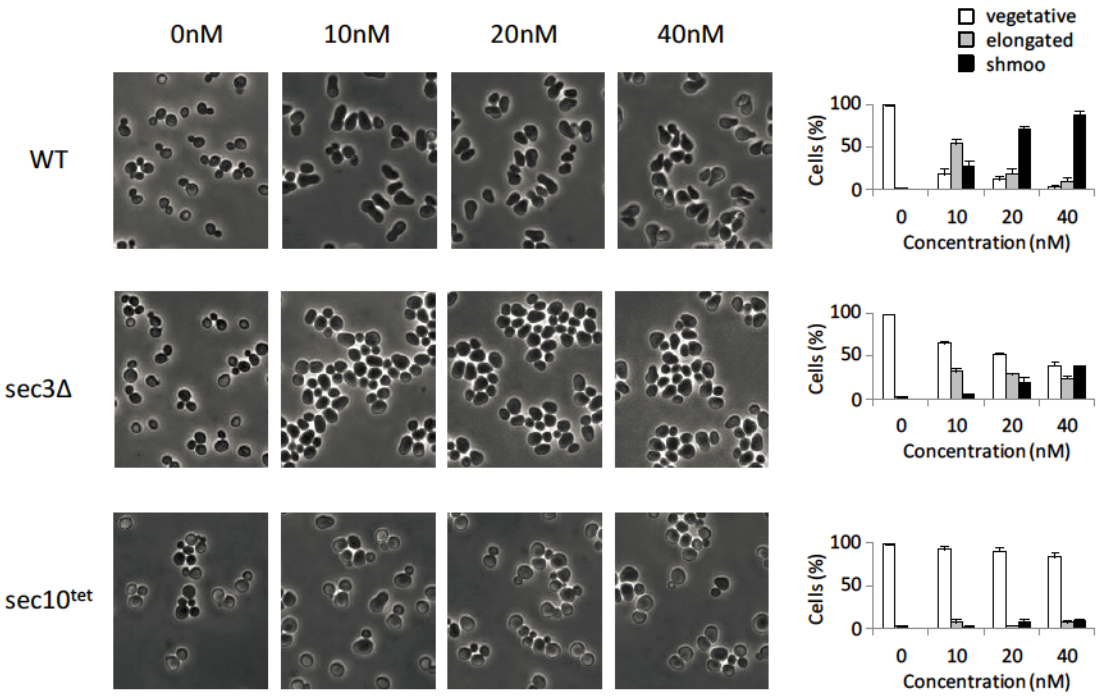

Figure 4.9. Pheromone-induced morphogenesis is altered in exocytic mutants. A) Indicated strains were treated with pheromone in liquid culture and scored as vegetative (budding), elongated (cell aspect ratio > 1.6), or shmooing (projections are pointed) after 3.5 hrs for each of the assayed concentrations. B) Percentage of cells exhibiting each phenotype is quantified at the right of each image set.

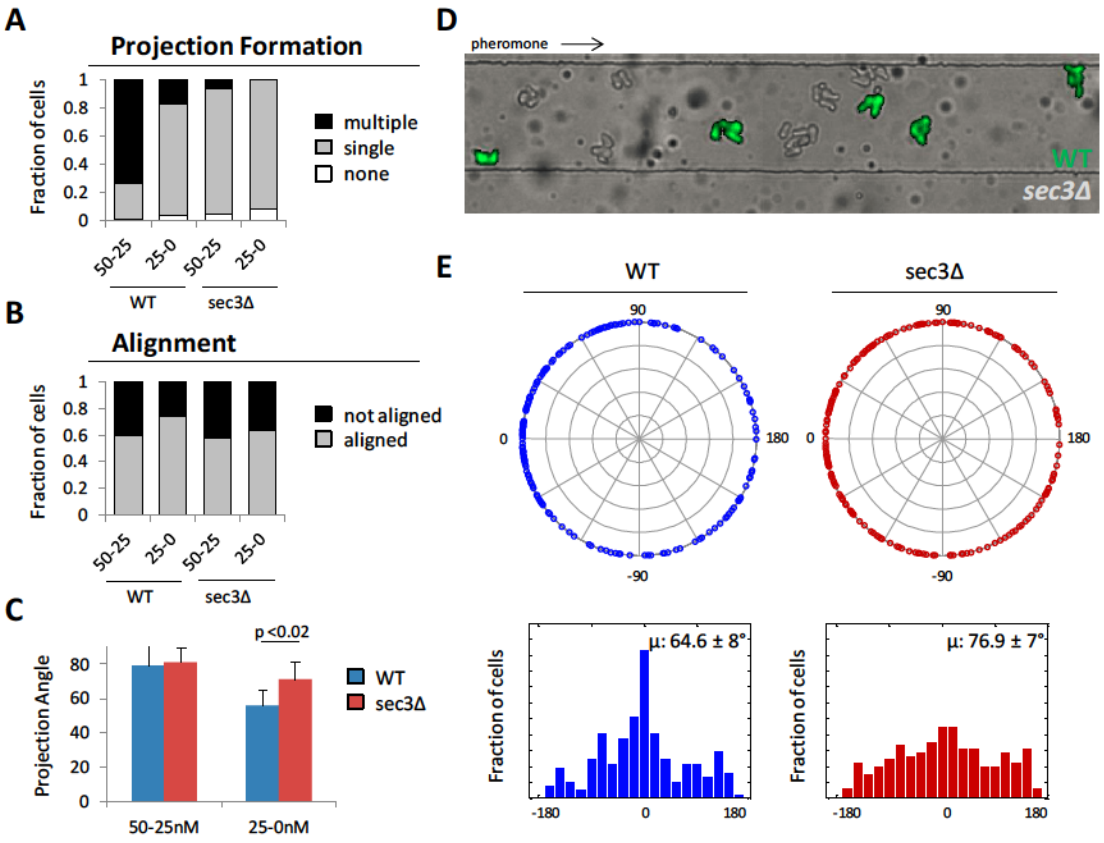

Figure 4.10. Gradient sensing is impaired in *sec3Δ* mutant. Wild-type and *sec3Δ* cells were co-stimulated in a 0-60nM pheromone gradient and chemotropic behavior was assessed after 7hrs. A) Fraction of cells exhibiting multiple projection growth, single projection growth, or no projection growth (arrested or budding cells) in both the high (50-25nM) and low (0-25nM) concentration ranges of the pheromone gradient. B) Percent of single-projection cells that aligned their growth with the direction of the gradient (angles < 90deg from gradient normal). C) Average projection angles for wt and sec3*Δ* cells in the high and low concentration ranges. D) Representative image of a cell chamber containing wt and *sec3Δ* cells exposed to a pheromone gradient. E) Polar plots (top) and histograms (bottom) of raw projection angles measured for both wt and *sec3Δ* cells exposed to the same pheromone gradient (n>200 cells per strain). Average angle ± 95% CI is indicated at topright of histogram.

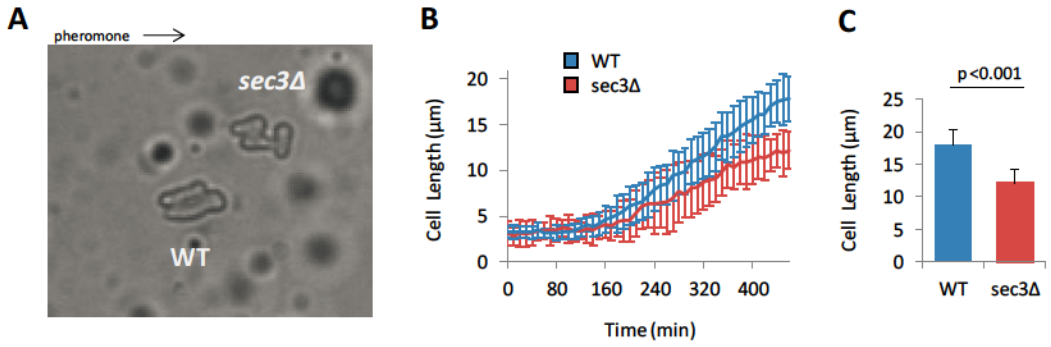

Figure 4.11. Projection growth-rate reduced in *sec3Δ* mutant. A) Representative image of wild-type and *sec3Δ* cells co-stimulated in a 0-60nM pheromone gradient. B) Cell length of single-projecting cells was measured over time during pheromone gradient exposure. Cell length was measured from the projection tip to the back of the cell for each time interval. C) Average single-projection cell length after 8 hrs of pheromone exposure was measured for each strain.

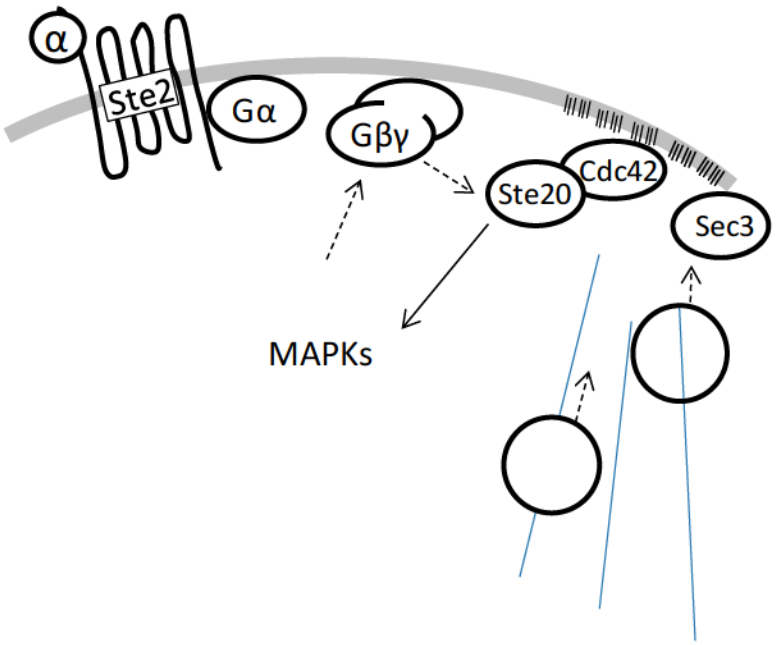

Figure 4.12. Schematic diagram of Sec3-mediated vesicle targeting during pheromone signaling. Sec3 may serve as a landmark for secretory vesicle targeting and fusion at sites on the plasma membrane where Cdc42 and PIP_2 (short black lines) are preferentially located.

Discussion

In summary, our genome-wide analysis of mating efficiency revealed a large number of mating deficient gene mutants with functions involving cell polarity and protein trafficking. To our knowledge this was the first attempt to systematically evaluate mating proficiency at a genome-level scale. In addition to identifying genes with known and lesser known roles in mating, several deletion mutants of uncharacterized putative proteins were also found to have a mating defect based on our screen. In this study we focused on two groups of vesicle trafficking gene hits, the ESCRT proteins and exocyst components, as regulators of endocytic and exocytic transport pathways, respectively.

While recycling pathways have been identified for several yeast proteins and internalized dyes in both wildtype and ESCRT-deficient cells[136,139], there is not much known about the mechanisms of Ste2 recycling or its potential impact on mating. Our initial findings indicate that ESCRT function and thus, an intact endocytosis pathway, is important for full mating competency. While ESCRT function did not appear important for gradient sensing precision, it did appear to be important for full morphogenic development as ESCRT mutants underwent less pronounced cell shape changes upon pheromone treatment. The concomitant reduction in mating gene expression in these mutants indicates that an alteration of upstream receptor trafficking may underlie these polarity and signaling defects. This may also support our finding that receptor localization at the plasma membrane was enhanced in the *vps27Δ* mutant. Ultimately, the aberrant recycling of potentially ubiquitinated or desensitized receptors back to the plasma membrane may cause this pool of receptors to either disrupt or compete with signaling-competent receptors at the cell surface.

In contrast to the endocytic ESCRT mutants, we found pheromone gradient sensing and projection growth rate to both be impaired in a *sec3Δ* mutant, in which secretory vesicle targeting is presumed to be defective. Sec3 has previously been characterized as a landmark protein that is important for leading secretory vesicles and their cargo to specific sites at the plasma

membrane[138]. It binds to both Cdc42 and PIP_2 and does not appear to require actin-based secretion to attain its polarized membrane distribution during cell budding[140,141]. Cdc42 and PIP2 also become polarized at incipient projection sites during pheromone gradient exposure (Figure 4.12). These finding indicate that connections made by Sec3 to both the Cdc42 polarity patch and secretory vesicles may ultimately help in targeting vesicles and important cargo proteins to sites at the membrane where receptors and heterotrimeric G proteins are activated.

Materials and Methods

To obtain images of the mating mixture cells (SGA mCherry mutants cells and wild-type GFP cells), mating reactions were fixed in paraformaldehyde, transferred to glass bottom dishes, and imaged on an automated epifluorescence microscope. Brightfield and fluorescence images (GFP and mCherry) were captured for a minimum of 4 fields of view per mutant, resulting in more than 40,000 fluorescence images for the first full genomic screen. Images were subsequently fed through a custom MATLAB pipeline to perform thresholding, filtering, and counting of the haploid and diploid cell types. To adjust for cases where the mutant and wild-type cells differed in their abundance, the mating fraction was computed to take the minimum (or limiting) number of haploid cell types as the total number of potential mating candidates. To obtain the normalized mating fraction, resulting mating fractions for each mutant were divided by the average mating fraction for all the mutants on the 384- well plate.

V. General Conclusions

Over the past several decades, the yeast mating pathway has served as a model extracellular signaling system, from which many aspects of MAPK and G protein signaling have been elucidated. Despite its genetic simplicity compared to higher eukaryotes, the cellular response to pheromone is a highly sophisticated response relying on layers of complex molecular machinery to coordinate diverse and dynamic cellular processes. In some ways, the chemotropic response is similar to chemotactic responses in other organisms by its dependence on spatial patterns of G protein activity for driving actin-mediated cell polarization. The initiation and maintenance of polarized growth in the presence of pheromone gradients, however, is a phenomenon that is unique to yeast and is still largely not understood. Our lack of understanding of these processes has in part been due to limitations in the experimental techniques available to study yeast at the single-cell level. Recent advances in microfluidic technology have enabled aspects of single-cell behavior, such as cell growth dynamics and protein localization, to be observed over long durations of time and at high spatial resolution. Additionally, the rapid development of new genetically-encoded biosensors in mammalian systems has opened new possibilities for studying analogous processes in simpler eukaryotes. While the advancement and application of genetic techniques have led to the identification and characterization of many important signaling components, many proteins involved in cell polarity remain poorly characterized in the context of mating differentiation. In this thesis, we took an integrative approach to explore outstanding questions relating to the scaffold-PM interaction, MAPK dynamics and variability, and chemotropic growth regulation.

In the first aim, we examined the role of membrane binding by the MAPK scaffold protein, Ste5, in mediating the chemotropic behavior of cells exposed to gradients of pheromone. We developed improved microfluidic devices for stable gradient generation and fluorescently-tagged mutant reporter strains to assess projection orientation and Ste5 localization dynamics,

respectively. Our findings indicate that modulation of scaffold binding to the membrane does not alter directional sensing, but rather sets a chemotropic sensitivity range by modulating the dose response of downstream pathway activity. In the second aim, we explored how the spatial and temporal patterns of Fus3/Kss1 activity contribute to developmental outcomes in cells, such as the decision to bud, mate, and undergo polarized morphogenesis in the presence of pheromone. We first applied the Erk Kinase Activity Reporter (EKAR) to specifically report Fus3 and Kss1 activity in live yeast cells. We demonstrate that overall mating MAPK activity exhibits rapid reversibility, a graded dose-dependence around the K_D of the receptor, and a biphasic kinetic profile that closely resembles Fus3/Kss1 phosphorylation. Interestingly, we observed significant cell-to-cell variability in responses and found this variability to depend on both cell-cycle position and heritability, and also correlate with mating gene expression. Furthermore, long-term imaging in microfluidic devices revealed that gradients of MAPK activity emanate from mating projection tips and develop over time as projections grow. These results illustrate new features of MAPK signaling dynamics in a unicellular differentiation system. In the third aim, we systematically examined mating at the genome-level with the goal of identifying new or previously unidentified mediators of chemotropism in yeast. First, we devised and executed a fluorescence-based genome-wide screen of mating efficiency and identified new groups of characterized and uncharacterized gene mutants, which exhibit defects in mating. We then attempted to characterize the specific cause of the mating deficiency in two separate groups of protein trafficking mutants: the ESCRT proteins and a membrane-localized component of the exocyst complex, Sec3. Our results indicate previously unidentified roles for these proteins in supporting optimal mating pathway activation and chemotropic behavior. In summary, we hope these findings may motivate future studies to further examine the mechanisms and consequences of dynamic MAPK and polarity regulation in yeast.

Appendix

Genes Absent from Screen

ORF	Gene	MF
YOR212W	STE4	na
YDR103W	STE5	na
YDL159W	STE7	na
YLR362W	STE11	na
YNL271C	BNI1	na
YDL090C	STE16/RAM1	na
YDR227W	STE9/SIR4	na
YDR410C	STE14	na
YLR442C	STE8	na
YJR086W	STE18	na
YHR084W	STE12	na
YKL209C	STE6	na

Known Positive Regulator Genes

ORF	Gene	MF
YHL007C	STE20	0
YGL032C	AGA2	0.061
YPR122W	STE22	0.072
YCL032W	STE50	0.078
YIL015W	BAR1	0.086
YBL016W*	FUS3	0.089
YLR229C	CDC42	0.105
YJR117W	STE24	0.107
YBR200W	BEM1	0.177
YJL157C	FAR1	0.185
YLR452C	SST2	0.191
YLR319C	BUD6	0.204
YDR461W	MFA1	0.237
YAL041W	CDC24	0.256
YOR219C	STE13	0.261
YCL027W	FUS1	0.273
YKL178C	STE3	0.278
YHR005C	GPA1	0.283
YHR061C	GIC1	0.292
YLL021W	SPA2	0.304

Known Negative Regulator Genes

ORF	Gene	MF
YLR113W	HOG1	0.731
YJL128C	PBS2	0.685
YNL053W	MSG5	0.725
YER075C	PTP3	0.621

References

1. Bardwell, L. A walk-through of the yeast mating pheromone response pathway. *Peptides* **25,** 1465–1476 (2004).

2. Chen, R. E. & Thorner, J. Function and regulation in MAPK signaling pathways: lessons learned from the yeast Saccharomyces cerevisiae. *Biochim Biophys Acta* **1773,** 1311–1340 (2007).

3. Merlini, L., Dudin, O. & Martin, S. G. Mate and fuse: how yeast cells do it. *Open Biol.* **3,** 130008 (2013).

4. Klein, S., Reuveni, H. & Levitzki, a. Signal transduction by a nondissociable heterotrimeric yeast G protein. *Proc. Natl. Acad. Sci.* **97,** 3219–3223 (2000).

5. Butty, a C., Pryciak, P. M., Huang, L. S., Herskowitz, I. & Peter, M. The role of Far1p in linking the heterotrimeric G protein to polarity establishment proteins during yeast mating. *Science (80-.).* **282,** 1511–1516 (1998).

6. Leeuw, T., C. Wu, J. D. Schrag, M. Whiteway, D. Y. Thomas, and E. L. Interaction of a G-protein -subunit with a conserved sequence in Ste20/PAK family protein kinases. *Nature* **391,** 191–195 (1998).

7. Ste, K., Lamson, R. E., Winters, M. J. & Pryciak, P. M. Cdc42 Regulation of Kinase Activity and Signaling by the Yeast. **22,** 2939–2951 (2002).

8. Wu, C. *et al.* Genetic Analysis of the Interface Between Cdc42p and the CRIB Domain of Ste20p in Saccharomyces cerevisiae. **20,** 9–20 (2003).

9. Pryciak, P. M. & Huntress, F. a. Membrane recruitment of the kinase cascade scaffold protein Ste5 by the Gbetagamma complex underlies activation of the yeast pheromone response pathway. *Genes Dev.* **12,** 2684–2697 (1998).

10. Whiteway, M. S. *et al.* Association of the yeast pheromone response G protein beta gamma subunits with the MAP kinase scaffold Ste5p. *Science (80-.).* **269,** 1572–1575 (1995).

11. Choi, K., Satterberg, B., Lyons, D. M. & Elion, E. A. Ste5 Tethers Multiple Protein Kinases in the MAP Kinase Cascade Required for Mating in S . cerevisiae. *Cell* **78,** 499–512 (1994).

12. Marcus, S., Polverino, A., Barr, M. & Wigler, M. Complexes between STE5 and components of the pheromone- responsive mitogen-activated protein kinase module. *Proc. Natl. Acad. Sci.* **91,** 7762–7766 (1994).

13. Printen, J. A. & Sprague, G. F. Protein-protein interactions in the yeast pheromone response pathway: Ste5p interacts with all members of the MAP kinase cascade. *Genetics* **138,** 609–19 (1994).

14. Van Drogen, F. *et al.* Phosphorylation of the MEKK Ste11p by the PAK-like kinase Ste20p is required for MAP kinase signaling in vivo. *Curr. Biol.* **10,** 630–639 (2000).

15. Winters, M. J., Lamson, R. E., Nakanishi, H., Neiman, A. M. & Pryciak, P. M. A membrane binding domain in the Ste5 scaffold synergizes with Gβγ binding to control localization and signaling in pheromone response. *Mol. Cell* **20,** 21–32 (2005).

16. Garrenton, L. S., Young, S. L. & Thorner, J. Function of the MAPK scaffold protein, Ste5, requires a cryptic PH domain. *Genes Dev.* **20,** 1946–1958 (2006).

17. Takahashi, S. & Pryciak, P. M. Membrane localization of scaffold proteins promotes graded signaling in the yeast MAP kinase cascade. *Curr. Biol.* **18,** 1184–91 (2008).

18. Yu, R. C. *et al.* Negative feedback that improves information transmission in yeast signalling. *Nature* **456,** 755–761 (2008).

19. Strickfaden, S. C. *et al.* A Mechanism for Cell-Cycle Regulation of MAP Kinase Signaling in a Yeast Differentiation Pathway. *Cell* **128,** 519–531 (2007).

20. Sabbagh, W., Flatauer, L. J., Bardwell, a. J. & Bardwell, L. Specificity of MAP kinase signaling in yeast differentiation involves transient versus sustained MAPK activation. *Mol. Cell* **8,** 683–691 (2001).

21. Elion, E. A., J. A. Brill, and G. R. F. Functional redundancy in the yeast cell cycle: FUS3 and KSS1 have both overlapping and unique functions. *Cold Spring Harb. Symp. Quant. Biol.* **56,** 41–49 (1991).

22. Farley, F. W., Satterberg, B., Goldsmith, E. J. & Elion, E. a. Relative dependence of different outputs of the Saccharomyces cerevisiae pheromone response pathway on the MAP kinase Fus3p. *Genetics* **151,** 1425–1444 (1999).

23. Ma, D., Cook, J. G. & Thorner, J. Phosphorylation and Localization of Kssl, a MAP Kinase of the Saccharomyces cerevisiae Pheromone Response Pathway. *Mol. Biol. Cell* **6,** 889–909 (1995).

24. Cherkasova, V., Lyons, D. M. & Elion, E. A. Fus3p and Kss1p control G1 arrest in Saccharomyces cerevisiae through a balance of distinct arrest and proliferative functions that operate in parallel with Far1p. *Genetics* **151,** 989–1004 (1999).

25. Errede, B. & Ammerer, G. STE12 , a protein involved in cell-type- specific transcription and signal transduction in yeast , is part of protein- DNA complexes. 1349–1361 (1989).

26. Elion, E. a, Satterberg, B. & Kranz, J. E. FUS3 phosphorylates multiple components of the mating signal transduction cascade: evidence for STE12 and FAR1. *Mol. Biol. Cell* **4,** 495–510 (1993).

27. Jeanette, G., Bardwell, L., Kron, S. J. & Thorner, J. Two novel targets of the MAP kinase Kssl are ne gative regulators of invasive growth in the yeast Saccharom yces cerevisiae. **20,** 2831–2848 (1996).

28. Tedford, K., Kim, S., Sa, D., Stevens, K. & Tyers, M. Regulation of the mating pheromone and invasive growth responses in yeast by two MAP kinase substrates. *Curr. Biol.* **7,** 228–238 (1997).

29. Jeoung, D. *et al.* Pheromone-Dependent G1 Cell Cycle Arrest Requires Far1 Phosphorylation, but May Not Involve Inhibition of Cdc28-Cln2 Kinase, In Vivo. *Mol. Cell. Biol.* **18,** 3681–3691 (1998).

30. Parnell, S. C. *et al.* Phosphorylation of the RGS protein Sst2 by the MAP kinase Fus3 and use of Sst2 as a model to analyze determinants of substrate sequence specificity. *Biochemistry* **44,** 8159–66 (2005).

31. Gruhler, A. *et al.* Quantitative phosphoproteomics applied to the yeast pheromone signaling pathway. *Mol. Cell. proteomics* **4,** 310–327 (2005).

32. Li, X. *et al.* Large-Scale Phosphorylation Analysis of r -Factor-Arrested Saccharomyces cerevisiae. *J. Proteome Res.* **6,** 1190–1197 (2007).

33. Choi, K. Y., Kranz, J. E., Mahanty, S. K., Park, K. S. & Elion, E. a. Characterization of Fus3 localization: active Fus3 localizes in complexes of varying size and specific activity. *Mol. Biol. Cell* **10,** 1553–1568 (1999).

34. Van Drogen, F., Stucke, V. M., Jorritsma, G. & Peter, M. MAP kinase dynamics in response to pheromones in budding yeast. *Nat. Cell Biol.* **3,** 1051–1059 (2001).

35. Blackwell, E. *et al.* Effect of the Pheromone-Responsive Gα and Phosphatase Proteins of Saccharomyces cerevisiae on the Subcellular Localization of the Fus3 Mitogen-Activated Protein Kinase. *Mol. Cell. Biol.* **23,** 1135–1150 (2003).

36. Chen, R. E., Patterson, J. C., Goupil, L. S. & Thorner, J. Dynamic localization of Fus3 mitogen-activated protein kinase is necessary to evoke appropriate responses and avoid cytotoxic effects. *Mol. Cell. Biol.* **30,** 4293–4307 (2010).

37. Maeder, C. I. *et al.* Spatial regulation of Fus3 MAP kinase activity through a reaction-diffusion mechanism in yeast pheromone signalling. *Nat. Cell Biol.* **9,** 1319–1326 (2007).

38. Hilioti, Z. *et al.* Oscillatory phosphorylation of yeast Fus3 MAP kinase controls periodic gene expression and morphogenesis. *Curr. Biol.* **18,** 1700–6 (2008).

39. Inouye, C., Dhillon, N. & Thorner, J. Ste5 RING-H2 domain: role in Ste4-promoted oligomerization for yeast pheromone signaling. *Science (80-.).* **278,** 103–106 (1997).

40. Bhattacharyya, R. P. *et al.* The Ste5 scaffold allosterically modulates signaling output of the yeast mating pathway. *Science (80-.).* **311,** 822–826 (2006).

41. Good, M., Tang, G., Singleton, J., Reményi, A. & Lim, W. a. The Ste5 scaffold directs mating signaling by catalytically unlocking the Fus3 MAP kinase for activation. *Cell* **136,** 1085–97 (2009).

42. Malleshaiah, M. K., Shahrezaei, V., Swain, P. S. & Michnick, S. W. The scaffold protein Ste5 directly controls a switch-like mating decision in yeast. *Nature* **465,** 101–105 (2010).

43. Takahashi, S. & Pryciak, P. M. Membrane Localization of Scaffold Proteins Promotes Graded Signaling in the Yeast MAP Kinase Cascade. *Curr. Biol.* **18,** 1184–1191 (2008).

44. Bush, A. & Colman-Lerner, A. Quantitative measurement of protein relocalization in live cells. *Biophys. J.* **104,** 727–736 (2013).

45. Flotho, A., Simpson, D. M., Qi, M. & Elion, E. a. Localized feedback phosphorylation of Ste5p scaffold by associated MAPK cascade. *J. Biol. Chem.* **279,** 47391–401 (2004).

46. Jackson, C. L., Konopka, J. B. & Hartwell, L. H. S. cerevisiae α pheromone receptors activate a novel signal transduction pathway for mating partner discrimination. *Cell* **67,** 389–402 (1991).

47. Ayscough, K. R. & Drubin, D. G. A role for the yeast actin cytoskeleton in pheromone receptor clustering and signalling. *Curr. Biol.* **8,** 927–931 (1998).

48. Davis, N. G., Horecka, J. L. & Sprague, G. F. Cis- and trans-acting functions required for endocytosis of the yeast pheromone receptors. *J. Cell Biol.* **122,** 53–65 (1993).

49. Suchkov, D. V *et al.* Polarization of the yeast pheromone receptor requires its internalization but not actin-dependent secretion. *Mol. Biol. Cell* **21,** 1737–1752 (2010).

50. Jenness, D. D. & Spatrick, P. Down Regulation of the a-factor Pheromone Receptor in S . cerevisiae. *Cell* **46,** 345–353 (1986).

51. Schandel, K. a & Jenness, D. D. Direct evidence for ligand-induced internalization of the yeast alpha-factor pheromone receptor. *Mol. Cell. Biol.* **14,** 7245–7255 (1994).

52. Reneke, J. E., Blumer, K. J., Courchesne, W. E. & Thorner, J. The CarboxyTerminal Segment of the Yeast a-factor Receptor Is a Regulatory Domain. *Cell* **55,** 221–234 (1988).

53. Zanolari, B., Raths, S., Singer-kruger, B. & Riezman, H. Yeast Pheromone Receptor Endocytosis and Hyperphosphorylation Are Independent of G Protein-Mediated Signal Transduction. *Cell* **71,** 755–763 (1992).

54. Hicke, L. & Riezman, H. Ubiquitination of a Yeast Plasma Membrane Receptor Signals Its Ligand-Stimulated Endocytosis. *Cell* **84,** 277–287 (1996).

55. Hicke, L., Zanolari, B. & Riezman, H. Cytoplasmic Tail Phosphorylation of the alpha-Factor Receptor Is Required for Its Ubiquitination and Internalization. *J. Cell Biol.* **141,** 349–358 (1998).

56. Terrell, J., Shih, S., Dunn, R. & Hicke, L. A function for monoubiquitination in the internalization of a G protein-coupled receptor. *Mol. Cell* **1,** 193–202 (1998).

57. Konopka, J. B., Jenness, D. D. & Hartwell, L. H. The C-Terminus of the S . cerevisiae a-Pheromone Receptor Mediates an Adaptive Response to Pheromone. *Cell* **54,** 609–620 (1988).

58. Rohrer, J., Benedetti, H., Zanolari, B. & Riezman, H. Identification of a Novel Sequence Mediating Regulated Endocytosis of the G Protein-Coupled a-Pheromone Receptor in Yeast. *Mol. Biol. Cell* **4,** 511–521 (1993).

59. Jackson, C. L. & Hartwell, L. H. Courtship in S. cerevisiae: Both cell types choose mating partners by responding to the strongest pheromone signal. *Cell* **63,** 1039–1051 (1990).

60. Vallier, L. G., Segall, J. E. & Snyder, M. The alpha-factor receptor C-terminus is important for mating projection formation and orientation in Saccharomyces cerevisiae. *Cell Motil. Cytoskeleton* **53,** 251–66 (2002).

61. Moore, T. I., Chou, C. S., Nie, Q., Jeon, N. L. & Yi, T. M. Robust spatial sensing of mating pheromone gradients by yeast cells. *PLoS One* **3,** e3865 (2008).

62. Arkowitz, R. a. Chemical gradients and chemotropism in yeast. *Cold Spring Harb. Perspect. Biol.* **1,** a001958 (2009).

63. Sahin, A., Daignan-Fornier, B. & Sagot, I. Polarized growth in the absence of F-actin in Saccharomyces cerevisiae exiting quiescence. *PLoS One* **3,** e2556 (2008).

64. Yamamoto, T. *et al.* Initial Polarized Bud Growth by Endocytic Recycling in the Absence of Actin Cable-dependent Vesicle Transport in Yeast. *Mol. Biol. Cell* **21,** 1237–1252 (2010).

65. Bi, E. & Park, H.-O. Cell polarization and cytokinesis in budding yeast. *Genetics* **191,** 347–87 (2012).

66. Valtz, N., Peter, M. & Herskowitz, I. FAR1 is required for oriented polarization of yeast cells in response to mating pheromones. *J. Cell Biol.* **131,** 863–873 (1995).

67. Nern, A. & Arkowitz, R. A. A GTP-exchange factor required for cell orientation. *Nature* **391,** 195–198 (1998).

68. Hao, N. *et al.* Regulation of Cell Signaling Dynamics by the Protein Kinase-Scaffold Ste5. *Mol. Cell* **30,** 649–656 (2008).

69. Yu, L., Qi, M., Sheff, M. A. & Elion, E. A. Counteractive Control of Polarized Morphogenesis during Mating by Mitogen-activated Protein Kinase Fus3 and G1 Cyclin-dependent Kinase. **19,** 1739–1752 (2008).

70. Metodiev, M. V, Matheos, D., Rose, M. D. & Stone, D. E. Regulation of MAPK function by direct interaction with the mating-specific Galpha in yeast. *Science (80-.).* **296,** 1483–1486 (2002).

71. Deflorio, R. *et al.* Phosphorylation of Gβ is crucial for efficient chemotropism in yeast. *J. Cell Sci.* **126,** 2997–3009 (2013).

72. Dyer, J. M. *et al.* Tracking shallow chemical gradients by actin-driven wandering of the polarization site. *Curr. Biol.* **23,** 32–41 (2013).

73. Johnson, J. M., Jin, M. & Lew, D. J. Symmetry breaking and the establishment of cell polarity in budding yeast. *Curr. Opin. Genet. Dev.* **21,** 740–6 (2011).

74. Wedlich-Soldner, R., Altschuler, S., Wu, L. & Li, R. Spontaneous cell polarization through actomyosin-based delivery of the Cdc42 GTPase. *Science (80-.).* **299,** 1231–1235 (2003).

75. Wedlich-Soldner, R., Wai, S. C., Schmidt, T. & Li, R. Robust cell polarity is a dynamic state established by coupling transport and GTPase signaling. *J. Cell Biol.* **166,** 889–900 (2004).

76. Dorer, R., Pryciak, P. M. & Hartwell, L. H. Saccharomyces cerevisiae cells execute a default pathway to select a mate in the absence of pheromone gradients. *J. Cell Biol.* **131,** 845–861 (1995).

77. Follette, P. J. & Arkowitz, R. A. Chemotaxis. **571,** 99–110 (2009).

78. Segall, J. E. Polarization of yeast cells in spatial gradients of alpha mating factor. *Proc. Natl. Acad. Sci. U. S. A.* **90,** 8332–8336 (1993).

79. Paliwal, S. *et al.* MAPK-mediated bimodal gene expression and adaptive gradient sensing in yeast. *Nature* **446,** 46–51 (2007).

80. Lee, S. S. *et al.* Quantitative and dynamic assay of single cell chemotaxis. *Integr. Biol.* **4,** 381 (2012).

81. Kumar, A. *et al.* Subcellular localization of the yeast proteome. *Genes Dev.* **16,** 707–719 (2002).

82. Ding, D. *et al.* Large-scale screening of intracellular protein localization in living fission yeast cells by the use of a GFP-fusion genomic DNA library. *Genes to cells* **5,** 169–190 (2000).

83. Frommer, W. B., Davidson, M. W. & Campbell, R. E. Genetically encoded biosensors based on engineered fluorescent proteins. *Chem. Soc. Rev.* **38,** 2833–41 (2009).

84. Moreno, D. *et al.* A fluorescent reporter for mapping cellular protein-protein interactions in time and space. *Mol. Syst. Biol.* **9,** 647 (2013).

85. Siekhaus, D. E. & Drubin, D. G. Spontaneous receptor-independent heterotrimeric G-protein signalling in an RGS mutant. *Nat. Cell Biol.* **5,** 231–235 (2003).

86. Mateus, C. & Avery, S. V. Destabilized green fluorescent protein for monitoring dynamic changes in yeast gene expression with flow cytometry. *Yeast* **16,** 1313–1323 (2000).

87. Oldach, L. & Zhang, J. Genetically encoded fluorescent biosensors for live-cell visualization of protein phosphorylation. *Chem. Biol.* **21,** 186–97 (2014).

88. Ramsey, S. A. *et al.* Dynamic analysis of MAPK signaling using a high-throughput microfluidic single-cell. *Proc. Natl. Acad. Sci.* **106,** (2009).

89. Rowat, A. C., Bird, J. C., Agresti, J. J., Rando, O. J. & Weitz, D. a. Tracking lineages of single cells in lines using a microfluidic device. *Proc. Natl. Acad. Sci. U. S. A.* **106,** 18149–54 (2009).

90. Rines, D. R., Thomann, D., Dorn, J. F., Goodwin, P. & Sorger, P. K. Live cell imaging of yeast. *Cold Spring Harb. Protoc.* **2011,** (2011).

91. Deuschle, K. *et al.* Construction and optimization of a family of genetically encoded metabolite sensors by semirational protein engineering. *Protein Sci.* **14,** 2304–2314 (2005).

92. Okada, S., Ota, K. & Ito, T. Circular permutation of ligand-binding module improves dynamic range of genetically encoded FRET-based nanosensor. *Protein Sci.* **18,** 2518–2527 (2009).

93. Wegner, S. V, Sun, F., Hernandez, N. & He, C. The tightly regulated copper window in yeast. *Chem. Commun.* **47,** 2571–3 (2011).

94. Vevea, J. D., Wolken, D. M. A., Swayne, T. C., White, A. B. & Pon, L. a. Ratiometric biosensors that measure mitochondrial redox state and ATP in living yeast cells. *J. Vis. Exp.* 1–12 (2013). doi:10.3791/50633

95. Smith, S. E. *et al.* Independence of symmetry breaking on Bem1-mediated autocatalytic activation of Cdc42. *J. Cell Biol.* **202,** 1091–106 (2013).

96. Strickfaden, S. C. *et al.* A Mechanism for Cell-Cycle Regulation of MAP Kinase Signaling in a Yeast Differentiation Pathway. *Cell* **128,** 519–531 (2007).

97. Leeuw, T. *et al.* Pheromone Response in Yeast: Association of Bem1p with Proteins of the MAP Kinase Cascade and Actin. *Science (80-.).* **270,** 1210–1213 (1995).

98. Lyons, D. M., Mahanty, S. K., Choi, K., Manandhar, M. & Elion, E. A. The SH3-Domain Protein Bem1 Coordinates Mitogen-Activated Protein Kinase Cascade Activation with Cell Cycle Control in Saccharomyces cerevisiae. *Mol. Cell. Biol.* **16,** 4095–4106 (1996).

99. Garrenton, L. S., Stefan, C. J., McMurray, M. a, Emr, S. D. & Thorner, J. Pheromone-induced anisotropy in yeast plasma membrane phosphatidylinositol-4,5-bisphosphate

distribution is required for MAPK signaling. *Proc. Natl. Acad. Sci. U. S. A.* **107,** 11805–11810 (2010).

100. Goldstein, A. L. & McCusker, J. H. Three New Dominant Drug Resistance Cassettes for Gene Disruption in Saccharomyces cerevisiae. *Yeast* **15,** 1541–1553 (1999).

101. Bahler, J. *et al.* Heterologous Modules for Efficient and Versatile PCR-based Gene Targeting in Schizosaccharomyces pombe. *Yeast* **14,** 943–951 (1998).

102. Xia, Y. & Whitesides, G. M. Soft Lithography. *Annu. Rev. Mater. Sci.* **28,** 153–184 (1998).

103. Doncic, A., Eser, U., Atay, O. & Skotheim, J. M. An algorithm to automate yeast segmentation and tracking. *PLoS One* **8,** e57970 (2013).

104. Colman-Lerner, A. *et al.* Regulated cell-to-cell variation in a cell-fate decision system. *Nature* **437,** 699–706 (2005).

105. Slaughter, B. D., Schwartz, J. W. & Li, R. Mapping dynamic protein interactions in MAP kinase signaling using live-cell fluorescence fluctuation spectroscopy and imaging. *Proc. Natl. Acad. Sci. U. S. A.* **104,** 20320–5 (2007).

106. Harvey, C. D. *et al.* A genetically encoded fluorescent sensor of ERK activity. *Proc. Natl. Acad. Sci. U. S. A.* **105,** 19264–19269 (2008).

107. Komatsu, N. *et al.* Development of an optimized backbone of FRET biosensors for kinases and GTPases. *Mol. Biol. Cell* **22,** 4647–4656 (2011).

108. Fritz, R. D. *et al.* A versatile toolkit to produce sensitive FRET biosensors to visualize signaling in time and space. *Sci. Signal.* **6,** rs12 (2013).

109. Vandame, P. *et al.* Optimization of ERK activity biosensors for both ratiometric and lifetime FRET measurements. *Sensors (Basel).* **14,** 1140–54 (2013).

110. Zhai, S., Ark, E. D., Parra-Bueno, P. & Yasuda, R. Long-distance integration of nuclear ERK signaling triggered by activation of a few dendritic spines. *Science* **342,** 1107–11 (2013).

111. Albeck, J. G., Mills, G. B. & Brugge, J. S. Frequency-modulated pulses of ERK activity transmit quantitative proliferation signals. *Mol. Cell* **49,** 249–61 (2013).

112. Aoki, K. *et al.* Stochastic ERK activation induced by noise and cell-to-cell propagation regulates cell density-dependent proliferation. *Mol. Cell* **52,** 529–40 (2013).

113. Poritz, M. a, Malmstrom, S., Kim, M. K., Rossmeissl, P. J. & Kamb, A. Graded mode of transcriptional induction in yeast pheromone signalling revealed by single-cell analysis. *Yeast* **18,** 1331–1338 (2001).

114. Yi, T., Kitano, H. & Simon, M. I. A quantitative characterization of the yeast heterotrimeric G protein cycle. *Proc. Natl. Acad. Sci.* **19,** 10764–10769 (2003).

115. Jenness, D. D., Burkholder, A. C. & Hartwell, L. H. Binding of ot-Factor Pheromone to Saccharomyces cerevisiae a Cells : Dissociation Constant and Number of Binding Sites. **6,** 318–320 (1986).

116. Zanolari, B. & Riezman, H. Quantitation of ot-Factor Internalization and Response during the Saccharomyces cerevisiae Cell Cycle. **11,** 5251–5258 (1991).

117. Oehlen, L. J. & Cross, F. R. G1 cyclins CLN1 and CLN2 repress the mating factor response pathway at Start in the yeast cell cycle. *Genes Dev.* **8,** 1058–1070 (1994).

118. Oehlen, L. J. W. M. & Cross, F. R. Potential Regulation of Ste20 Function by the Cln1-Cdc28 and Cln2-Cdc28 Cyclin-dependent Protein Kinases. *J. Biol. Chem.* **273,** 25089–25097 (1998).

119. Wassmann, K. & Ammerer, G. Overexpression of the G1-cyclin Gene CLN2Represses the Mating Pathway in Saccharomyces cerevisiae at the Level of the MEKK Ste11. *J. Biol. Chem.* **272,** 13180–13188 (1997).

120. Ricicova, M. *et al.* Dissecting genealogy and cell cycle as sources of cell-to-cell variability in MAPK signaling using high-throughput lineage tracking. *Proc. Natl. Acad. Sci. U. S. A.* **110,** 11403–8 (2013).

121. Blackwell, E., Kim, H.-J. N. & Stone, D. E. The pheromone-induced nuclear accumulation of the Fus3 MAPK in yeast depends on its phosphorylation state and on Dig1 and Dig2. *BMC Cell Biol.* **8,** 44 (2007).

122. Marshall, C. J. & Laboratories, C. B. Specificity of Receptor Tyrosine Kinase Signaling : Transient versus Sustained Extracellular Signal-Regulated Kinase Activation. **2,** 179–185 (1995).

123. Kriegsheim, A. Von *et al.* Europe PMC Funders Group Cell fate decisions are specified by the dynamic ERK interactome. **11,** (2013).

124. Cohen-Saidon, C., Cohen, A. a., Sigal, A., Liron, Y. & Alon, U. Dynamics and Variability of ERK2 Response to EGF in Individual Living Cells. *Mol. Cell* **36,** 885–893 (2009).

125. Shankaran, H. *et al.* Rapid and sustained nuclear-cytoplasmic ERK oscillations induced by epidermal growth factor. *Mol. Syst. Biol.* **5,** 332 (2009).

126. Doncic, A., Falleur-Fettig, M. & Skotheim, J. M. Distinct Interactions Select and Maintain a Specific Cell Fate. *Mol. Cell* **43,** 528–539 (2011).

127. Fukuda, M., Gotoh, I., Gotoh, Y. & Nishida, E. Cytoplasmic Localization of Mitogen-activated Protein Kinase Kinase Directed by Its NH2 -terminal, Leucine-rich Short Amino Acid Sequence, Which Acts as a Nuclear Export Signal. **271,** 20024–20028 (1996).

128. Bardwell, L., Cook, J. G., Chang, E. C., Cairns, B. R. & Thorner, J. Signaling in the yeast pheromone response pathway: specific and high-affinity interaction of the mitogen-activated protein (MAP) kinases Kss1 and Fus3 with the upstream MAP kinase kinase Ste7. *Mol. Cell. Biol.* **16,** 3637–3650 (1996).

129. Cappell, S. D., Baker, R., Skowyra, D. & Dohlman, H. G. Systematic analysis of essential genes reveals important regulators of G protein signaling. *Mol. Cell* **38,** 746–57 (2010).

130. Grote, E. Cell fusion assays for yeast mating pairs. *Methods Mol. Biol.* **475,** 165–196 (2008).

131. Breslow, D. K. *et al.* A comprehensive strategy enabling high-resolution functional analysis of the yeast genome. **5,** (2008).

132. Cohen, Y. & Schuldiner, M. *Network Biology*. **781,** (Humana Press, 2011).

133. Bilodeau, P. S., Winistorfer, S. C., Kearney, W. R., Robertson, A. D. & Piper, R. C. Vps27-Hse1 and ESCRT-I complexes cooperate to increase efficiency of sorting ubiquitinated proteins at the endosome. *J. Cell Biol.* **163,** 237–243 (2003).

134. Odorizzi, G., Babst, M. & Emr, S. D. Fab1p Ptdlns(3)P 5-kinase function essential for protein sorting in the multivesicular body. *Cell* **95,** 847–858 (1998).

135. Babst, M., Odorizzi, G., Estepa, E. J. & Emr, S. D. Mammalian tumor susceptibility gene 101 (TSG101) and the yeast homologue, Vps23p, both function in late endosomal trafficking. *Traffic* **1,** 248–258 (2000).

136. Bugnicourt, A. *et al.* Antagonistic roles of ESCRT and Vps class C/HOPS complexes in the recycling of yeast membrane proteins. *Mol. Biol. Cell* **15,** 4203–4214 (2004).

137. Gelin-Licht, R., Paliwal, S., Conlon, P., Levchenko, A. & Gerst, J. E. Scp160-dependent mRNA trafficking mediates pheromone gradient sensing and chemotropism in yeast. *Cell Rep.* **1,** 483–94 (2012).

138. Finger, F. P., Hughes, T. E. & Novick, P. Sec3p Is a Spatial Landmark for Polarized Secretion in Budding Yeast. *Cell* **92,** 559–571 (1998).

139. Wiederkehr, A., Avaro, S., Prescianotto-Baschong, C., Haguenauer-Tsapis, R. & Riezman, H. The F-box protein Rcy1p is involved in endocytic membrane traffic and recycling out of an early endosome in Saccharomyces cerevisiae. *J. Cell Biol.* **149,** 397–410 (2000).

140. Zhang, X. *et al.* Cdc42 interacts with the exocyst and regulates polarized secretion. *J. Biol. Chem.* **276,** 46745–50 (2001).

141. Zhang, X. *et al.* Membrane association and functional regulation of Sec3 by phospholipids and Cdc42. *J. Cell Biol.* **180,** 145–58 (2008).

Vitae

Patrick Conlon was born in Bloomington, Illinois in 1984. He received a B.S. degree in Chemical Engineering at the University of Florida in 2008. He worked in the lab of Weihong Tan where his undergraduate thesis focused on the design and construction of DNA biosensors. In 2008, he entered the Ph.D. program in Biomedical Engineering at Johns Hopkins University and in 2009, joined the lab of Andre Levchenko where his graduate thesis focused on understanding single-cell MAPK signaling behavior.